ZMP BASED REFERENCE GENERATION FOR A BIPEDAL HUMANOID ROBOT

by
ÖZER KOCA

Submitted to the Graduate School of Engineering and Natural Sciences
in partial fulfillment of
the requirements for the degree of
Master of Science

Sabanci University
August 2009

ZMP BASED REFERENCE GENERATION FOR A BIPEDAL HUMANOID ROBOT

APPROVED BY:

Assist. Prof. Dr. Kemalettin ERBATUR (Thesis Advisor) .....

Prof. Dr. Asif SABANOVIC .....

Assoc. Prof. Dr. Mustafa ÜNEL .....

Assoc. Prof. Dr. Mahmut F. AKŞİT .....

Assist. Prof. Dr. Hakan ERDOĞAN .....

DATE OF APPROVAL: 10.08.2009

ZMP BASED REFERENCE GENERATION FOR A BIPEDAL HUMANOID ROBOT

Özer KOCA

ME, Ms Thesis, 2009

Thesis Supervisor: Assist. Prof. Dr. Kemalettin ERBATUR

Keywords: Linear Inverted Pendulum Model, Zero Moment Point, Reference Generation.

ABSTRACT

Recent fifteen years witnessed fast improvements in the field of humanoid robotics. The human-like robot structure is more suitable to human environment with its supreme obstacle avoidance properties when compared with wheeled service robots. However, the walking control for bipedal robots is a challenging task due to their complex dynamics.

Stable reference generation plays a very important role in control. Linear Inverted Pendulum Model (LIPM) and the Zero Moment Point (ZMP) criterion are applied in a number of studies for stable walking reference generation of biped walking robots. This thesis takes this main approach too.

This thesis proposes a natural and continuous ZMP reference trajectory for a stable and human-like walk. Natural, human-like walking is obtained by ZMP trajectories which move forward under the sole of the support foot when the robot body is supported by a single leg. Robot center of mass trajectory is obtained from predefined ZMP reference trajectories by a Fourier series approximation method. The Gibbs phenomenon problem common with Fourier approximations of discontinuous functions is avoided by employing continuous ZMP references. Also, these ZMP reference trajectories, unlike many examples in the literature, possess pre-assigned single and double support phases, which are very useful in experimental tuning work.

In this thesis, a method for generating a stepping sequence of finite number of steps is proposed too.

The ZMP based reference generation strategy is applied on the full body humanoid robot SURALP designed at Sabanci University. Experimental results indicate that the proposed reference trajectory generation technique is successful.

İKİ BACAKLI İNSANSI BİR ROBOT İÇİN SMN TABANLI REFERANS SENTEZİ

Özer KOCA

ME, Master Tezi, 2009

Tez Danışmanı: Yrd. Doç. Dr. Kemalettin ERBATUR

Anahtar Kelimeler: Doğrusal Ters Sarkaç Modeli, Sıfır Moment Noktası, Referans Sentezi.

ÖZET

Son on beş yılda insansı robot alanındaki çalışmalar hızlı bir artış göstermiştir. Tekerlekli robotlarla karşılaştırıldıklarında, insansı yapıya sahip olmaları insanların yaşam alanlarına uyum sağlamaları açısından daha elverişlidir. Fakat karmaşık dinamikleri, iki ayaklı insansı robotların kontrolünü büyük bir ölçüde zorlaştırmaktadır.

Kararlı bir yürüyüş referans yörüngesi sentezi, insansı robotların kontrolünde önemli bir rol oynamaktadır. Çok sayıda çalışma, iki ayaklı insansı robotlar için kararlı bir yürüyüş referans yörüngesi sentezinde Doğrusal Ters Sarkaç Modeli'ni (LIMP) ve Sıfır Moment Noktası (ZMP) kriterini kullanmıştır. Bu tezde de, bu ana yaklaşım benimsenmiştir.

Bu tezde kararlı ve insanınkine benzer bir yürüyüş elde edebilmek için doğal ve sürekli ZMP referans yörüngeleri önerilmektedir. Bu doğal ve insanınkine benzer yürüyüş, robot gövdesi tek bacak tarafından desteklendiği esnada destek ayak tabanı altında ileriye doğru hareket eden ZMP yörüngeleri kullanılarak elde edilmiştir. Robot ağırlık merkezi yörüngeleri de, daha önceden tanımlanmış olan ZMP referans yörüngelerinden Fourier serileri yakınsaması yöntemi kullanılarak oluşturulmaktadır. Kesikli fonksiyonların Fourier yakınsamalarında sıkça görülen Gibbs fenomeni sorunu tanımlanan sürekli ZMP referansları ile engellenmiştir. Ayrıca, bu alandaki birçok çalışmanın aksine, bu ZMP referansları deneysel parametre ayarlamalarında çok faydalı olan önceden tanımlanmış tek ve çift ayak destek evrelerine sahiptir.

Bunlara ek olarak, bu tezde sınırlı adım sayısına sahip olan bir yürüyüş elde edebilmek için de bir yöntem sunulmuştur.

ZMP tabanlı referans sentezi yöntemi Sabancı Üniversitesi'nde tasarlanmış olan iki ayaklı insansı robot SURALP'te uygulanmıştır. Deneysel sonuçlar, önerilen referans yörüngesi sentezi yönteminin başarılı olduğunu göstermektedir.

to my beloved family

ACKNOWLEDGEMENTS

This thesis would not have been a real fulfillment without the cooperation from various individuals through various means. It is a pleasure to present my gratitude to them all in my humble acknowledgement.

In the first place, I would like to express my deepest gratitude to my supervisor, Assist. Prof. Dr. Kemalettin Erbatur for his endless support, encouragement, supervision and useful advices throughout my Masters education and thesis study. Without his invaluable patience of teaching and academic guidance, this thesis would not have been possible. I am indebted to him for providing me a friendly working environment. I would like to thank Prof. Dr. Asif Sabanovic, Assoc. Prof. Dr. Mustafa Ünel, Assoc. Prof. Dr. Mahmut F. Akşit and Assist. Prof. Dr. Hakan Erdoğan for attending to my thesis jury and for their valuable comments.

I would like to acknowledge the financial support provided by The Scientific & Technological Research Council of Turkey (TÜBİTAK) through project “Two Legged Humanoid Robot Design, Construction and Control” under the grant 106E040.

I would gratefully like to thank SURALP team members Utku Seven, Evrim Taşkıran and Metin Yılmaz for their endless efforts which make this thesis possible and for their valuable friendship.

Furthermore I would like to thank Burak Karaboğa, Berkay Kaya, Berkay Topçu, Cihan Şahin and Özlem Can for always supporting me throughout my thesis writing period and having fun with me in several activities. I am also happy to acknowledge Ahmetcan Erdoğan, Ahmet Yasin Yazıcıoğlu, Berk Çallı, Caner Hamarat, Hakan Kaynar, Hümay Esin, Kaan Öner and all my other friends.

Finally, I would like to give my greatest thanks to my family, Fevzi Koca, Neriman Koca, Deniz Koca Çeliktaş, Remzi Çeliktaş, Özgür Koca and Seval Koca for their incomparable support, trust and unconditional love.

TABLE OF CONTENTS

LIST OF FIGURES

LIST OF TABLES

LIST OF SYMBOLS

H_{ij}	:	Sub-matrices of the robot inertia matrix for $(i, j) \in \{1,2,3\}$
v_B	:	Linear velocity of the robot body frame
ω_B	:	Angular velocity of the robot body frame
θ	:	Joint displacements vector
c_1, c_2, c_3	:	Bias vector terms
u_E	:	Generalized force vector generated by external forces
$\tau_{jo\,\mathrm{int}}$	:	Generalized joint control vector
c	:	Coordinates of the point mass in inverted pendulum model
p_x	:	ZMP coordinate in the x-direction
p_y	:	ZMP coordinate in the y-direction
z_c	:	Fixed height of the Linear Inverted Pendulum
g	:	Gravity constant
A	:	Distance between the foot centers in the y-direction
B	:	Distance between the foot centers in the x-direction
T	:	Half of the walking period
b	:	Range of the ZMP motion under the foot sole
p_x^{ref}	:	Reference ZMP in the x-direction
p_y^{ref}	:	Reference ZMP in the y-direction
c_x	:	CoM coordinate in the x-direction
c	:	CoM coordinate in the y-direction
	:	Lanczos sigma factor parameter
	:	Reference CoM in the x-direction
	:	Reference CoM in the y-direction
	:	Half of the double support period
	:	Double support period
	:	Periodic component of

δ	:	Magnitude of peak difference between p_x^{ref} and the nonperiodic component of p_x^{ref}
u	:	Unit step function
ω_n	:	Square root of g/z_c
a_0, a_k, b_k	:	Fourier coefficients of c_y^{ref}
$\alpha_0, \alpha_k, \beta_k$	:	Fourier coefficients of c_x^{ref}
$\hat{s}_b^b$	:	Coordinates of the body center of mass in the body coordinate
R_a^b	:	Orientation of “b” frame with respect to “a” frame
h_h	:	Height of the hip frame from ground level
$x_{ref\ \text{asymmetry}}$	:	Initial coordinates of the feet in the x-direction
N_{swing}	:	Number of foot swings
N_{phase}	:	Phase description number
N_{step}	:	Traveled distance in terms of step size
s_s	:	Toe-to-toe step size
T_s	:	Single support period
T_w	:	Full walking period
h_s	:	Step height
t	:	Generic time variable
A_s	:	Traveled distance variable in the x-direction
d_a^b	:	Coordinate of “b” frame expressed in “a” frame

LIST OF ABBREVIATIONS

ZMP	:	Zero Moment Point
LIPM	:	Linear Inverted Pendulum Model
CoM	:	Center of Mass
3D-LIPM	:	Three-Dimensional Linear Inverted Pendulum Model
DOF	:	Degrees of Freedom
CoG	:	Center of Gravity
3D	:	Three Dimensional
CMB	:	Center of Mass of Body
FSR	:	Force Sensing Resistor

Chapter 1

1. INTRODUCTION

Recent fifteen years witnessed fast improvements in the field of humanoid robotics. The human-like robot structure is suitable for our homes and offices due to its supreme obstacle avoidance properties when compared with wheeled service robots. Robots in the human shape can be accepted as a social being by human beings. Their integration into human life as assistants will be much easier than with differently shaped robots. These facts make this robotics field very attractive for researchers and promising for the future.

However, there are many problems which should be solved before realizing the daily life human-robot coexistence. The large number of degrees of freedom cause pronounced coupling effects. The bipedal free-fall manipulator is inherently difficult to stabilize. This makes the walking control a challenging task. In biped robot systems, control and gait planning go hand in hand. A stable walking reference generation is essential.

The Zero Moment Point (ZMP) criterion is the most widely accepted and used stability measure for the legged locomotion. The criterion states that, during the walk, the ZMP should lie within the supporting area - often called the support polygon - of the feet in contact with the ground.

The Zero Moment Point coordinates are functions of the positions and accelerations of the numerous links and the body of the humanoid robot. Though they can be computed – even online, – it is quite difficult to use these expressions of many variables in the design of reference generation and control algorithms. The same is true for the complicated dynamics equations of the biped robot. This is where an approximate model, rather than a detailed one, would be of better use.

The Linear Inverted Pendulum Model (LIPM) is such an approximate model of the legged robot. It consists of a point mass of constant height and a massless rod connecting the point mass with the ground. By virtue of this model, a quite simple

relation between the Zero Moment Point and the robot Center of Mass (CoM) coordinates is obtained. It is this relation that opened a route for Zero Moment Point based stable reference generation. The Linear Inverted Pendulum Model and the Zero Moment Point criterion are applied in a number of studies successfully for stable walking reference generation of biped walking robots. In such works, robot center of mass trajectory is obtained from predefined stable ZMP reference trajectories. The reference trajectories for the leg joints are obtained then via inverse kinematics from the robot Center of Mass coordinates.

There is a freedom in choosing the Zero Moment Point reference trajectory as long as the criterion mentioned above is satisfied. A natural choice is to keep it fixed at the center of the foot sole when only one foot is supporting the body (single support phase) and interpolating between the foot centers when two feet support it (double support phase). However, studies have shown that a natural, human-like walk can be obtained by ZMP trajectories which move forward when the robot body is supported by a single leg.

In [33], Erbatur and Kurt introduce a forward moving discontinuous ZMP reference trajectory for a stable and human-like walk and employ Fourier series approximation to obtain CoM reference trajectory from this ZMP trajectory. The ZMP reference trajectory in the double support phases in [33] is obtained indirectly with a smoothing process, which also provides smoothing of the Gibbs phenomenon peaks due to Fourier approximation. Although the walk period is defined by the user, the partition of the period into the single and double support phases is due to the smoothing process, and not predefined.

This thesis follows the same mechanism as in [33] in using Fourier series approximation for the computation of the CoM trajectory from a given ZMP reference curve. However, it defines a continuous ZMP reference and the durations of the single and double support phases are fully pre-assigned. This is quite useful since these parameters play an important role in the final parameter tuning in experimental work. The naturalness of the walk is preserved, in that the single support ZMP reference is forward moving. Further, the continuity of the introduced ZMP reference makes the after-Fourier-approximation smoothing process unnecessary. In addition, in this thesis, a walk planning algorithm which generates references for a predefined number of steps with smooth starting and stopping motion is designed, in contrast to infinitely cycling references in [33].

The thesis is organized as follows. The next chapter briefs humanoid robot terminology and presents a survey on reference generation and control of biped walking robots. Chapter 3 introduces the simulation environment and the experimental humanoid robot SURALP on which the designed reference generation algorithms are tested. The ZMP based reference generation for bipedal walk and created CoM reference trajectories are presented in Chapter 4. In Chapter 5, the foot reference trajectory generations and the modifications on the CoM reference are detailed in order to have a finite walk with a predefined number of steps. Chapter 6 is devoted to experiments on SURALP using the generated reference trajectories. Conclusion is presented lastly.

Chapter 2

2. LITERATURE REVIEW

In this chapter, a literature review is presented in the context of humanoid locomotion terminology, walking reference trajectory generation and control for the bipedal humanoid robots.

2.1. Humanoid Locomotion Terminology

It is important to introduce some useful terms in the humanoid locomotion terminology to get familiar with the humanoid robotics research area. In this area, to define sets of motions of the bipedal robot in one specific direction, different reference planes are used. In this thesis, the following reference frames presented in Figure 2.1 are used.

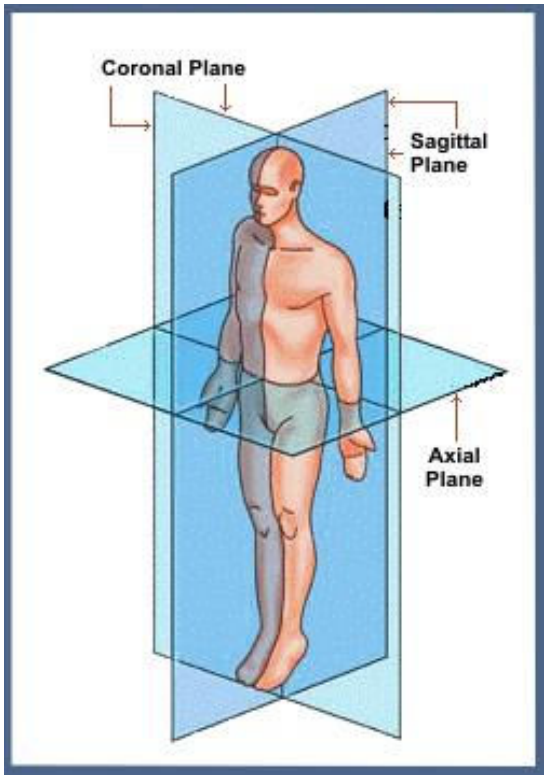

Figure 2.1: Reference body planes [1]

Only the motions in the sagittal plane are considered to achieve a walking gait for the bipedal robots in several works [2-4]. The term of gait defines the pattern of steps and gait cycle is used for the successful cyclic motion of this pattern. Mentioned gait cycle can be divided into two phases called swing and support (stance) phases. Swing phase occurs when a leg starts to move in the air freely without touching the ground and it ends with the touch of the foot to the ground, after that moment support phase starts for this leg. Support phase can also be thought as the combination of two phases, so-called single support and double support phases. During the single support phase, all of the body weight is carried by one of the legs while in the double support phase both of the legs are at the ground supporting the whole body. In Figure 2.2, the mentioned phases above are visualized for a better understanding.

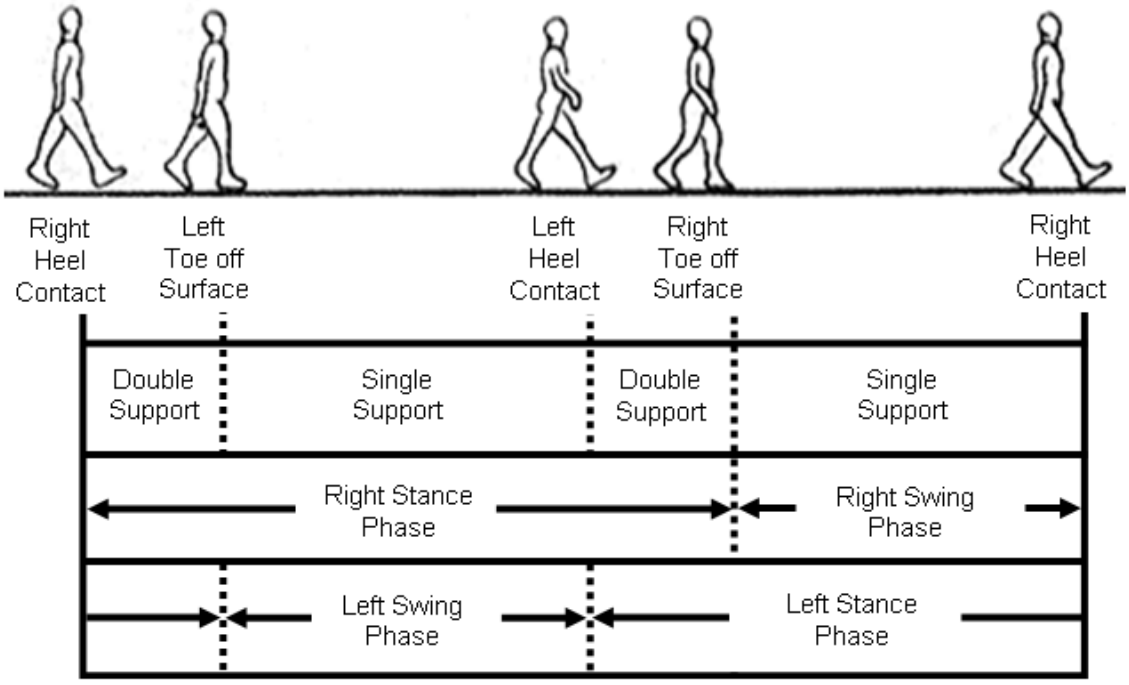

Figure 2.2: A complete walking cycle defined with several stages [5]

Since the phases in a complete walking gait cycle is observed, the stability of this walking process can be examined by defining what a support polygon is. Support polygon is the area on the ground where the corners of the support foot (feet) envelop (Figure 2.3).

Stable walking gait synthesis is highly related with the position of the ground projection of the Center of Mass (Figure 2.4) in the support polygon during the gait cycle. In other words, characteristics of the gait cycle can be defined with the position of the CoM. If the CoM stays in the support polygon at all times during the walk, this

walking gait is called static gait (Figure 2.5) which leads a stable but relatively slower walking process. Since the CoM always stays in the supporting polygon during static locomotion, even if the robot ends its motion, it does not have an intention to fall.

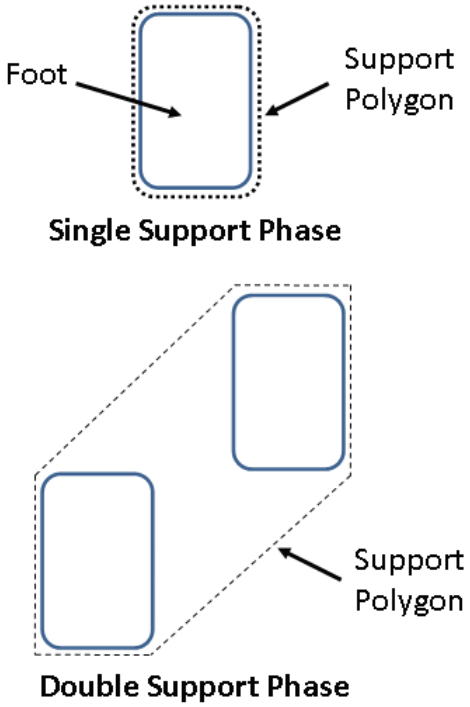

Figure 2.3: Supporting polygon

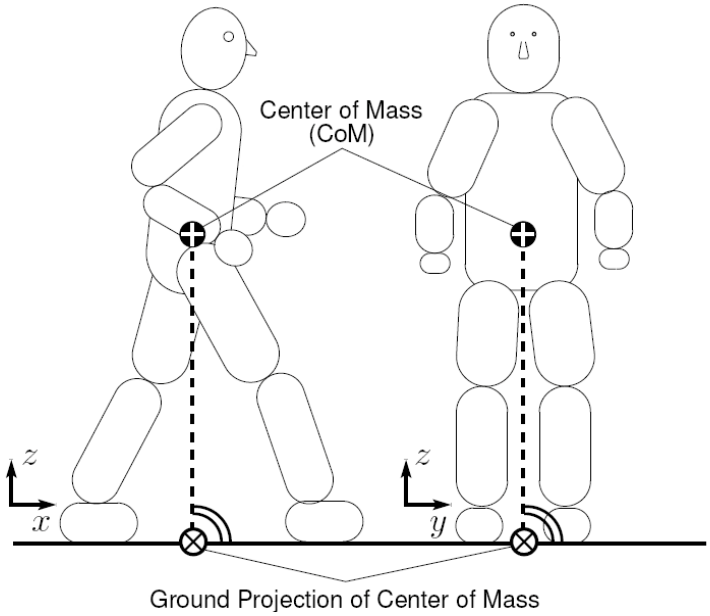

Figure 2.4 CoM and its ground projection [6]

On the other hand, in the dynamic gait the CoM does not have to stay in the supporting polygon at all times. In this type of walking gait, stability is provided by the

inertial effects. If it is to be compared, dynamic gait stability is harder to achieve than the static gait stability, but a fast dynamic gait can be realized by the correct adjustment of the walking speed in the means of arranging single and double support phases. In other words, walking speed should be fast enough to take back the CoM position into the support polygon before the robot starts to fall down completely with the effect of the gravity.

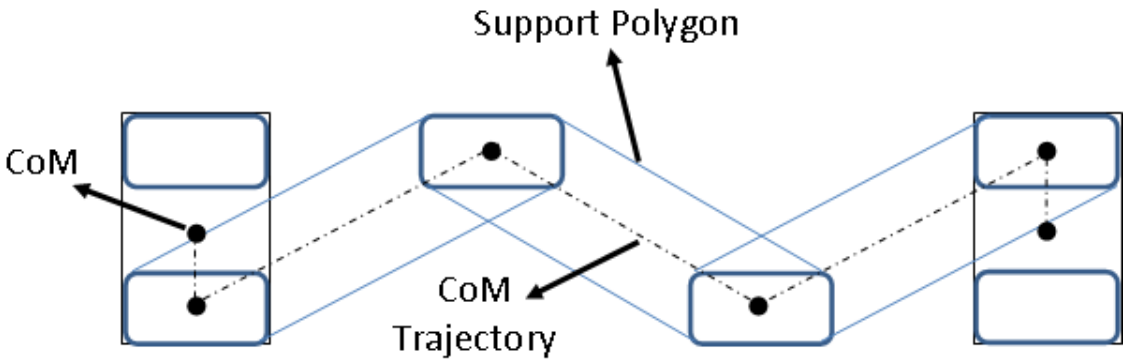

Figure 2.5 Static walking gait and CoM trajectory

As the position of the CoM in the supporting polygon indicates the stability of the robot, another and more powerful criterion for achieving dynamically stable biped locomotion is the Zero Moment Point criterion. This concept was introduced by Vukobratovic, M. in 1968 and then in the beginning of 1970s, its name was given as the Zero Moment Point. It is the point on the ground surface which the total reaction force at the contact of the foot does not create any moment; in other words, it is the point where the total inertial force equals zero [7]. If the ZMP lies inside the support polygon during the walking gait at all times, this gait is considered to be stable even if the created gait is a dynamic gait which the CoM position leaves the support polygon. On the other hand, if the ZMP gets closer to the boundary of the supporting polygon, it may lead tipping moment acting on the robot body and the robot may fall eventually. For prevent such a situation, generally a stability region is created for the ZMP trajectories in reference generation of bipedal humanoid robots.

2.2. Reference Generation and Control for the Bipedal Humanoid Robots

The bipedal humanoid robots which are thought to be served with full capacity in our daily life in future have many challenging problems when the subject comes to the stability of these robots. Since the biped robots have highly complex and nonlinear dynamics, it is hard to stabilize the bipedal walking even if they walk on a flat ground. However, the human environment has flat surfaces such as floors; most parts of this environment have irregularities, discontinuities and uneven surfaces. From this point of view, generation of stable bipedal walking references is one of the key solutions for the bipedal humanoid robots to serve in such a complex environment. For this purpose, in a number of studies, Linear Inverted Pendulum Model and the Zero Moment Point criterion are applied for stable walking reference generation of biped walking robots. In such works, robot center of mass trajectory is obtained either from predefined ZMP reference trajectories or with the online modification of the ZMP reference trajectories. The reference generation and the control of the obtained trajectories through the direct or indirect manipulation of the predefined ZMP trajectories are the main and inextricable topics for the stable walking of the bipedal robots. Since this is the fact, in this subsection of literature survey, both of these are considered together and some of the studies in this area are examined.

Lim and Kim, in 1995, proposed a Zero Moment Point control algorithm for dynamic bipedal walking [8]. In their work, a new walking step without the double support phase is introduced to overcome the difficulties of analyzing the difference of reaction force created by the instant landing or take-off of the foot between the single support phase and double support phase. For this purpose, in this new designed walking step, the foot pushes itself ahead and swing occurs simultaneously in one single supporting phase. Therefore, the ZMP becomes independent of the supporting phase and the walking algorithm is simplified because there are only two different steps of walk, which are left-leg-supporting step and right-leg-supporting step. Thus, only open kinematics chain during the walking period is considered and instead of using ZMP trajectory, the ZMP is placed to the origin of the foot support polygon.

In contrast to [8], Zhang, Wang, Qiang and Fu worked on a new method of gait generation which uses the reaction force between the feet and the ground [9]. After achieving the relation between the reaction force and joint motions by using the D'Alembert's principle, the desired joint trajectories of the walk is designed. The

desired gait is composed of the desired joint trajectories and the desired ground reaction force pattern for a walking period. While creating the desired joint trajectories, after several analysis, it is noted that the Center of Mass (CoM) displacement of the swing leg in sagittal plane and the position of the hip joint of the supporting leg have the most significant effect on the ZMP trajectory. A fuzzy logic based determination for the desired ZMP trajectory is implemented based on the human locomotion observations. According to these observations, the heel of the swing foot touches the ground firstly, and the toe touches at last such that the ZMP moves continuously under the foot in this case. It is stated that the proposed method in this work can decrease the trunk oscillations and can be applied both single and double support phases.

In 2002, Kajita et al. worked on real-time walking control of a biped robot with a simplified three-dimensional inverted pendulum model [10]. In such simplified models, because the controller knows a limited knowledge of the dynamics of the model, feedback control is used mostly. In their work, a Three-Dimensional Linear Inverted Pendulum Mode (3D-LIPM) (Figure 2.6) is represented which is a derivation of three-dimensional inverted pendulum whose motion is constrained. The new model simplifies the walking pattern generation by allowing a separate controller design for the sagittal and lateral motions. The biped robot HRP-2L (Figure 2.7) is governed by an input device which is a gamepad and experiments carried out for moving forward, turning right and then moving backwards. In this experiment, step size is also changed during the change of the moving direction with online modification of the two foot placements. Experimental results show that proposed pattern generation performed well on the biped robot HRP-2L.

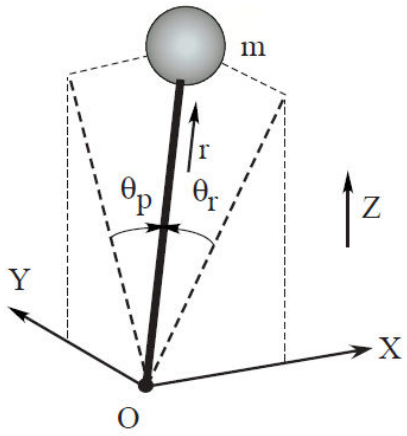

Figure 2.6: 3D inverted pendulum model

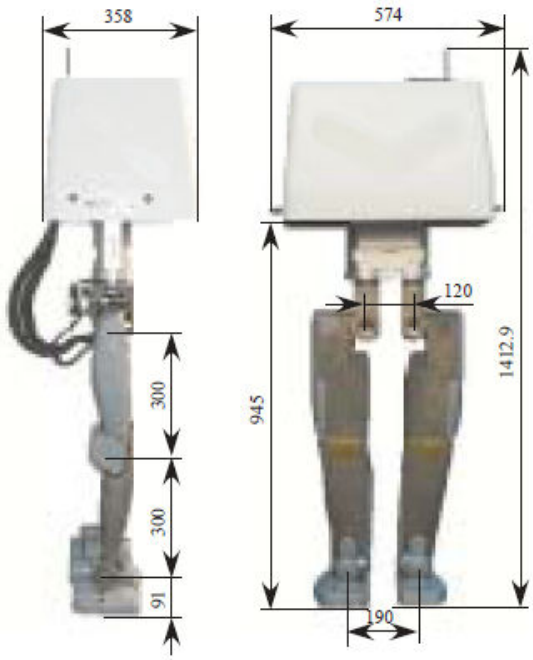

Figure 2.7: The biped robot – HRP-2L

Nishiwaki et al. presented an efficient online trajectory generation algorithm which also satisfies the desired upper body trajectories [11]. For this purpose, the desired ZMP is followed by a fast motion pattern generation method which modifies horizontal torso trajectory from given initial trajectory. Control inputs that controls the upper body motion and walking direction given by a joystick are updated and connected to the old trajectory inputs in real-time. In their work, repetitive generation and update method is proposed to be able to apply position based trajectory generation algorithm for online walk control (Figure 2.8). One step cycle control system is applied on the humanoid robot H7 (Figure 2.9).

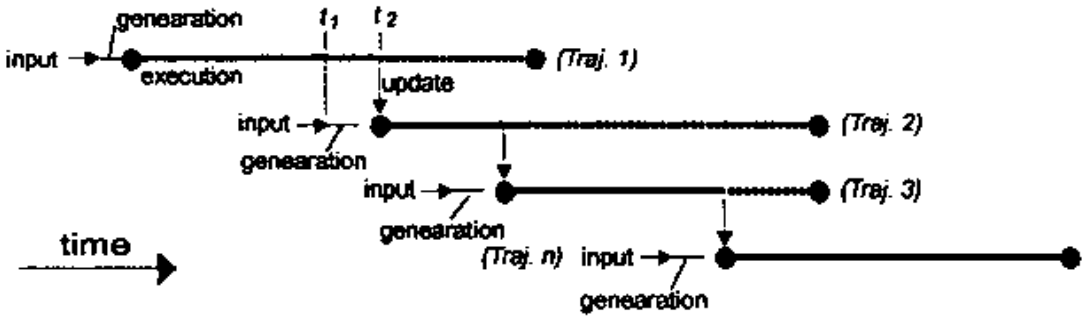

Figure 2.8: Trajectory update method for online walk control

Figure 2.9: The humanoid robot H7

Similar to the work in [11], in 2002, Lim, Kaneshima and Takanishi proposed an online walking pattern generation method for biped humanoids with a trunk [12]. This walking pattern generation consists of two parts. In the first part, lower-limb motion patterns are updated and connected to the preceding pattern smoothly depending on the walking command created online. In the second part, for the upper body stable pattern generation, based on the ZMP trajectory and the motion of the lower-limbs, a trunk and a waist motion is generated to compensate the moments generated by the lower-limbs. In this work, a walking cycle is composed of five phases (Figure 2.10).

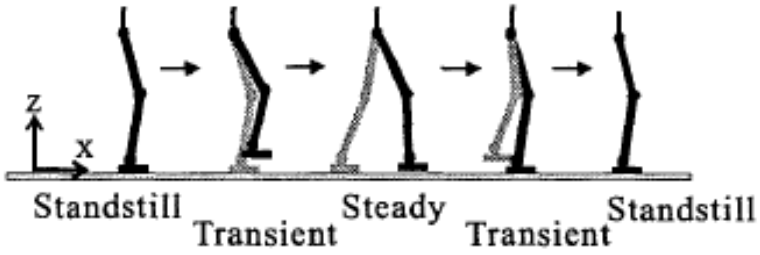

Figure 2.10: A complete walking cycle

There is a transient phase before and after the steady phase which deals with the created momentum by the lower- limbs. Online pattern generator which is depicted in Figure 2.11, leads a continuous and stable walk. Walking parameters such as step

length, step height and step direction are given as inputs to the pattern generator by inspection firstly. Then lower-limb pattern is created by making a five-step and the ZMP pattern is set in the support polygon. After this step, the trunk and waist compensation is calculated from the lower-limb and ZMP trajectories created before. Lastly, the middle step of the preceding five-step pattern and the compensation pattern is set for the next step.

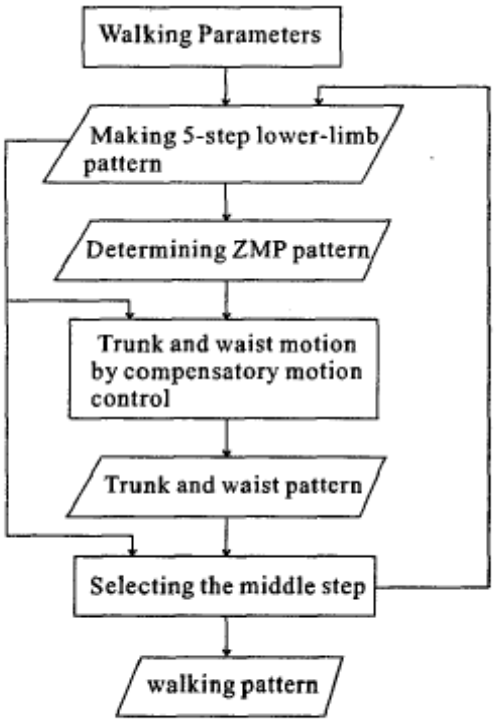

Figure 2.11: Online pattern generation architecture

Peng et al. stated that online walking pattern generation computing the whole dynamics is nearly impossible because of the complexity of the nonlinear differential equations of dynamics of the humanoid robots [13]. Thus, in this work, an approach of online trajectory generation is proposed which is based on offline typical walking pattern parameters such as hip parameters, step length, walking cycle and so on as in [12]. After this step, stability optimization which is based on ZMP is done online and online trajectories are created. The method proposed in this study is first tried in simulations and then experiments are carried out with the humanoid robot BHR-01 (Figure 2.12) which has 33-DOF. These simulations and experiments showed that the proposed method is effective for creating online trajectory generation.

Figure 2.12: The humanoid robot BHR-01

Sugihara, Nakamura and Inoue, in 2002, controlled the Center of Gravity (CoG) by manipulation of the ZMP indirectly, to develop a real-time motion generation algorithm [14]. This algorithm consists of four parts, 1) the referential ZMP planning, 2) the ZMP manipulation, 3) the CoG velocity decomposition for joint angles and 4) local control of joint angles which provide high –mobility to the humanoid robots. One of the advantages of this method is its applicability to the high degrees of freedom humanoid robots although the method itself is created using a simple linear inverted pendulum model. The authors also verified the effectiveness of the proposed methods using computer simulations.

Similar to the work in [14], in 2004, Harada, Kajita, Kaneko and Hirukawa presented a real-time gait planning method for a humanoid robot by planning the CoG and ZMP trajectories simultaneously [15]. With this method a fast and smooth transition between the respective gaits is obtained by connecting newly calculated gait to the previous gait pattern, as in the work in [11]. Although this work is similar to the work in [14], there is a new method called the quasi-real-time connection method (besides real-time connection method) which can change the gait even if the change of the step position is significant. The proposed methods are carried out successfully by simulations and real-time experiments with the humanoid robot HRP-2 (Figure 2.13).

Figure 2.13: The humanoid robot HRP-2

In 2003, Nishiwaki et al. presented an online walking control system that follows a given desired motion by generating body trajectories [16]. Layered control architecture (Figure 2.14) is used to form this control system to create autonomous locomotion behaviors. With created autonomous locomotion, the humanoid robot can move a destination point automatically by inspecting the environment and planning a suitable motion. Many techniques should be used to create this autonomy, such as environment map generation, localization, path planning, gait planning, avoiding obstacles, dynamic stabilization control and motor servo control. In this work, implemented system generates stable walking trajectories on a horizontal plane and satisfies the motion parameters such as walking speed and direction, upper body posture and walk cycle timing given online. In experiments, the humanoid robot H7 is used and it successfully tracked and followed a moving target using stereo vision feedback.

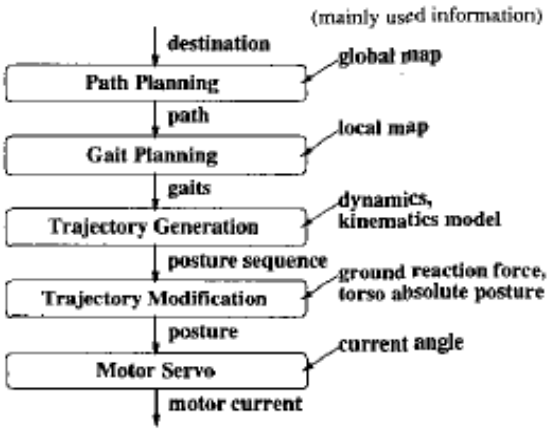

Figure 2.14: Layered structure for online walking control

In 2003, Kajita et al. proposed a new method of a biped walking pattern generation by using a preview control of the Zero Moment Point [17]. The mentioned preview control consists of three terms, 1) the integral action on the tracking error, 2) the state feedback and 3) the preview action using the future reference. A table-cart model (Figure 2.15) is used to model the dynamics of the biped robot which is useful to obtain a suitable representation to get ZMP references. After designing a ZMP tracking servo controller with an optimal preview control used, the effectiveness of the proposed method is proved by a simulation of the biped robot HRP-2 Prototype (HRP-2P) walking on spiral stairs. It is also shown that the ZMP error can be compensated by the preview controller too.

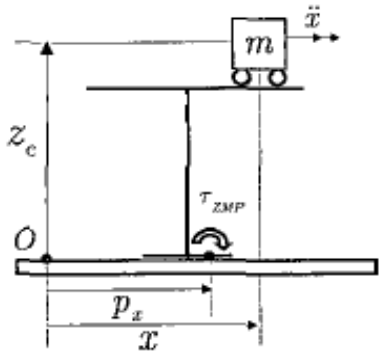

Figure 2.15: A table-cart model

In 2006, similar to the work in [14], Tanaka, Takubo, Inoue and Arai proposed a control algorithm to change the gait motion of the humanoid robot which leads it to stop by modifying pre-defined Zero Moment Point trajectory in real-time [18]. For this purpose, the amount of the ZMP modification is adjusted with the given timing of stop command and the relation map between them is employed to generate the stable gait change. The relation between the predicted ZMP trajectory using a preview controller and the support polygon defines the modification criteria in this approach**.** Mentioned preview controller above, includes a Table-Cart model [17] and it creates the CoM trajectory from the ZMP reference trajectory in real-time. With the proposed method, the humanoid robot HRP-2 is used to verify that it can stop immediately within one step to avoid a collision if an unexpected object appears in front of the robot during the walk.

Verrelst, Stasse, Yokoi and Vanderborght presented a work whose main aim is stepping over obstacles of the humanoid robots in complex environments in 2006 [19]. In this work, the ZMP is used as stability criteria instead of CoG for stepping over

obstacles in a fluent dynamic motion. The proposed method also uses a preview controller defined in [17] for maintaining dynamic balance of the robot and includes trajectory generation for the feet and waist. Although there are some practical implementation difficulties, this method successfully applied to the humanoid robot HRP-2 and for dynamically stepping over obstacles, several methods are implemented such as overstretching the knee and reducing the impact at landing. An example of this experiment is given that HRP-2 steps over an obstacle of 15 cm height and 5 cm width.

Nishiwaki and Kagami applied a dynamically stable walking pattern algorithm that can update the pattern at a short cycle such as 40 milliseconds to the humanoid robot HRP-2 [20]. With the proposed algorithm, the robot can change the walking pattern in a short time after the change of the command input which is the force information transmitted via the force sensor at its wrist. Frequent update of the pattern leads a stable walk such that the robot maintains its balance according to its dynamics. The ZMP is used as the stability criteria and it is employed to create horizontal torso trajectory with the preview control method [17].

Huang, Chew, Zheng and Hong proposed a motion pattern generation for the humanoid robots walking on a terrain which has a slope [21]. Based on Table-Cart model, using preview control [17], the CoM trajectory of the biped robot is generated to maintain the ZMP at the desired location and the future ZMP locations are selected according to the known slope gradient. Several experiments carried out such as walking up slope and down slope, walking on slopes with different gradients to demonstrate of walking on uneven terrains and staircase walking. With the proposed pattern generation method, a 42-DOF robot simulator achieved a stable walk.

In 2004, Kong, Lee and Kim proposed an optimal gait generation which uses genetic algorithm [22]. A genetic algorithm is defined as a searching algorithm in the global area and its advantage is to find an optimal solution without using any differential equations. Thus, calculations for the optimal gait generation are simplified. It is stated that for a stable walking, gait planning has the most effect. In this work, not only for stable walk, also for saving the electric power, a smooth and optimal gait is implemented for a robot to have a long working time. Genetic algorithm is used to guarantee to have the optimal gait trajectory and the robot gets a smooth movement via this algorithm. All process is done by a PC-based program and optimal solution is obtained from the simulation of a biped robot.

Similar to the work in [22], in 2007, Dau, Chew and Poo proposed a method of trajectory planning for humanoid robots using genetic algorithm searches the key parameters to create the optimal trajectory that has large stability margin and low energy consumption [23]. In this work, the hip and foot trajectories are created using polynomial interpolation in Cartesian space and for stability criterion the ZMP is used. Experiments carried out on the humanoid robot NUSBIP-II.

Ha, Han and Hahn proposed a method that imitates the human gait to generate a natural and stable gait pattern for humanoid robots [24]. Human gait patterns are inspected and the torque parameter for the sagittal plane and the ZMP for the lateral plane are decided to use as gait parameters for the modified genetic algorithm as in [22] which determines the joint angles of the biped robot. With the proposed algorithm, a natural and stable walk pattern is achieved for a 5-link biped robot.

Hoonsuwan, Sillapaphiromsuk, Sukvichai and Fish used a real human motion as in [24] to generate a walking trajectory for a stable robot motion [25]. For this purpose, the trajectory of a human motion is extracted by using image processing and transformation methods. The ZMP stability criterion is used to guarantee the dynamic stability of the robot. In the experiments, different human motions are applied to the robot in a simulation environment to verify this trajectory generation method.

Ayhan and Erbatur, in 2004, stated that the ground force interaction of the swing leg at the moment of landing is an important problem of the walking control [26]. For soft landing purposes and biped locomotion, a control scheme which employs gravity compensation and virtual potential fields applied to the swing leg is proposed and it is independent of the body reference position tracking. For the supporting leg, optimization methods are also employed to obtain suitable leg joint torques to be able to track body reference trajectories. 12-DOF (Degrees of Freedom) biped robot is used for the test of 3D dynamics and ground interaction simulations with the proposed method. These simulations show that this method can be applied in real implementations.

Naksuk, Mei and Lee proposed a trajectory generation method which minimizes the angular momentum at the CoM while the humanoid robot keeps its balance based on the ZMP stability criterion [27]. The authors stated that the angular momentum at the CoM is highly regulated during the gait cycles and needs an extensive computational work. For this purpose, a spline interpolation of the desired movement snapshots is taken to generate an initial humanoid robot trajectory. After this step, an iterative approach is investigated and employed for generating the robot trajectory which

maintains its angular momentum at CoM within the desired boundary of the ZMP criterion constraint. Numerical simulations are carried with a biped simulation which has 11 masses to verify the proposed trajectory generation method.

In 2006, Kim, Park and Oh proposed a control method for the dynamic walking of humanoid robots [28]. Firstly, the human walking process is observed to design a suitable off-line walking pattern for the biped humanoid robots. According to these observations, the walking cycle is divided into several parts which include different characteristics of motions (Figure 2.16). Finally, for controlling the dynamic walking in real-time, several control schemes are implemented. One of these schemes modifies the walking pattern periodically based on the sensory information during each walk cycle, while the others are used for the real-time balance control using the inertial sensor information and to predict the gait motion of the robot from the previous experimental data. This adaptive walking pattern generation algorithm is applied to the humanoid robot KHR-2 (KAIST Humanoid Robot-2) (Figure 2.17) and its effectiveness is proven throughout the experiments.

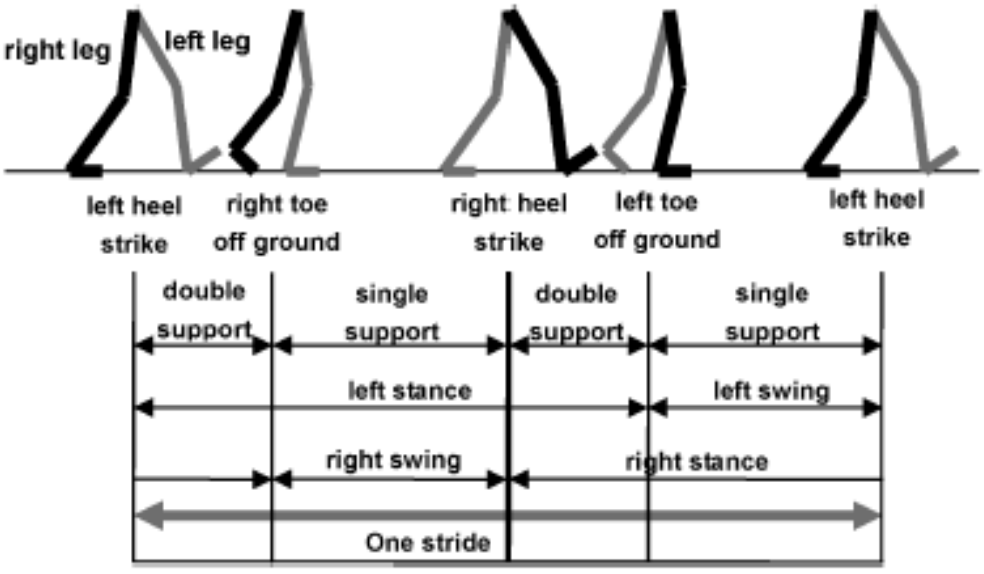

Figure 2.16: A complete walking cycle defined with several stages

Figure 2.17: The humanoid robot KHR-2

Erbatur and Seven proposed a new approach based on the Linear Inverted Pendulum Model which involves the dynamics of the swing leg, while the preceding works using LIPM ignore these dynamics in 2007 [29]. This new LIPM method can also be used when the legs are heavy. The model used in this work, has a two-mass LIPM and the dynamics of the robot body and the swing leg in the swing phase is described with a fifth order state space description. For given foot placement references and the desired ZMP trajectory, the Center of Mass of Body (CMB) reference trajectory is created and then an inverse kinematics based position controller is employed for biped locomotion. 3D full-dynamics simulations of a 12-DOF biped robot is used to compare the stability of the walking performances with one-mass and one-mass-two-mass switching linear inverted pendulum models and these simulations proved that switching algorithm is highly useful in improving the stability.

Morisawa et al. proposed an algorithm of a real-time gait planning based on an analytical solution of an inverted pendulum model [30]. The Center of Gravity and the Zero Moment Point trajectories are defined by polynomials and their coefficients are computed with given boundary conditions. The landing position of the foot can be changed before lifting up the swing leg and a stable walking gait can be generated by changing the single support period which is defined as an additional trajectory parameter to overcome the unexpected results of the immediate changes of the foot

placement. The ZMP fluctuation is also compensated by the anti-phase of the ZMP error to handle these unexpected results. The experimental results carried out on the humanoid robot HRP-2 show that the proposed algorithm can be used for real-time gait planning. In 2007, Tang and Er also used the inverted pendulum model to define the robot CoG motion, ankle, hip and knee trajectories as the leg trajectories [31].

In 2008, Lee et al. proposed an algorithm which can modify the walking period and the step length in both sagittal and lateral directions to be able to give complex commands to the humanoid robots. The CoM position and velocity is changed independently during the single support phase by creating a variation of the Zero Moment Point on the supporting polygon [32]. It is stated that the proposed method allows a range of dynamic motion by adopting the closed-form functions to calculate the algorithm in real-time, which is not achievable using 3D-LIPM. Both simulations and experiments on the humanoid robot HanSaRam-VII (Figure 2.18) are carried out to verify the effectiveness of the proposed algorithm.

Figure 2.18: The humanoid robot HanSaRam-VII

Erbatur and Kurt proposed a reference generation method based on the Linear Inverted Pendulum Model and moving support foot ZMP references in 2009 [33]. It is stated that generally the ZMP reference during the walk is kept fixed in the middle of the supporting foot sole. Although several works are reported using this approach, in this method moving ZMP references is employed because it is observed that in the human walk the ZMP moves forward under the supporting foot. The solutions of the

Linear Inverted Pendulum dynamics equations are obtained using Fourier series approximation and smooth ZMP references are generated. The CoM trajectory of the robot is derived from the desired ZMP trajectory and an inverse kinematics based independent joint control is applied. Simulations are carried out with a 12-DOF biped robot 3D simulation which has full dynamics. It is shown that the moving ZMP references are more energy efficient than the fixed ZMP under the supporting foot.

As mentioned in Chapter 1, although [33] obtains natural, human like bipedal humanoid walking, the durations of the single support and the double support phases cannot be adjusted by the user in a direct way. Rather, the double support phase is introduced as a result of a trajectory smoothing process. In this thesis, as an improvement on the method in [33], the durations of the single support and the double support phases are implemented as separate parameters to be adjusted by the choice of the user. Furthermore, the naturalness of the walk is preserved, in that the single support ZMP reference is forward moving and the continuity of the introduced ZMP reference makes the after-Fourier-approximation smoothing process unnecessary.

The next chapter introduces the simulation environment and the experimental robot SURALP on which the designed algorithms are tested.

Chapter 3

3. SIMULATION AND EXPERIMENTAL ENVIRONMENTS

3.1 Simulation and Animation Environment

In this thesis, a Newton-Euler method based full-dynamics 3D simulation and animation environment as described in [34] is used for simulation studies to observe the results of the proposed ZMP based reference generation method. In Figure 3.1, a view of the mentioned animation environment can be seen. In this model, an adaptive penalty based method is employed to model the ground contact. The details of the simulation algorithm and contact modeling can be found in [34].

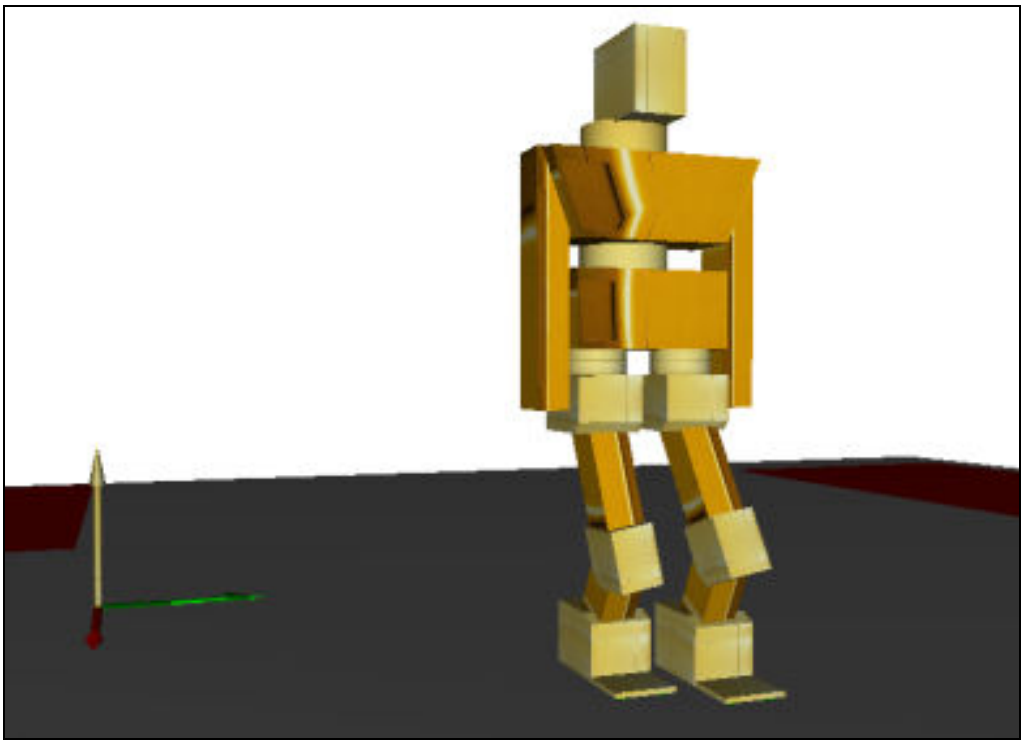

Figure 3.1: The animation window of the simulation environment

3.2 SURALP: A Full Body Bipedal Humanoid Robot

SURALP (Sabanci University Robotics ReseArch Laboratory Platform) is designed as the test platform for the bipedal walking experiments within the context of a project funded by TUBITAK (The Scientific and Technological Research Council of Turkey). Stable bipedal walking on flat or uneven surfaces and physical interaction between the humanoid robot and objects that can be recognized with visual feedback are the main aims of this project. SURALP is a full-body bipedal humanoid robot with 29-DOFs, including leg, arm, hand, neck and waist joints. Leg module of SURALP which consists of 12-DOF was introduced earlier in [35, 36]. This chapter introduces SURALP in the context of its mechanical design, actuation mechanism and sensory system.

The kinematic arrangement of SURALP is shown in Figure 3.2. Each leg consists of 6-DOF and each arm has 7-DOF. Hips and shoulders composed of three orthogonal joint axes intersecting each other at a common point. At the legs, the knee axis follows the hip pitch axis and the ankle accommodates two orthogonal axes which are ankle pitch and ankle roll joints. At the arms, revolute elbow joints come after the shoulder joints and the wrist is actuated by a roll and a pitch axes positioned in the forearm. Last link at the arms is the hand which has a single DOF linear movement. There is a waist yaw axis positioned on the pelvis and the neck is composed of two axes in the pan-tilt configuration. The link lengths and weight information is given in Table 3.2.

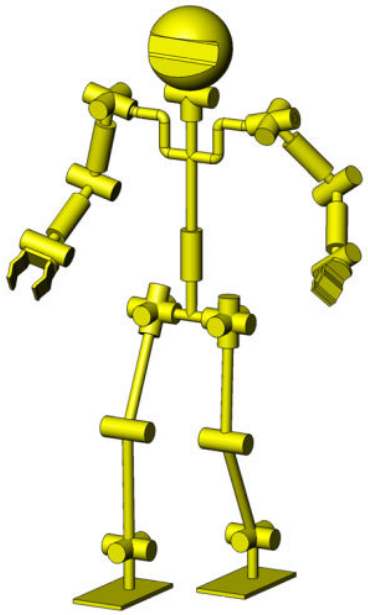

Figure 3.2: The kinematic arrangement of SURALP

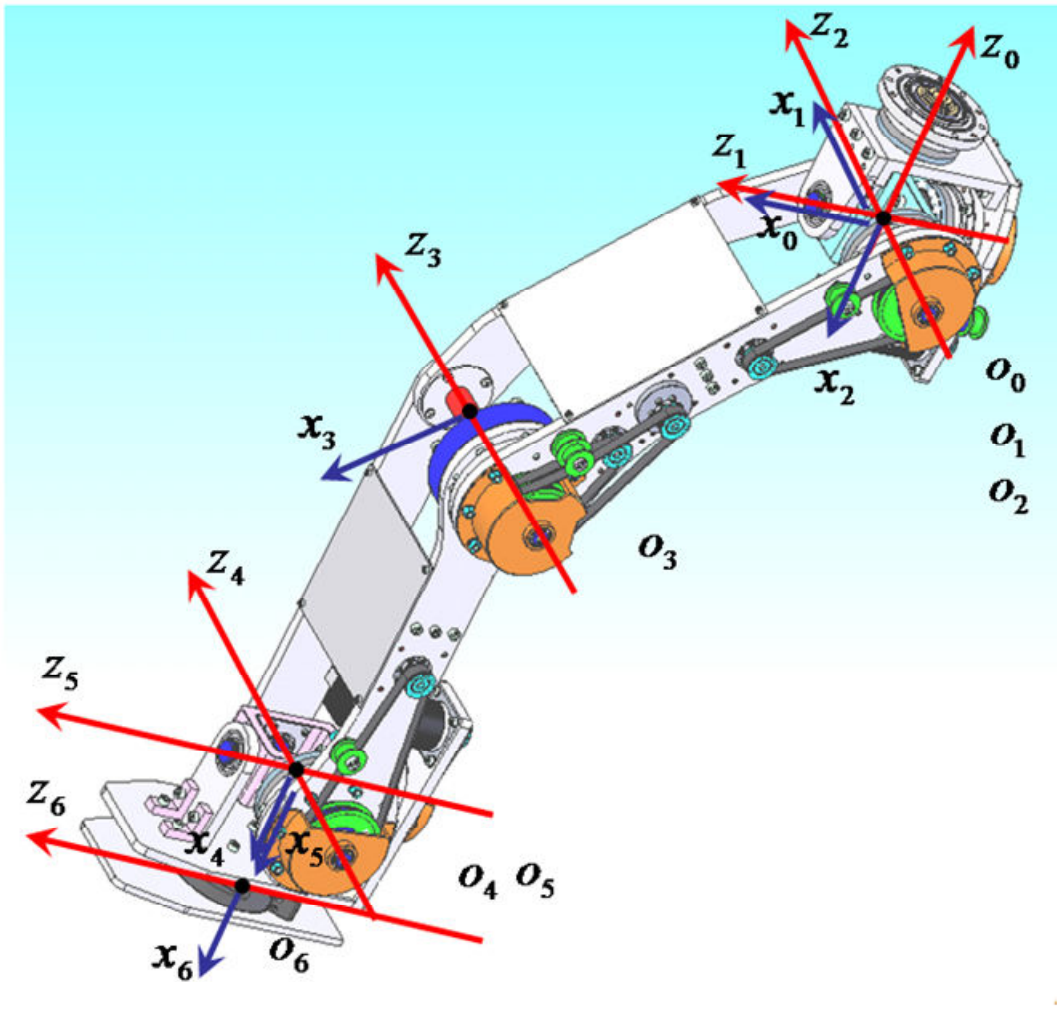

Figure 3.3: Denavit Hartenberg axis assignment for a 6-DOF Leg

Table 3.1: Denavit Hartenberg table with respect to Figure 3.3

	a	α	d	θ
Link 1	0	-90°	0	θ_1^*
Link 2	0	90°	0	θ_2^*
Link 3	L_3	0°	0	θ_3^*
Link 4	L_4	0°	0	θ_4^*
Link 5	0	-90°	0	θ_5^*
Link 6	L_6	0°	0	θ_6^*

Table 3.2: Length and weight parameters of the links

Upper Leg Length	280mm
Lower Leg Length	270mm
Sole-Ankle Distance	124mm
Foot Dimensions	240mm x 150mm
Upper Arm Length	219mm
Lower Arm Length	255mm
Robot Weight	101 kg

DC motors and reduction gears are used at the joints. Harmonic Drive reduction gears are selected to obtain very high reduction ratios in a very compact space. For transmitting the motor rotary motion to Harmonic Drive reduction gears belt-pulley systems are used. Except the knee joint, all joints are actuated by a single DC motor. The knee joint is driven by two DC motors for high torque capability. Table 3.3 displays the motor powers, belt-pulley and the Harmonic Drive reduction ratios. Working ranges of the joints are also shown in this table.

Table 3.3: Joint actuation systems

Joint	**Motor Power**	**Pulley Ratio**	**HD Ratio**	**Motor Range**
Hip-Yaw	90W	3	120	-50 to 90 deg
Hip-Roll	150W	3	160	-31 to 23 deg
Hip-Pitch	150W	3	120	-128 to 43 deg
Knee 1-2	150W	3	160	-97 to 135 deg
Ankle-Pitch	150W	3	100	-115 to 23 deg
Ankle Roll	150W	3	120	-19 to 31 deg
Shoulder Roll 1	150W	2	160	-180 to 180 deg
Shoulder Pitch	150W	2	160	-23 to 135 deg
Shoulder Roll 2	90W	2	120	-180 to 180 deg
Elbow	150W	2	120	-49 to 110 deg
Wrist Roll	70W	1	74	-180 to 180 deg
Wrist Pitch	90W	1	100	-16 to 90 deg
Gripper	4W	1	689	0 to 80 mm
Neck Pan	90W	1	100	-180 to 180 deg
Neck Tilt	70W	2	100	-24 to 30 deg
Waist	150W	2	160	-40 to 40 deg

For sensory feedback, joint incremental encoders which measure the motor angular positions, force/torque sensors, inertial measurement systems and CCD cameras are employed.

The motor angular positions are measured by 500 ppr (pulse per revolution) optic incremental encoders. Force and torque measurements are done with two different

force and torque sensors. One of these sensors is the 6 axis force/torque sensor which is positioned at the ankle. An alternative force and torque measurement system is obtained by the use of FSRs (Force Sensing Resistors).

FSRs are thick polymer film devices which show a decrease in their terminal resistance with an increasing force applied to their active surface [37]. The dimensions of FSRs used in the sensor design are 40 mm x 40 mm x 0.43 mm. The weight of the sensor is negligible and its thin structure enables assembling without a significant increase in the foot height. FSRs have a large contact area which provides a wide range of force measurement and this is the most important advantage of these sensors. However the force-resistance curve of FSRs is highly nonlinear (Figure 3.4), a piecewise linear approximation is used in the presented design to obtain force values from the voltage measured at the terminals of the FSRs.

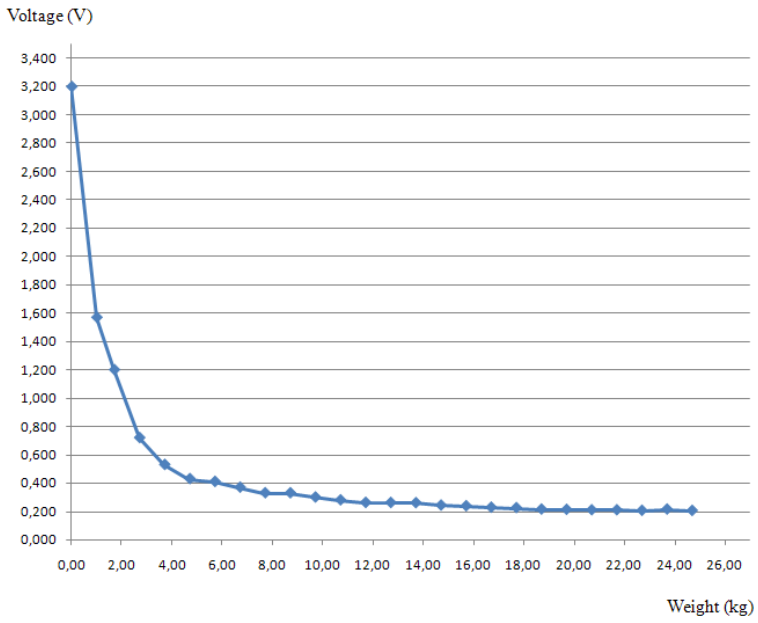

Figure 3.4: An applied force-measured voltage curve for a sample FSR

In early designs of SURALP, each foot consists of four FSRs whose places are at the four corners under the robot foot (Figure 3.5). The layers at the foot sole composed of various materials together which helps smooth landing of the foot are shown in this figure too. The aim in placing these FSRs at the four corners is to obtain rich tactile information and also singularities are handled with this way. This sensory system including FSRs can substitute the 6 axes force/torque sensor in some cases, also

it is used for the ankle torque and the vertical direction total ground interaction force measurements.

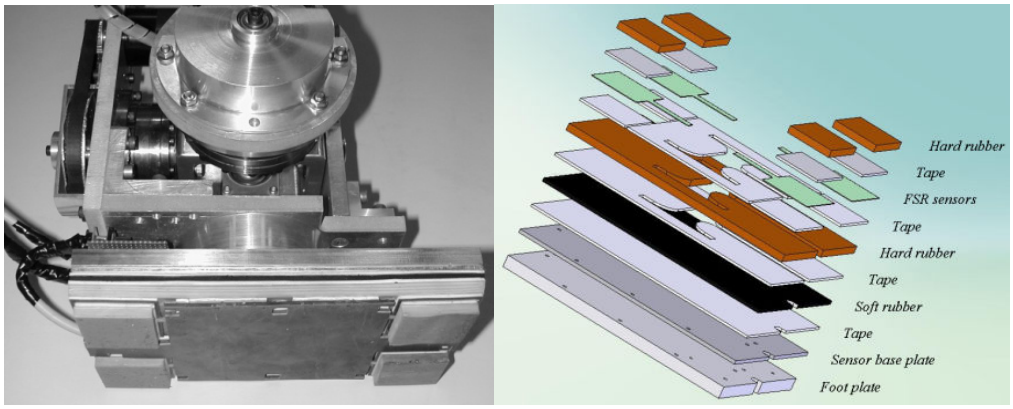

Figure 3.5: FSR based foot sensor and layers of the foot sensor with FSRs

The robot is also equipped by a rate gyro, an inclinometer and a linear accelerometer which are mounted at the robot torso too. These sensors are listed in Table 3.4 with their working ranges, mounting locations and allocated controller board channels.

Table 3.4: Sensors of SURALP

	Sensor	**Number of Channels**	**Range**
All joints	Incremental optic encoders	1 channel per joint	500 pulses/rev
Ankle	F/T sensor	6 channels per ankle	± 660 N (x, y-axes) ± 1980 N (z-axis) ± 60 Nm (all axes)
Foot	FSR	4 channels per foot	0 to 250 N
Torso	Accelerometer	3 channels	± 2 G
	Inclinometer	2 channels	± 30 deg
	Rate gyro	3 channels	± 150 deg/s
Wrist	F/T sensor	6 channels per wrist	± 65 N (x, y-axes) ± 200 N (z-axis) ± 5 Nm (all axes)
Head	CCD camera	2 with motorized zoom	640x480 pixels (30 fps)

The control electronics of SURALP is based on dSpace modular hardware. Central controller is the DS1005 board of the dSpace family in our controller. This is the board where all the biped locomotion algorithms run. Besides this central board, seven DS3001 incremental encoder input boards provide connectivity for 35 joint encoders. 31 of these connections are allocated with the encoders of the current design

of SURALP. A DS2002 and a DS2103 board are used for analog inputs and outputs, respectively. The rate gyro, accelerometer, inclinometer, FSR sensors and 6-axis force/torque sensors are integrated over the analog inputs. The analog outputs provide torque references for the four-quadrant Maxon & Faulhaber DC motor drivers. The control and data acquisition boards mentioned above are housed by a dSpace Tandem AutoBox enclosure, which is mounted in a backpack configuration in the robot assembly. The power source and a remote user interface computer are placed externally. The CCD cameras are connected to the remote control PC via Firewire interfaces.

The current design of the bipedal humanoid robot SURALP with control hardware in its trunk is shown in Figure 3.6 and 3.7.

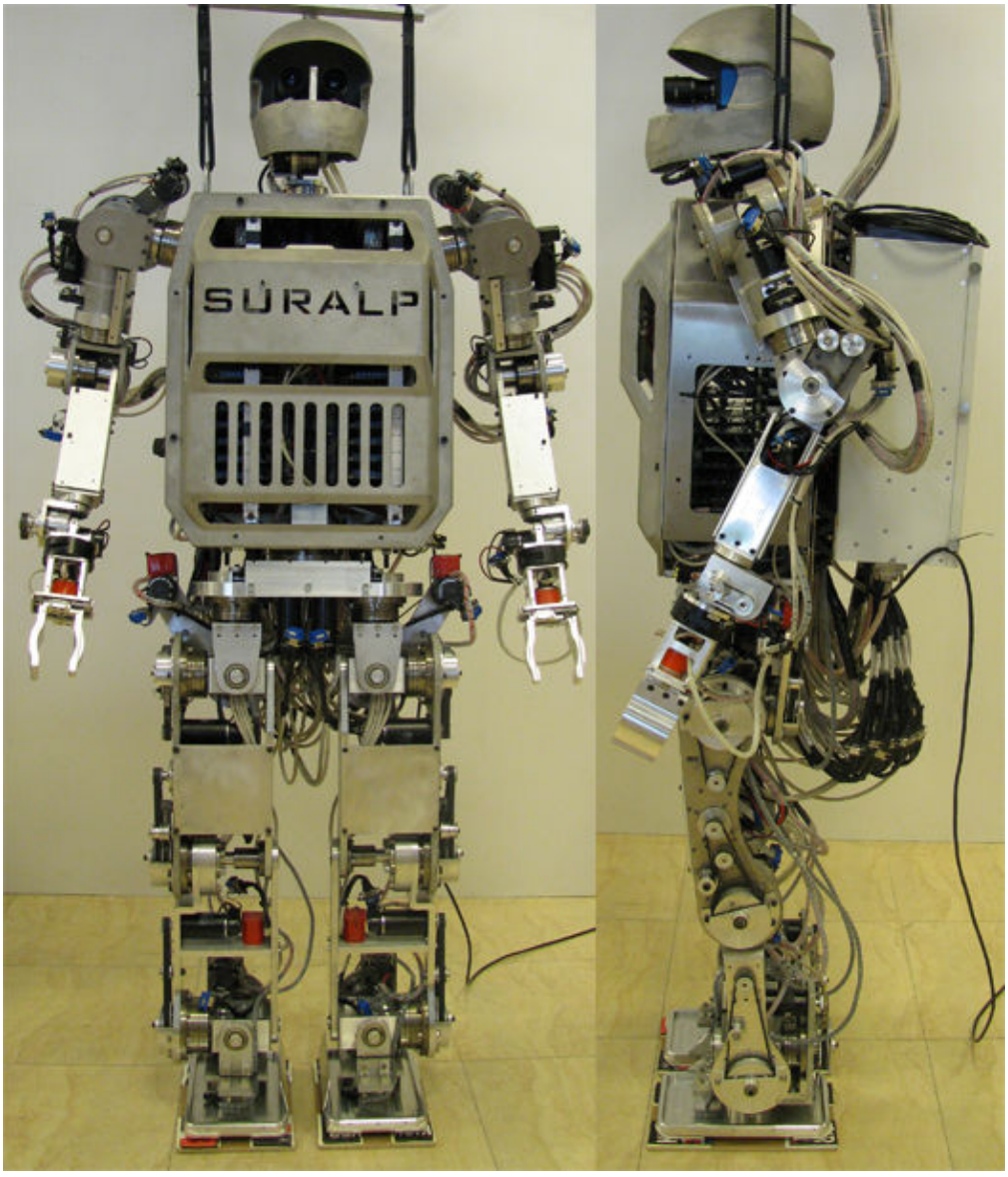

Figure 3.6: SURALP, side and front views

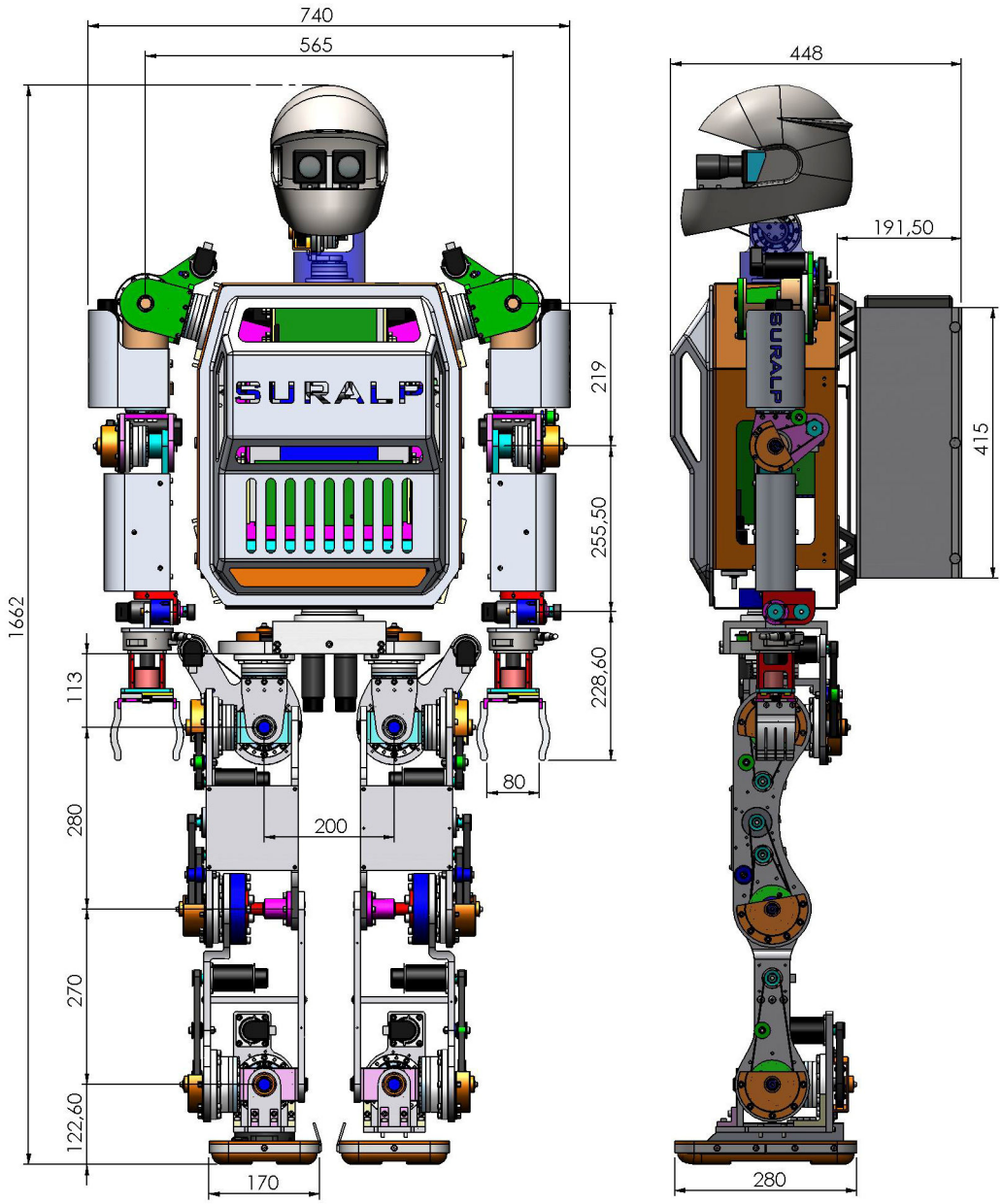

Figure 3.7: SURALP, dimensions

Chapter 4

4. ZMP BASED REFERENCE GENERATION FOR A BIPEDAL ROBOT

This chapter begins with the section that introduces the LIPM firstly and the relationship between the ZMP and the location of the robot CoM is derived. Following these, suitable ZMP references and methods for obtaining CoM reference trajectories from given ZMP references are discussed.

4.1 LIPM and ZMP

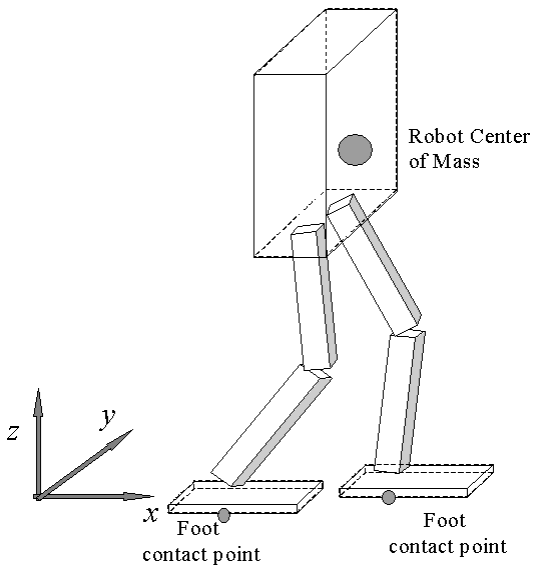

Figure 4.1: Biped robot typical kinematic arrangement. In single support phases, it behaves as an inverted pendulum.

In this section it is assumed that the mass of the legs should be much less than the robot mass. The sketch in Figure 4.1 shows the typical biped robot with 6-DOF legs for which the reference generation and control algorithms presented below can be applied.

A robot structure such as shown in this figure has a highly nonlinear, multiple-DOF and coupled full dynamics description. Equation of motion for this robot can be expressed as:

$$\begin{bmatrix} H_{11} & H_{12} & H_{13} \\ H_{21} & H_{22} & H_{23} \\ H_{31} & H_{32} & H_{33} \end{bmatrix} \begin{pmatrix} \dot{v}_B \\ \dot{\omega}_B \\ \ddot{\theta} \end{pmatrix} + \begin{pmatrix} c_1 \\ c_2 \\ c_3 \end{pmatrix} + \begin{pmatrix} u_{E_1} \\ u_{E_2} \\ u_{E_3} \end{pmatrix} = \begin{pmatrix} 0 \\ 0 \\ \tau_{jo\,\mathrm{int}} \end{pmatrix} \tag{1}$$

where H_{ij} are sub-matrices of the robot inertia matrix for $(i, j) \in \{1,2,3\}$. v_B is the linear velocity and ω_B is the angular velocity of the robot body coordinate frame with respect to a fixed coordinate frame. θ is the joint displacements vector. c_1, c_2 and c_3 terms form the bias vector in this dynamics equation. u_{E_1}, u_{E_2} and u_{E_3} stand for the net force effect, the net torque effect and the effect of reaction forces acting on the robot joints, respectively. These reactive forces are produced by environmental interaction. $\tau_{jo\,\mathrm{int}}$ is the generalized joint control vector which typically consists of torques actuating the joints of a robot with revolute joints. H_{11}, H_{12}, H_{21}, and H_{22} are 3×3 matrices. H_{13} and H_{23} are 3×12, H_{31} and H_{32} are 12×3, H_{33} is 12×12 matrices for a 12-DOF robot with 6-DOF at each leg [26]. It is important to note that it is very difficult to obtain the closed form solutions of the matrices in this expression. Because of this reason, Newton-Euler recursive formulations are used in their computation in [34] and [38].

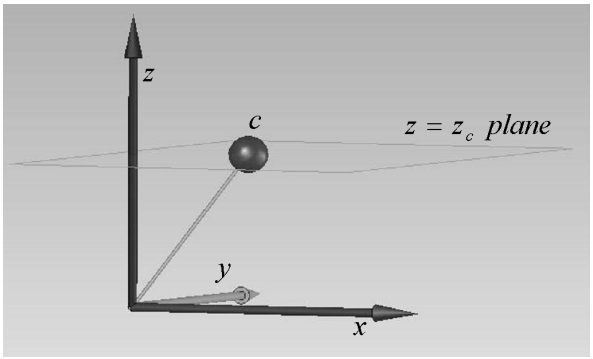

Figure 4.2: The linear inverted pendulum model

Generating such a model is very useful for the test of reference generation and control methods via the simulation; however, the structure in (1) is a highly complex model which can help in forming the basics for the walking control. Instead of using this complex model, simpler models such as the inverted pendulum model are more suitable for controller synthesis. A point mass is assigned to the CoM of the robot which represents the body (trunk) of the robot and this point mass is linked to a stable (not sliding) contact point on the ground via a massless rod, which is idealized model of a

supporting leg. In the same manner, the swing leg is assumed to be massless too. Described inverted pendulum above is shown in Figure 4.2. $c = (c_x \quad c_y \quad c_z)^T$ is the coordinates of the point mass in this figure. Although much simpler than (1), the inverted pendulum model has still coupled and nonlinear equations of motion. Rather, a linear system which is uncoupled in the x and y directions is assumed. This assumption yields a fixed height for the robot CoM and this model is called the Linear Inverted Pendulum Model. With the LIPM, it is simple enough to develop algorithms for reference generation [37].

Stability of the walk is the most desired feature of a reference trajectory. The ZMP criterion is the most widely accepted and used stability criterion in biped robotics [41]. The ZMP is defined as the point on the $x-y$ plane which no horizontal torque components exist on it for the model in Figure 4.2. For the point mass structure shown in this figure, the expressions for the ZMP coordinates p_x and p_y are [42]:

$$p_x = c_x - \frac{z_c}{g}\ddot{c}_x \tag{2}$$

$$p_y = c_y - \frac{z_c}{g}\ddot{c}_y \tag{3}$$

z_c is the height of the plane where the motion of the point mass is constrained and g is the gravity constant as 9.806 m/s^2. The torque balance equation in the $x-z$ plane as shown in Figure 4.3 gives the result in (2).

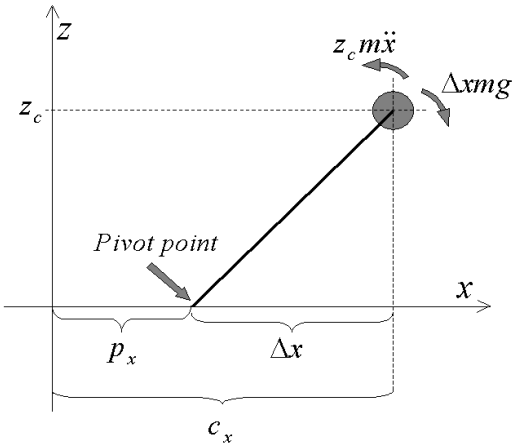

Figure 4.3: Torque balance in the $x-z$ plane

The torque due to the gravity (Δxmg) should be balanced by the torque generated by the reaction force which is created by the point mass acceleration in the x

direction ($z_c m\ddot{x}$) in order to have zero net moment at the "pivot point" in Figure 4.3. This zero moment condition gives a solution for Δx and for the touching point p_x. p_y, in equation (3), can be obtained with a similar method for the $y-z$ plane.

4.2 ZMP References in Related Work

The ZMP and the CoM can be related to each other with the equations (2) and (3). A suitable ZMP trajectory can be generated without difficulty for reference generation purposes. As the only stability constraint, the ZMP should always lie in the supporting polygon defined by the foot or feet touching the ground. The ZMP location is generally chosen as the middle point of the supporting foot sole. In [42], the reference ZMP trajectory shown in Figure 4.4 is created with this idea. A is the distance between the foot centers in the y direction, B is the step size and T is the half of the walking period in this figure. It can be observed that from the same figure, firstly, step locations are determined. The step location selections can be based on the size of the robot and the task performed by the robot. This selection of support foot locations defines the staircase-like p_x and the square-wave structured p_y curves, if the half period T is given too. The step period can also be determined by the physical properties of the robot and by the application, as similar to the step size.

However, in [42], the naturalness of the walk is not considered. As mentioned above, in that work ZMP stays at a fixed point under the foot sole, although investigations in [37] and [39] show that the human ZMP moves forward under the foot sole (Figure 4.5). Figure 4.4 also shows that the transition from left single support phase to the right single support phase is instantaneous, there exists no double support phase.

In order to address the naturalness issue, the p_x reference curve shown in Figure 4.6 is employed in [33]. In this figure, forward moving ZMP can be seen at the top. A complete definition of naturalness of the walk is difficult to obtain and the curve in this figure is not necessarily the most natural ZMP reference. However, it is more natural than a fixed ZMP curve because it is more similar to the human ZMP. b defines the range of the ZMP motion under the sole in Figure 4.6 and a symmetric trajectory centered at the foot center is assumed. Although b can be defined as the half of the foot

length, this is not a must: ZMP can move on the line connecting the heel to the toes without covering this line completely too.

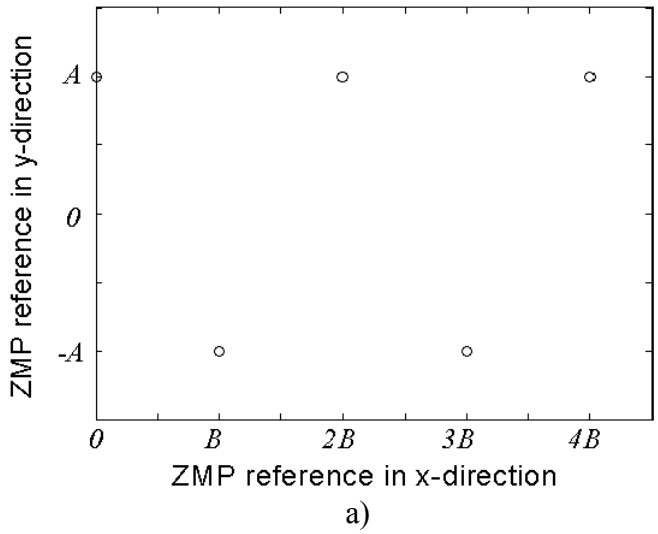

a)

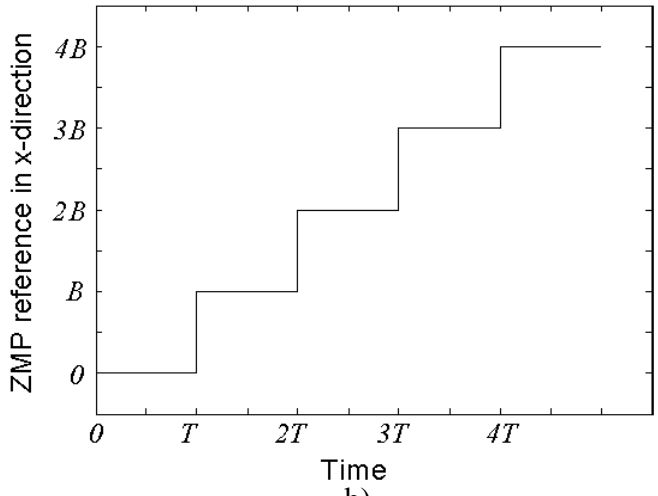

b)

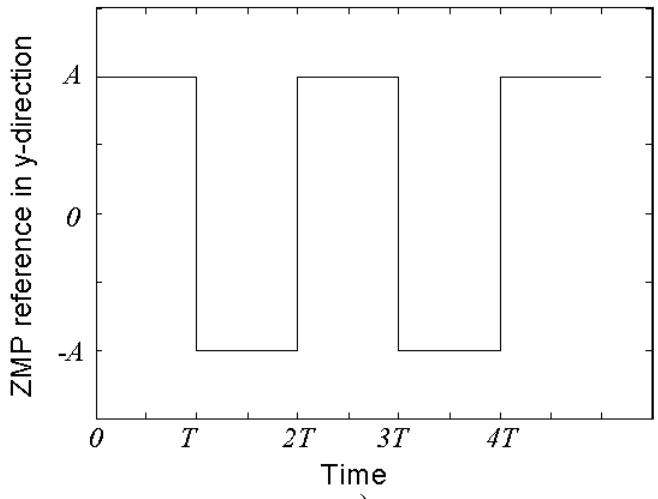

c)

Figure 4.4: Fixed ZMP references. a) $p_x^{ref} - p_y^{ref}$ Relation on the $x-y$ plane b) p_x^{ref}, the x-axis ZMP reference c) p_y^{ref}, the y-axis ZMP reference

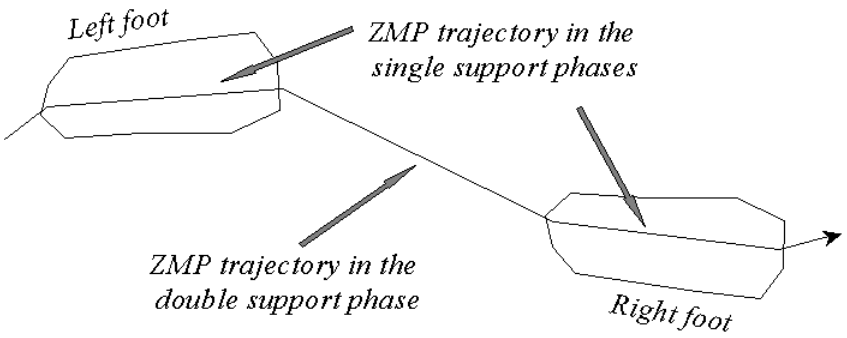

Figure 4.5: A natural ZMP trajectory

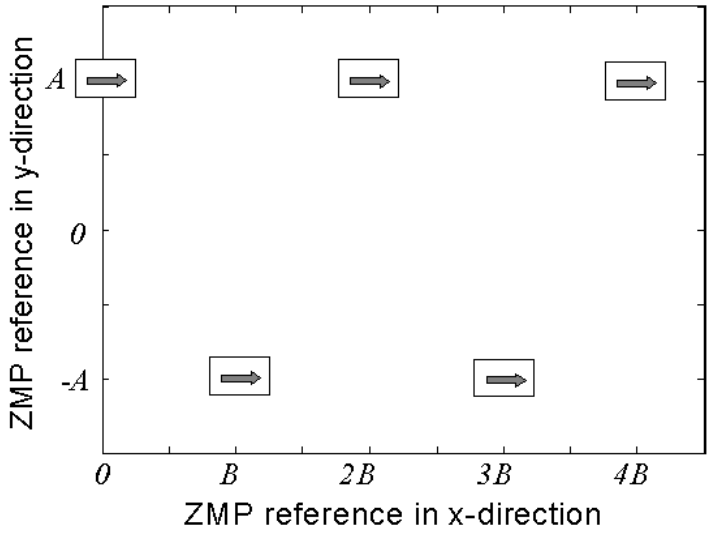

a)

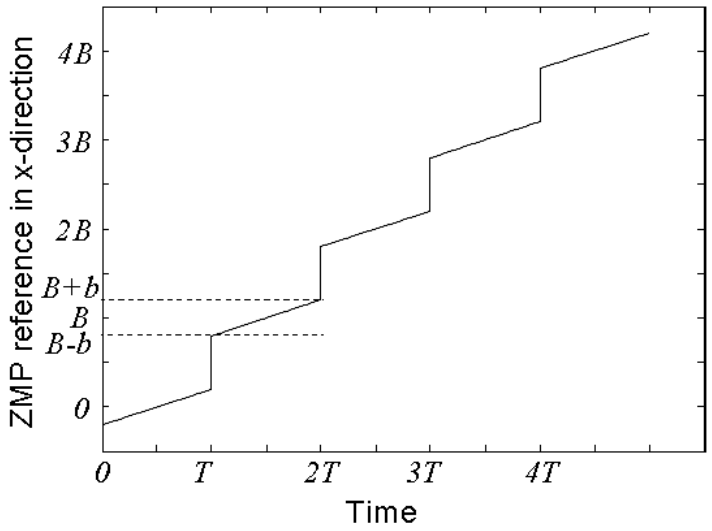

b)

Figure 4.6 (a, b): Forward moving ZMP reference. a) $p_x^{ref} - p_y^{ref}$ Relation on the $x-y$ plane. b) p_x^{ref}, a natural x-axis ZMP reference. Note the difference of the x-reference with the one shown in Figure 4.4.

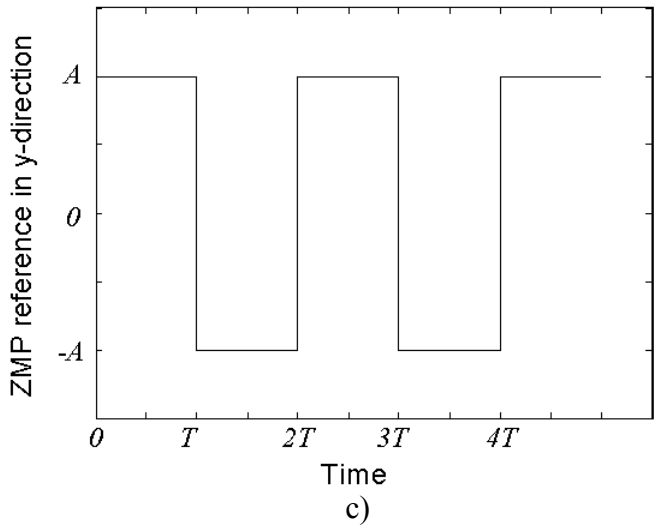

Figure 4.6 (c): c) p_y^{ref}, the y-axis ZMP reference.

Having defined the curves, and hence the mathematical functions for $p_x^{ref}(t)$ and $p_y^{ref}(t)$, and the next step is obtaining CoM reference trajectories from $p_x^{ref}(t)$ and $p_y^{ref}(t)$. Position control schemes for the robot joints with joint references obtained by inverse kinematics from the CoM locations can be obtained once the CoM trajectory is computed. The computation of CoM trajectory from the given ZMP trajectory can be carried out in a number of ways [17, 42].

[42], for the reference ZMP trajectories in Figure 4.4, proposes an approximate solution with the use of Fourier series representation to obtain CoM references for reference generation. Taking an approach similar to the one in [42], [33] develops an approximate solution for the c_x and c_y references corresponding to the moving ZMP references in Figure 4.6. In this process Fourier series approximations of the ZMP references $p_x^{ref}(t)$ and $p_y^{ref}(t)$ and of the CoM reference are obtained. Note that, although the ZMP reference in the x-direction in Figure 4.6 is forward moving and hence natural as desired, it is not continuous. So is the ZMP reference of Figure 4.6 in the y-direction. The y-direction reference is in the form of as square wave as in Figure 4.4. This discontinuous function corresponds to an instantaneous switching of the support foot, from right to left and from left to right foot, without an intermediate double support phase. Apart from the difficulties in the realization of such an instantaneous switching there is one more reason why such reference is undesirable: Natural, human-like motion will be lost with such a ZMP reference trajectory. Humans

walk with a double support phase of nonzero duration. In [33], smooth transition between single support phases with a double support phase is achieved by an additional smoothing action based on Lanczos sigma factors smoothing. Lanczos sigma factor smoothing is a technique in which the so called Gibbs Phenomenon – peaks of Fourier series approximations at the discontinuities of the original function - is cured by introducing weighting coefficients multiplying Fourier series coefficients. There weighting coefficients are called Lanczos sigma factors expressed as:

$$\mathrm{sinc}(k\pi/N) = \frac{\sin(k\pi/N)}{k\pi/N} \tag{4}$$

where N is one more that the number of terms in a Fourier series approximation.

In the work of Erbatur and Kurt [33], the same Lanczos sigma factors multiply the Fourier series coefficients of the ZMP and CoM references. This method of smoothing achieves two objectives at once: i) Suppressing the Gibbs phenomenon, ii) Introducing a double support phase. Different levels of smoothing can be achieved by modifying the Lanczos sigma factors. Also at the same time different double support periods can be obtained. This modification can be done with the parameter d. N is replaced with d in the Lanczos sigma factors in the sinc function:

$$\mathrm{sinc}(k\pi/d) \tag{5}$$

The effect of this modified Lanczos sigma smoothing is shown in Figure 4.8 for the $p_y^{ref}(t)$. For desired double support phase duration, different d values can be chosen. $d = 4$ creates the longest double support period in this figure.

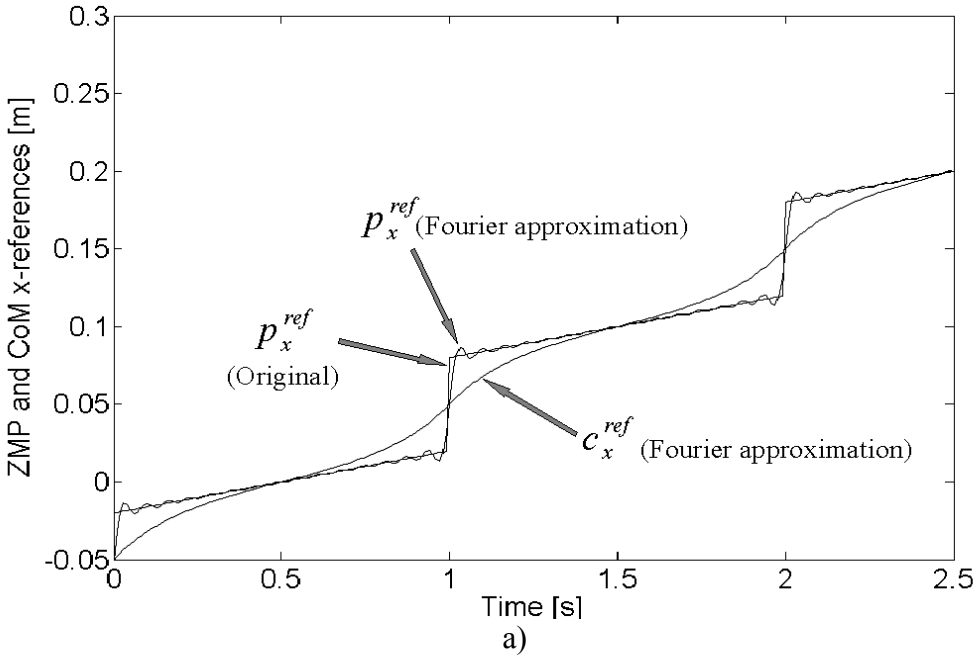

a)

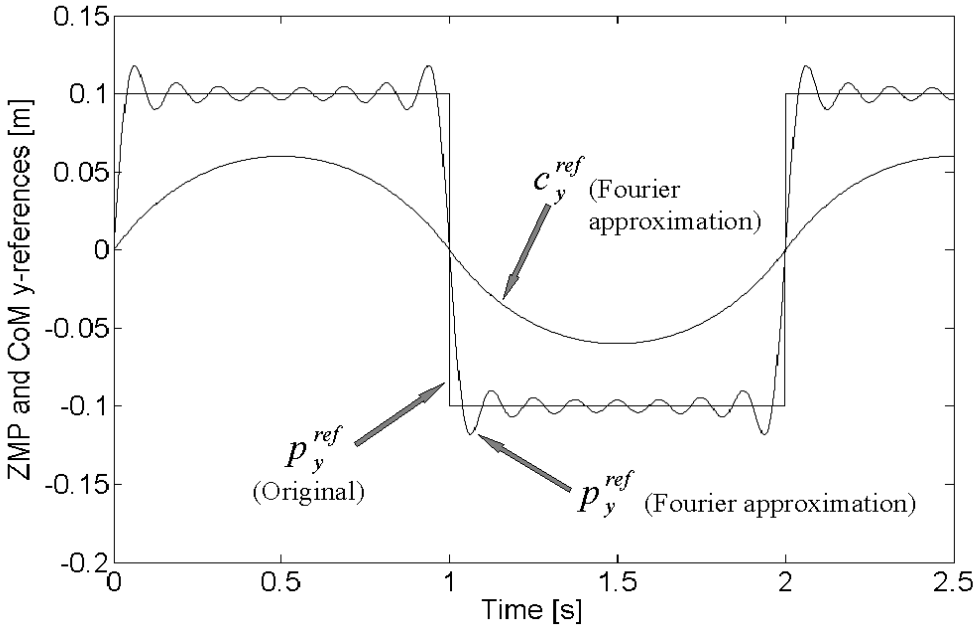

b)

Figure 4.7: The CoM reference curves with the original and the approximated ZMP reference curves. a) c_x^{ref} and b) c_y^{ref}

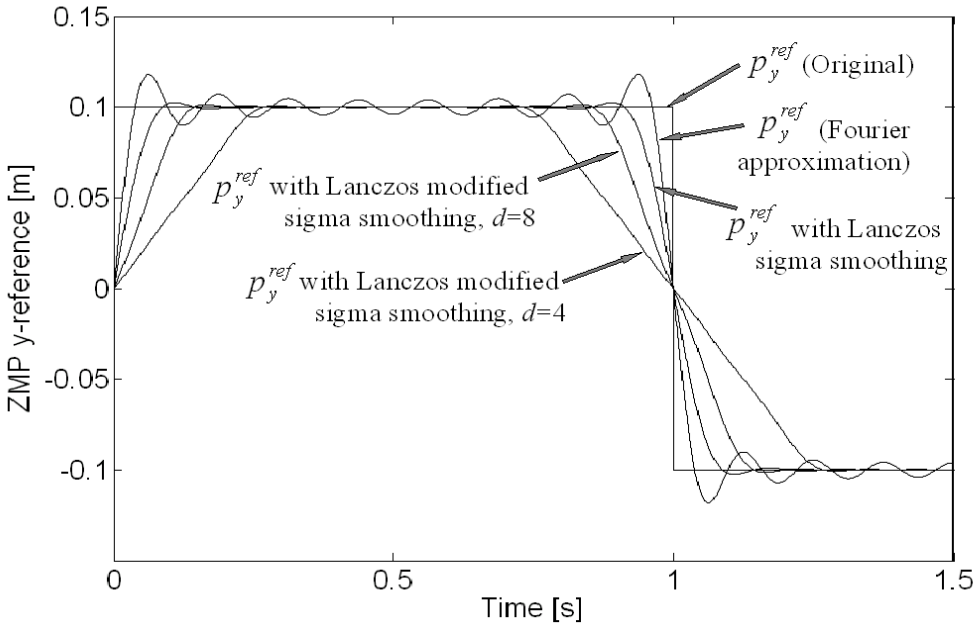

Figure 4.8: A double support phase is obtained with the modified Lanczos sigma smoothing factors in [42]. Different *d* values generate different double support phase durations.

This mechanism, however, introduces some shortcomings too: Gibbs suppression and double support period determination are coupled processes. Walk pattern design may impose a short double support phase (as in the case of humans), whereas this, due to the coupling between the this period and Gibbs suppression level, would lead to ZMP reference curves with pronounced oscillations at the foot switching times (Figure 4.8). Furthermore, our simulation studies and experimental work with a number of reference generation techniques [35-36, 43] suggest that having the single and double support periods a freely and directly adjustable parameters plays a vital role in final tuning of walking pattern.

4.3 ZMP Reference Trajectory with Predefined Single and Double Support Phases

With this motivation, in this thesis, a new ZMP reference trajectory is introduced. This trajectory, as in [33], has forward moving x-direction components for the naturalness of the walk. However, it is continuous and includes double support phases in its original description. The solution for the CoM trajectory from the given ZMP trajectory follows the same lines as in [33]. However, thanks to continuity of the ZMP reference signal, the Gibbs phenomenon is not observed and there is no need for smoothing. Also, the double and single support phase durations are freely selectable parameters of the reference generation algorithm. The newly introduced ZMP reference trajectory is presented in Figure 4.9. It is a modified version of the trajectory in Figure 4.6. The double support phase is introduced by using the parameter τ in this figure. A linear interpolation region is inserted around multiples of the half walking period T. The interpolation regions have widths of 2τ. The double support period T_d and τ are related by the expression

$$T_d = 2 * \tau \tag{6}$$

and hence the double support period is freely adjustable with the parameter τ.

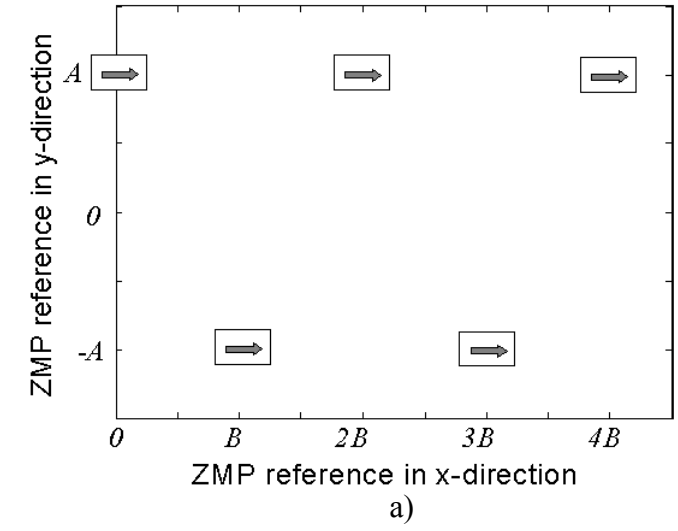

a)

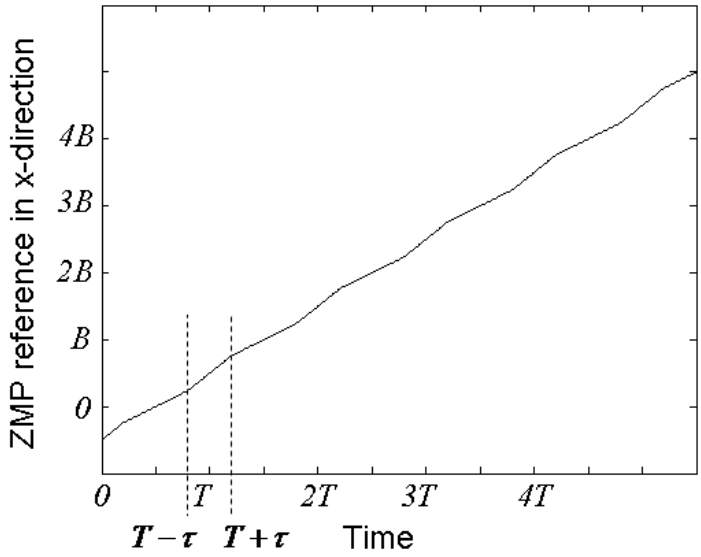

b)

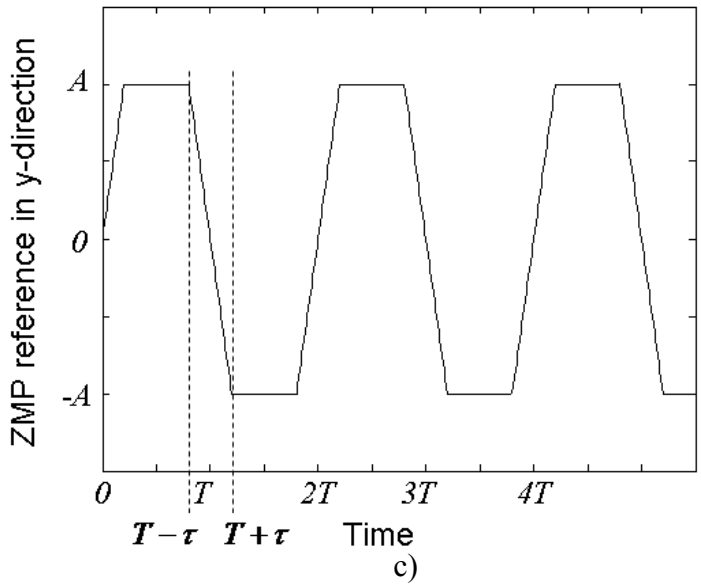

c)

Figure 4.9: Moving ZMP references with preassigned double support phases. a) $p_x^{ref} - p_y^{ref}$ Relation on the $x - y$ plane

b) p_x^{ref}, the x-axis ZMP reference **c)** p_y^{ref}, the y-axis ZMP reference

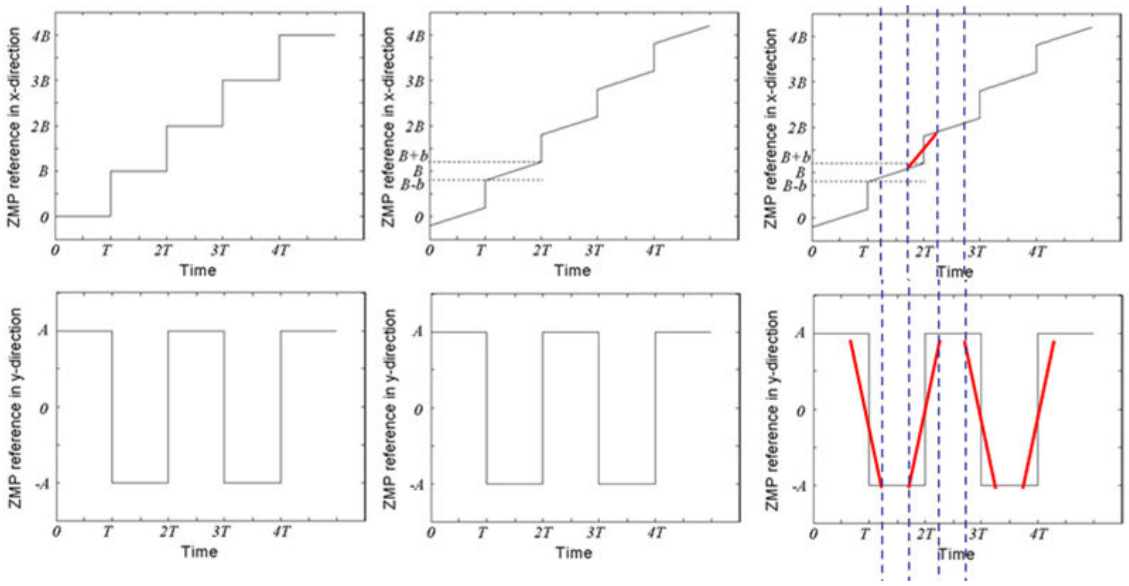

a) b) c)

Figure 4.10: Incremental development of the ZMP reference in this thesis. a) Fixed ZMP references [42]. b) The approach in [33] with moving ZMP references. c) The approach in this thesis: Moving ZMP references with predefined double support periods.

4.4 Fourier Approximation and the Solution for the CoM Trajectory

The mathematical description of the $p_x^{ref}(t)$ in Figure 4.9 is given by

$$p_x^{ref} = \frac{B}{T}(t - \frac{T}{2}) + p_x'^{ref} \tag{7}$$

where $p_x'^{ref}$ is periodic with period T. $p_x'^{ref}$ can be expressed as a combination of three line segments on $[0, T]$.

$$p_x'^{ref} = \begin{cases} \Omega_1 + \sigma_1 t & \text{if} \quad 0 \le t \le \tau \\ \Omega_2 + \sigma_2 t & \text{if} \quad \tau < t \le T - \tau \\ \Omega_3 + \sigma_3 t & \text{if} \quad T - \tau < t \le T \end{cases} \tag{8}$$

Here,

$$\begin{aligned} &\Omega_1 = 0, \\ &\sigma_1 = \frac{\delta}{\tau}, \\ &\sigma_2 = \frac{-2\delta}{T - 2\tau}, \Omega_2 = \delta - \tau\sigma_2, \\ &\sigma_3 = \sigma_1, \\ &\Omega_3 = -\delta - (T - \tau)\sigma_3. \end{aligned} \tag{9}$$

with

$$\delta = \frac{\frac{T}{2} - \tau}{\frac{T}{2}}(\frac{B}{2} - b). \tag{10}$$

Note that δ is the magnitude of peak difference between p_x^{ref} and the nonperiodic component $\frac{B}{T}(t - \frac{T}{2})$ of p_x^{ref}. δ can be computed form Figure 4.11 geometrically.

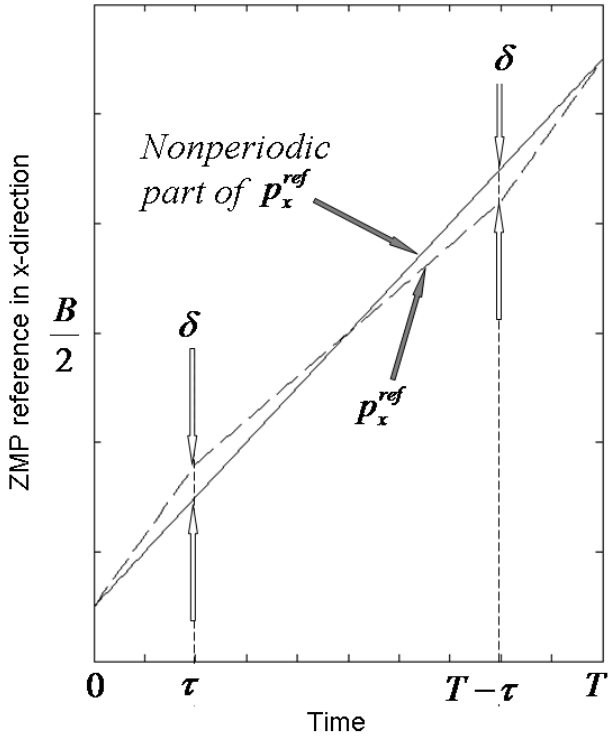

Figure 4.11: The parameter δ

$p_y^{ref}(t)$ is Figure 4.9 is expressed as

$$p_y^{ref} = \sum_{k=1}^{\infty} \mathrm{A}(-1)^k \left[\frac{2}{2\tau}(t - kT)\left[u(t - (kT - \tau)) - u(t - (kT + \tau))\right] + \left[u(t - (kT + \tau)) - u(t - (kT + T - \tau))\right] \right] \tag{11}$$

where $u(\cdot)$ represents the unit step function.

Defining $\omega_n \equiv \sqrt{g/z_c}$, we can rewrite (2) and (3) for the reference variables as follows.

$$\ddot{c}_x^{ref} = \omega_n^2 c_x^{ref} - \omega_n^2 p_x^{ref} \tag{12}$$

$$\ddot{c}_y^{ref} = \omega_n^2 c_y^{ref} - \omega_n^2 p_y^{ref} \tag{13}$$

Note that the y-direction ZMP reference $p_y^{ref}(t)$ is a periodic function with the period $2T$. It is reasonable to assume that $c_y^{ref}(t)$ is a periodic function too and that it has the same period. Hence, it can be approximated by a Fourier series

$$c_y^{ref}(t) = \frac{a_0}{2} + \sum_{k=1}^{\infty} a_k \cos(\frac{2\pi kt}{2T}) + b_k \sin(\frac{2\pi kt}{2T}) \tag{14}$$

By (13) and (14), p_y^{ref} can be expressed as

$$\begin{aligned} p_y^{ref}(t) &= c_y^{ref} - \frac{1}{\omega_n^2}\ddot{c}_y^{ref} \\ &= \frac{a_0}{2} + \sum_{k=1}^{\infty} a_k (1 + \frac{\pi^2 k^2}{\omega_n^2 T^2}) \cos(\frac{2\pi kt}{2T}) \\ &\qquad + b_k (1 + \frac{\pi^2 k^2}{\omega_n^2 T^2}) \sin(\frac{2\pi kt}{2T}) \end{aligned} \tag{15}$$

Noting that this expression in the form of a Fourier series for $p_y^{ref}(t)$, and since $p_y^{ref}(t)$ is an odd function, we can conclude that the coefficients $a_0/2$ and $a_k(1+(\pi^2k^2)/(\omega_n^2T^2))$ for $k = 1,2,3,\cdots$ are zero. In order to compute the coefficients $b_k(1+(\pi^2k^2)/(\omega_n^2T^2))$ we can employ the Fourier integral:

$$b_k(1 + \frac{\pi^2 k^2}{\omega_n^2 T^2}) = \frac{2}{2T}\int_0^{2T} p_y^{ref} \sin(\frac{2\pi kt}{2T}) dt \tag{16}$$

As a result, as derived in Appendix Section A of this thesis, the Fourier coefficients b_k of $c_y^{ref}(t)$ in (14) can be obtained as

$$b_k = \begin{cases} \dfrac{\omega_n^2 T^2}{\omega_n^2 T^2 + \pi^2 k^2} 2\dfrac{A}{\pi k}\left\{\left[\dfrac{2}{\tau}\left\langle \dfrac{T}{\pi k}\sin(\dfrac{\pi k\tau}{T}) - \tau\cos(\dfrac{\pi k\tau}{T})\right\rangle\right] + \left[\cos(\dfrac{\pi k\tau}{T}) - \cos(\dfrac{\pi k(T-\tau)}{T})\right]\right\} & \text{if } k \text{ is odd} \\ 0 & \text{if } k \text{ even} \end{cases}$$

for $k = 1,2,3,\cdots$. (17)

The second step is finding the Fourier series coefficients for c_x^{ref}. $p_x^{ref}(t)$ in Figure 4.9 is not a periodic function. It cannot be expressed as a Fourier series. However, as expressed above, this function is composed of the periodic function $p_x'^{ref}$ and the non-periodic function $(\frac{B}{T}(t - \frac{T}{2}))$. The periodic part of $p_x^{ref}(t)$ are shown in Figure 4.12. It is again a reasonable assumption that c_x^{ref} has a periodic part and a non-periodic part too. Further, if we suppose that the two non-periodic parts (of $p_x^{ref}(t)$ and

c_x^{ref}) are non-equal, then the difference $p_x^{ref}(t) - c_x^{ref}$ will be non-periodic. This is not expected in a continuous walk as the one described in Figure 4.9.

Therefore we conclude that the non-periodic parts of the two functions are equal. Note that, as shown in Figure 4.9, the period of the periodic part of $p_x^{ref}(t)$ is T and we can make the same statement for the period of the periodic part of c_x^{ref}. Finally, c_x^{ref} can be expressed as

$$c_x^{ref} = \frac{B}{T}(t - \frac{T}{2}) + \frac{\alpha_0}{2} + \sum_{n=1}^{\infty} \alpha_k \cos(\frac{2\pi nt}{T}) + \beta_k \sin(\frac{2\pi nt}{T}) \tag{18}$$

Recalling (12), with (18) the expression for $p_x^{ref}(t)$ with a Fourier series is

$$\begin{aligned} p_x^{ref}(t) &= c_x^{ref} - \frac{1}{\omega_n^2}\ddot{c}_x^{ref} \\ &= \frac{B}{T}(t - \frac{T}{2}) + \frac{\alpha_0}{2} + \sum_{n=1}^{\infty} \alpha_k (1 + \frac{\pi^2 k^2}{\omega_n^2 T^2}) \cos(\frac{2\pi kt}{T}) \\ &\qquad + \beta_k (1 + \frac{\pi^2 k^2}{\omega_n^2 T^2}) \sin(\frac{2\pi kt}{T}) \end{aligned} \tag{19}$$

Therefore the Fourier coefficients of $p_x'^{ref}(t)$, the periodic part of $p_x^{ref}(t)$, are $\alpha_0/2$, $\alpha_k(1+\pi^2k^2/\omega_n^2T^2)$ and $\beta_k(1+\pi^2k^2/\omega_n^2T^2)$ for $k = 1, 2, 3, \cdots$ The Fourier coefficients $\alpha_0/2$, $\alpha_k(1+\pi^2k^2/\omega_n^2T^2)$ of $p_x'^{ref}(t)$ shown in Figure 4.12 are zero because this is an odd function. The coefficients for $\beta_k(1+(\pi^2k^2)/(\omega_n^2T^2))$ can be found by

$$\beta_k(1 + \pi^2k^2/\omega_n^2T^2) = \frac{2}{T}\int_0^T p_x'^{ref}(t)\sin(\frac{2\pi kt}{T})dt \tag{20}$$

This yields the result

$$\beta_k = \frac{\omega_n^2T^2}{\pi^2k^2 + \omega_n^2T^2}\frac{2}{\pi k}\left[\begin{aligned} &\sigma_1\left[-\tau\cos(\frac{2\pi k\tau}{T}) + \frac{T}{2\pi k}\sin(\frac{2\pi k\tau}{T})\right] \\ &+ \sigma_2\left[\tau\cos(\frac{2\pi k\tau}{T}) - \frac{T}{2}\left(\cos\left(\frac{2\pi k\tau}{T}\right)\right) - \frac{T}{2\pi k}\sin(\frac{2\pi k\tau}{T})\right] \end{aligned}\right] \tag{21}$$

for $k = 1, 2, 3, \cdots$.

with the derivation in the Appendix Section B.

The curves obtained for c_x^{ref} and c_y^{ref} are shown in Figure 4.13 together with the corresponding original ZMP references (as defined in Figure 4.9). The original and Fourier approximation ZMP reference curves are shown in Figure 4.14. In figures 4.13

and 4.14, the following parameter values are used: $A = 0.1$ m, $B = 0.1$ m, $b = 0.04$, $T = 1$ s and $\tau = 0.2$ s. The infinite sums in (14), (15), (18) and (19) are approximated by finite sums of N terms ($N = 24$).

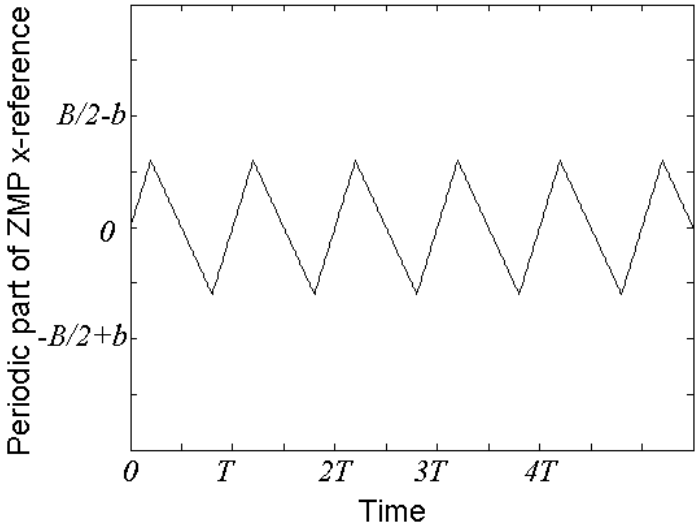

Figure 4.12: $p_x'^{ref}(t)$, the periodic part of the x-direction ZMP reference $p_x^{ref}(t)$

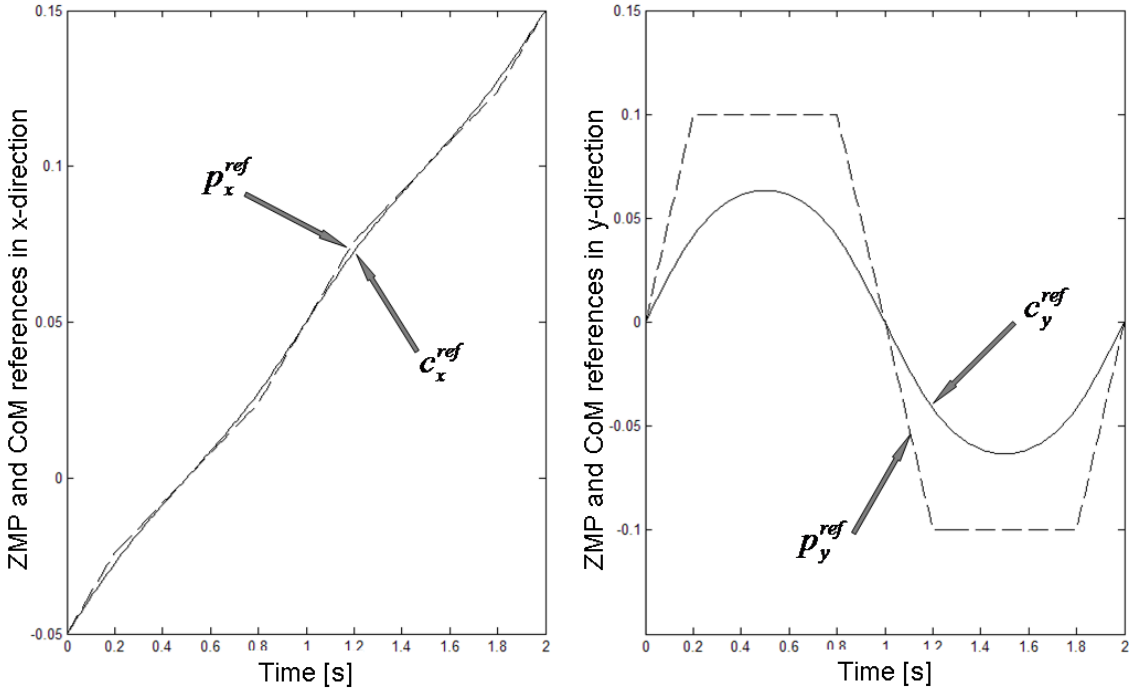

a) b)

Figure 4.13: c_x^{ref} and c_y^{ref} CoM references together with the corresponding original ZMP references a) c_x^{ref} b) c_y^{ref}

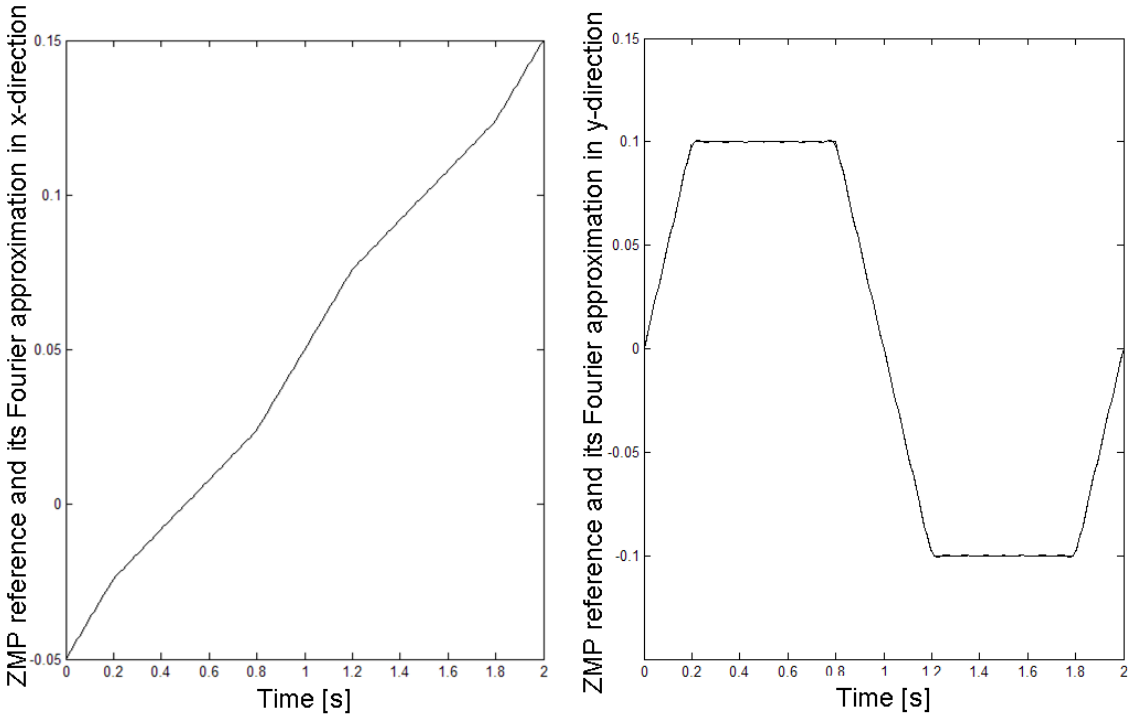

a) b)

Figure 4.14: The original and approximated ZMP reference curves a) the x-direction ZMP reference p_x^{ref} b) the y-direction ZMP reference p_y^{ref}

In this chapter of the thesis, firstly, footstep locations are planned with respect to the physical properties of the bipedal robot in order to shape our natural, human-like ZMP references in x and y- directions for an infinite time. Created continuous ZMP references are approximated with Fourier Series approximation and Fourier coefficients for the ZMP references in x and y- directions are obtained separately. After this step, the CoM references are created by using the approximated ZMP references. It should be noted that the newly defined ZMP references have no discontinuities and this property prevents the Gibbs phenomenon when they are approximated with Fourier Series. Continuity also gives us the opportunity to introduce the double support phases in our references.

Although the CoM references created in this chapter are among the main necessities for generating reference trajectories for obtaining a bipedal walk, there are other reference trajectories to be designed too: Foot position reference trajectories have to be created. Inverse kinematics then can be employed to find the reference positions of the leg joints which bridge the CoM and the feet. The next chapter works on the foot trajectories and on various modifications of the CoM references for a forward walk of a predetermined number of steps.

Chapter 5

5. PLANNING THE STEPPING SEQUENCE AND MODIFICATIONS ON THE CoM REFERENCE TRAJECTORY

As mentioned in the previous chapter, the trajectory for the CoM is only part of the required reference trajectories. If foot Cartesian trajectories are assigned too, then the walking reference generation task will be complete. Figure 5.1 shows coordinate frames employed for this purpose and the CoM. The world coordinate frame is assumed to be on the ground level. Another frame is fixed to the body of the robot. The CoM is located in a known and fixed position $\hat{s}_b^b$ in this coordinate frame. (Note that, this is an approximation, since, when the legs or other extremities of the robot are in motion, the CoM moves with respect to the body coordinate frame too.) The notation $\hat{s}_b^b$ corresponds to "coordinates of the body center of mass in the body coordinate frame." Two coordinate frames (identical to Frame 6 in Figure 3.3) are attached rigidly at the soles of the right and left feet, respectively. The frame origins of these centers are just below the ankle joints in Figure 5.1. The hip frames in Figure 5.1 correspond to the base frame (Frame 0) of Figure 3.3. The axis assignments of the hip frames are not shown in Figure 5.1 for simplicity of illustration. However, as the Denavit-Hartenberg axis assignment in Chapter 3 suggests, the body and hip frame orientations are identical.

Our task is to find the reference homogeneous transformation matrices which relate the foot frame coordinates to their respective hip frame coordinates at any given time. Inverse kinematics for the six-degrees-of-freedom legs can then provide the joint position references, which are used directly in servo routines.

5.1 Walk Planning Assumptions

A number of walk planning assumptions have to be made in order to close the gap between the knowledge of the CoM reference trajectory and the reference leg configurations (equivalently the leg homogeneous transformation matrices):

1) The reference trajectory for the CoM computed in the previous chapter is described in world coordinates. In the computation, it is already assumed that the walk direction is along the x-axis of the world coordinate frame.

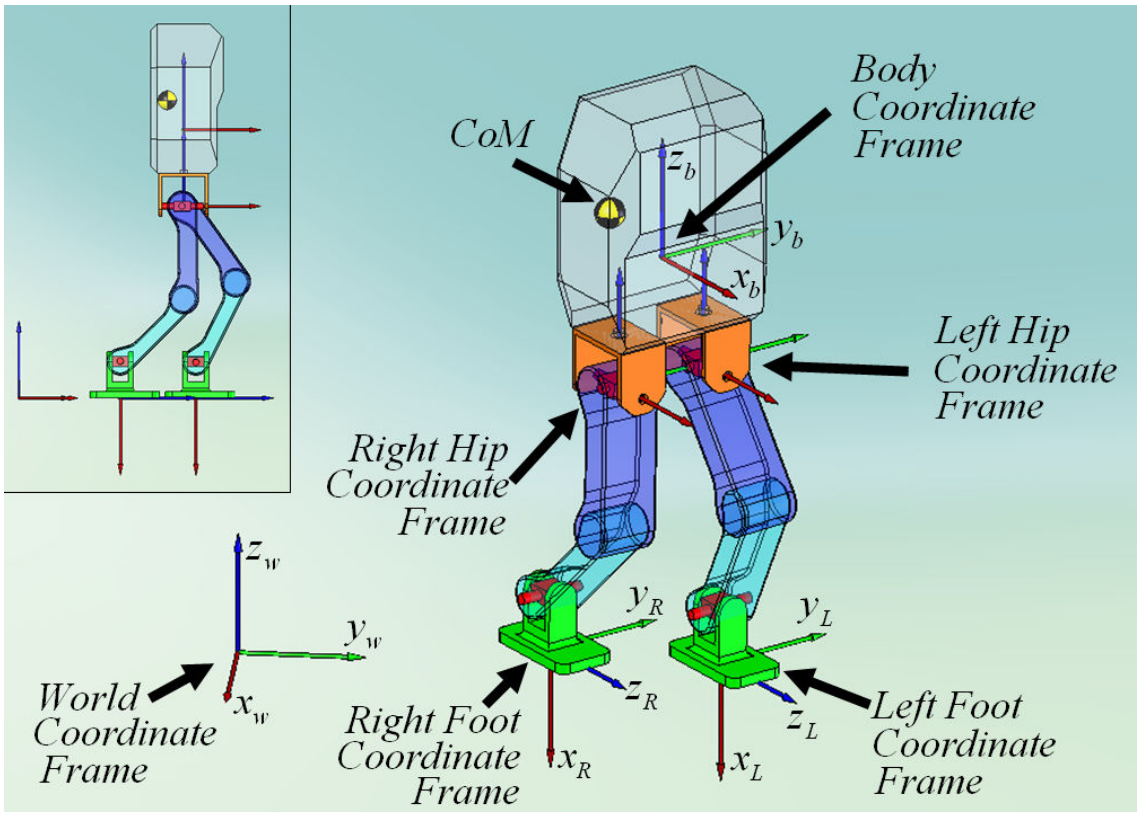

Figure 5.1: Coordinate frames employed on the bipedal robot

2) The orientation reference for the body frame is always parallel to the world frame (Figure 5.2). This can be expressed as

$$R_w^b = \begin{bmatrix} 1 & 0 & 0 \\ 0 & 1 & 0 \\ 0 & 0 & 1 \end{bmatrix} \tag{22}$$

where the notation R_w^b reads "the orientation of the body frame with respect to the world frame."

3) The foot soles are planned to be parallel to the ground, foot fronts showing into the walking direction. Hence, from Figure 5.1, the foot orientations are given by

$$R_w^R = R_w^L = \begin{bmatrix} 0 & 0 & 1 \\ 0 & 1 & 0 \\ -1 & 0 & 0 \end{bmatrix} \tag{23}$$

Since by (22) and the discussion above, the world, body and hip coordinate frames are identical in orientation, we conclude that

$$R_{R_0}^{R} = R_{L_0}^{L} = \begin{bmatrix} 0 & 0 & 1 \\ 0 & 1 & 0 \\ -1 & 0 & 0 \end{bmatrix} \tag{24}$$

where R_0 and L_0 denote the right and left hip frames, respectively. These matrices, as computed in (24) constitute the orientation part of the leg reference configurations.

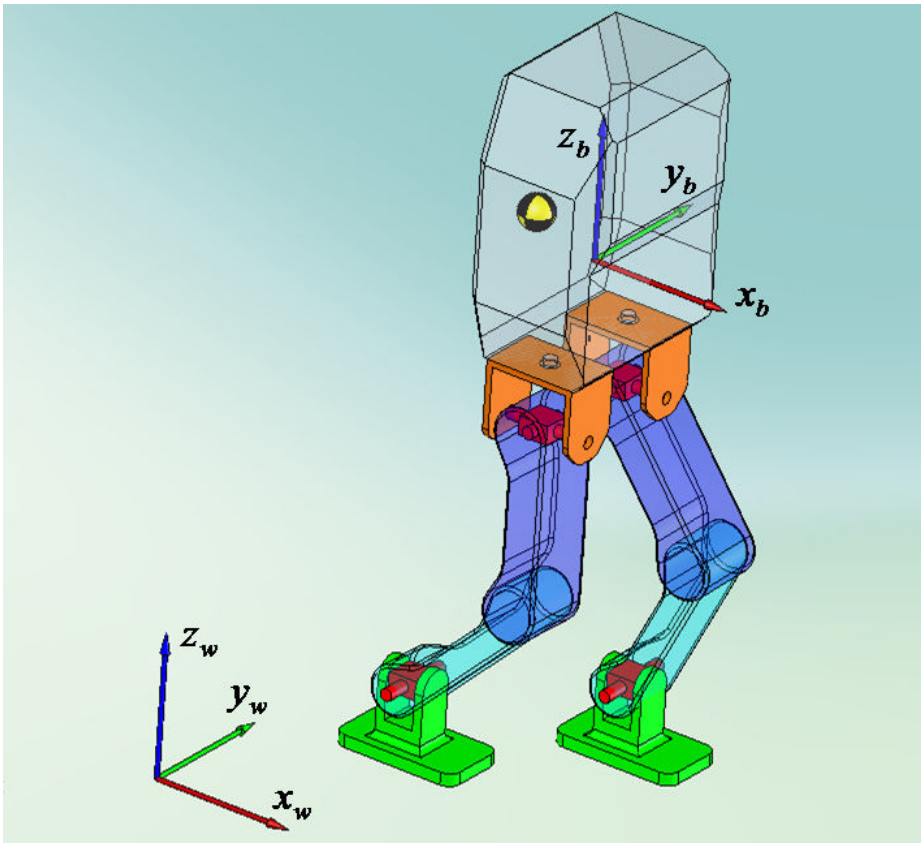

Figure 5.2: Attached world and body frames

4) The body frame is initially (at time $t = 0$) positioned just above the world frame (Figure 5.3).

5) The hip frame height from ground level, h_h in Figure 5.3, is fixed for all times. Its value is adjusted experimentally in such a way that the walking motion of the feet remains in the workspace of the legs.

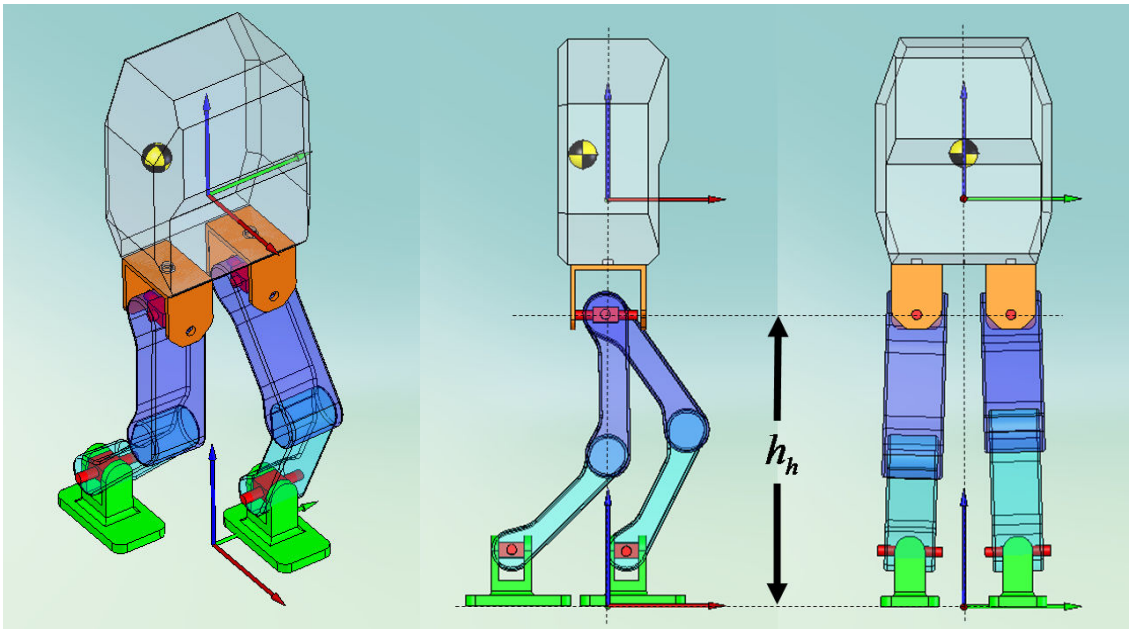

Figure 5.3: World and body frames. Note that this is the configuration at $t = 0$

6) The discussion for the CoM reference generation in the previous chapter starts with predetermined step locations as shown in Figure 4.9. The step locations in this figure are chosen to yield and exploit the periodic nature of ZMP trajectories. However, many applications can impose foot positions relative to each other different than in Figure 4.9, before and after the periodic motion (initially, and lastly). Some of the (infinitely many) options for this positioning are shown in Figure 5.4. One of the two feet can be in front of the body and the other one at the back in the beginning of the walk. Another option for the beginning configuration is to start with feet in the same position in the walking direction (x- direction). The last option shown in Figure 5.4, with foot fronts in line with each other, is chosen in this thesis, for both of the initial and final foot configurations. This choice is suitable for the biped robot to come close to desks, shelves and other work environments. It will, however, make modifications in the originally designed CoM trajectory necessary. These modifications are discussed later in this chapter. As shown in Figure 5.5, the initial coordinates of the feet in x-direction, as expressed in the hip frame is a design parameter denoted by $x_{ref\ asymmetry}$.

7) The right foot will be swung firstly in the walk.

8) Without restriction of generality, for simplicity, it is assumed that the hip frame x-direction coordinates as expressed in the body frame are zero.

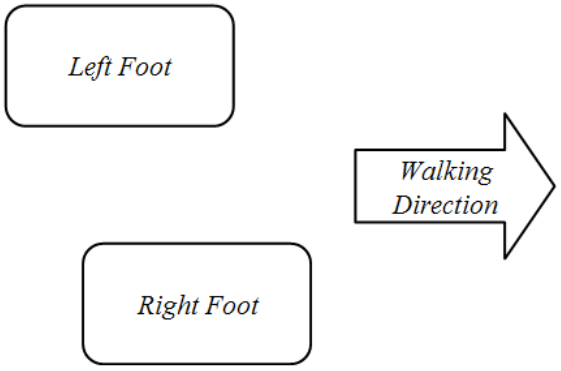

a)

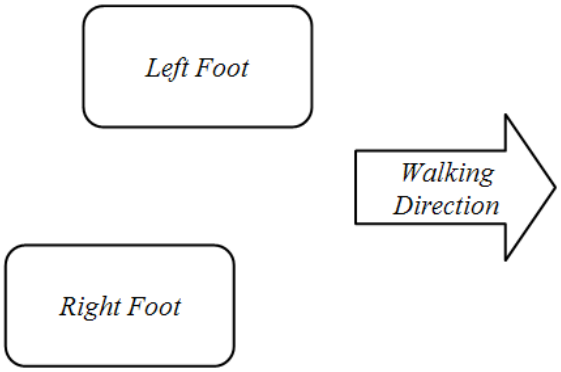

b)

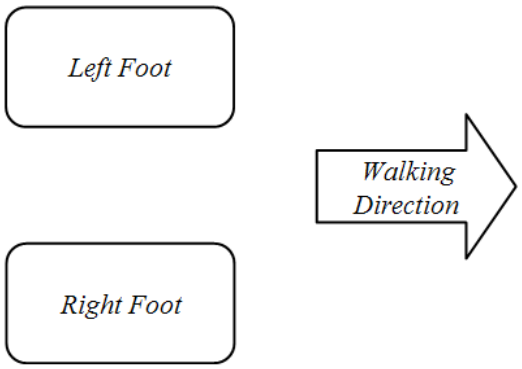

c)

Figure 5.4: Some of the options for foot positioning: a) Right foot in front of the body b) Left foot in front of the body c) Two feet in the same position in the x-direction

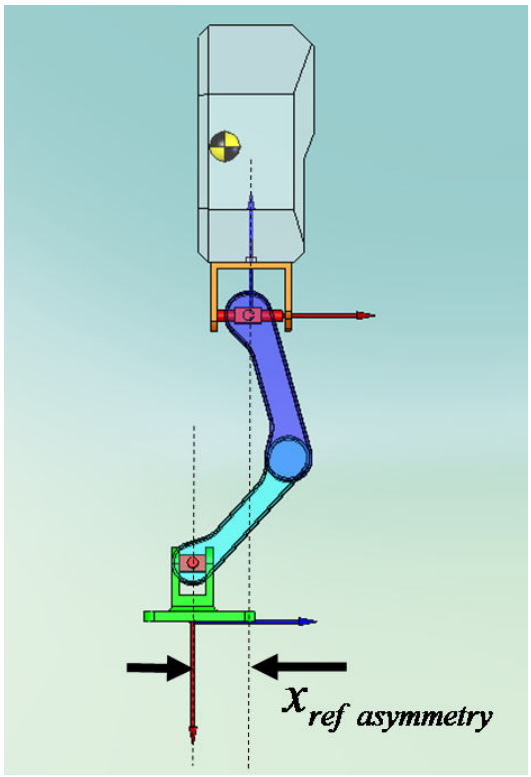

Figure 5.5: Initial coordinates of the two feet positioned at $x_{ref\ asymmetry}$

5.2 Planning the Stepping Sequence

With assumption 6 above, the first and last steps of the walk have to be special ones: Unlike all other steps of the walk, the first one starts with foot fronts in line with each other, and the last one ends with foot fronts in line with each other. Figure 5.6 shows stepping locations of such a walk.

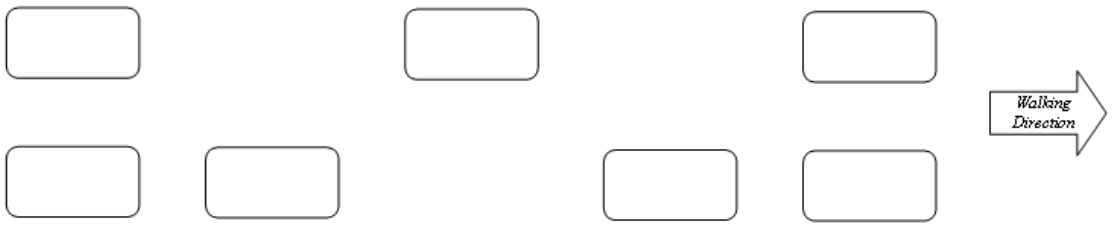

Figure 5.6: Stepping locations of the two feet

With the assumptions 6 and 7 above, this stepping sequence is fully defined once the number of foot swings, N_{swing}, is specified. In order to describe the stepping

phases, we also introduce another parameter, the *phase description number* N_{phase}. On a sketch of stepping locations like in Figure 5.6, each single and double support phase is indicated with increasing numbers starting from 1 marked on the corresponding supporting foot prints. The maximum number of phases of the walk reached at the end of the walk is called the phase description number. Examples of this numbering of the phases are shown in Figure 5.7.

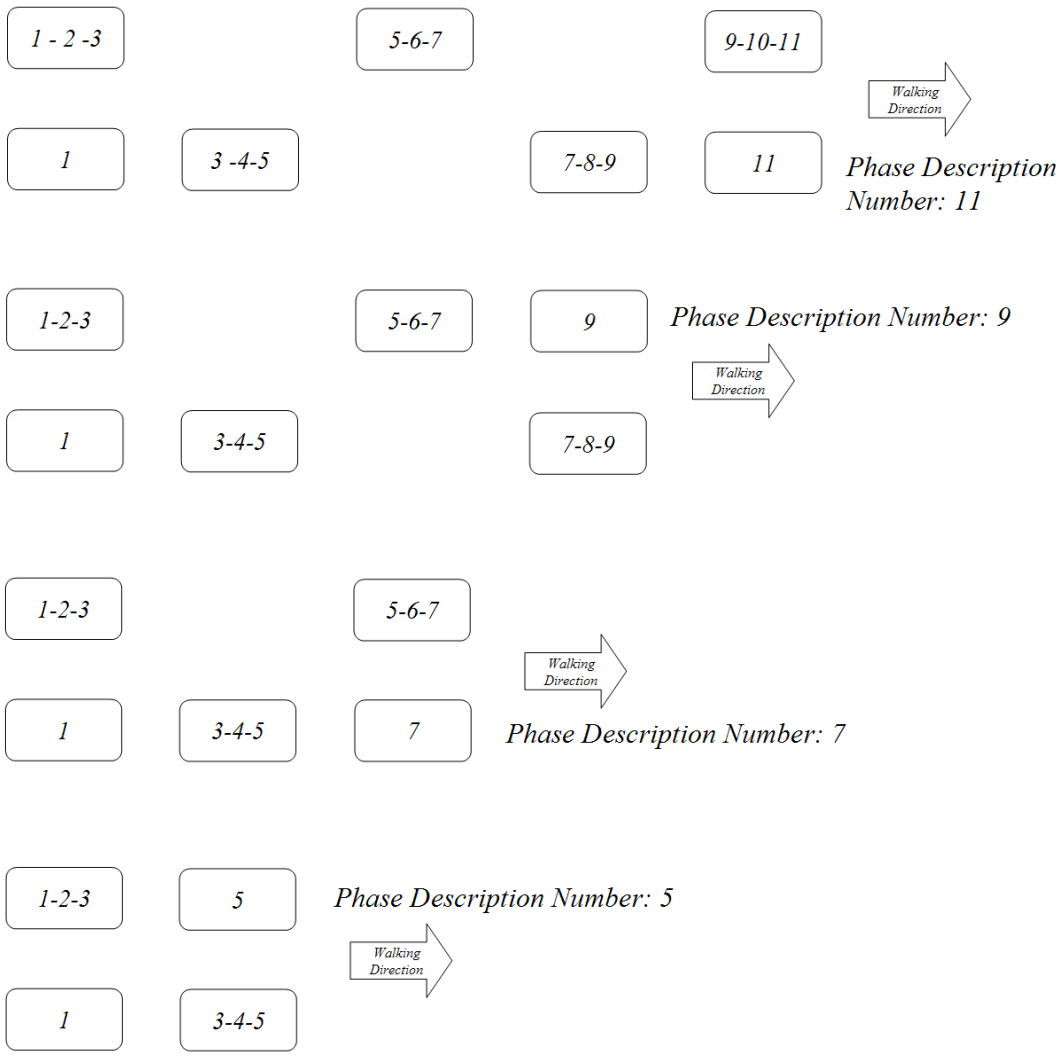

Figure 5.7: Phase description number visualization

Yet another way of describing the step sequence is in terms of the distance traveled N_{step} measured in units of "step size." This requires the definition of the step size s_s. We define it as the toe-to-toe distance after a swing phase as shown in Figure 5.8. N_{step} is 4 for the step sequence shown in Figure 5.8.

The three numbers, N_{swing}, N_{phase} and N_{step} are equivalent in describing step sequences. Once one of them is specified, the other two can uniquely determined from straight forward equations:

$$N_{phase} = 2N_{swing} + 1 \tag{25}$$

$$N_{step} = N_{swing} - 1 \tag{26}$$

Once the stepping sequence is specified, Cartesian foot references as expressed in the world coordinate frame can be generated. This reference generation process follows in the next sections.

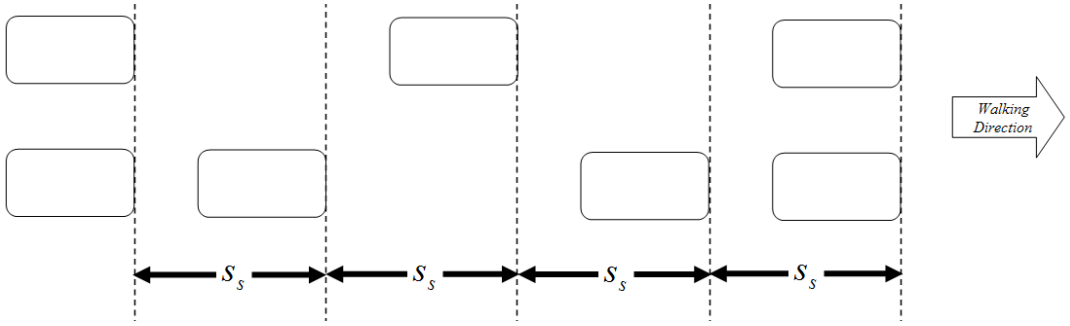

Figure 5.8: s_s, toe-to-toe distance after a swing phase

5.3 Foot References in the z-Direction

The feet are on the ground when not in the swing phase. In the swing phases they are lifted from the ground level. The swing phase is divided into two sub-phases of equal duration. The first of these is the take-off phase, followed by the landing phase. The timing is specified by two timing parameters: The double support T_d and the single support period T_s. These two parameters are linked with the timing parameters of the previous chapter with

$$T = T_d + T_s \tag{27}$$

and

$$\tau = \frac{T_d}{2} \tag{28}$$

Note that the full walking period T_w is computed as

$$T_w = 2T\,. \tag{29}$$

Parallel with the common robotics practice of using smooth references, a sinusoidal function is used for the take-off and landing of the swung foot. This sinusoid is in the form of a "*1-cosine*" curve as shown in Figure 5.9 and described by

$$z = \tfrac{1}{2} h_s \left(1 - \cos(t \frac{2\pi}{T_s}) \right) \tag{30}$$

The parameter h_s is called step height in this thesis. As given above, T_s is the single support period. t is a generic time variable. The function in Figure 5.9 is shifted in time to swing start instants to generate the vertical motion. Note also that it is defined in world coordinate frame coordinates. Figure 5.10 shows right and left foot swing references for a walk of 5 swings with their appropriate timing. T_s is 1 s, T_d is 0.5 s, and h_s is 0.02 m in this plot.

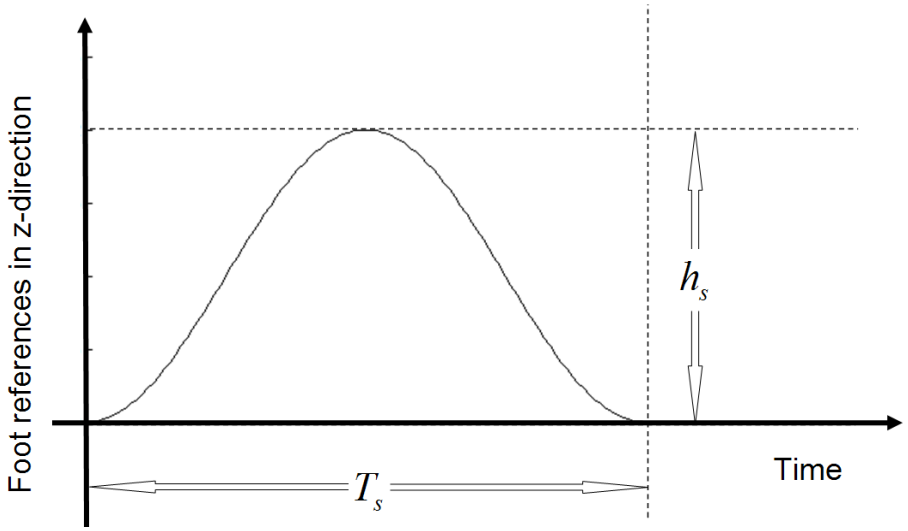

Figure 5.9: Foot reference in the z -direction in the form of "*1-cosine*" curve during a swing phase

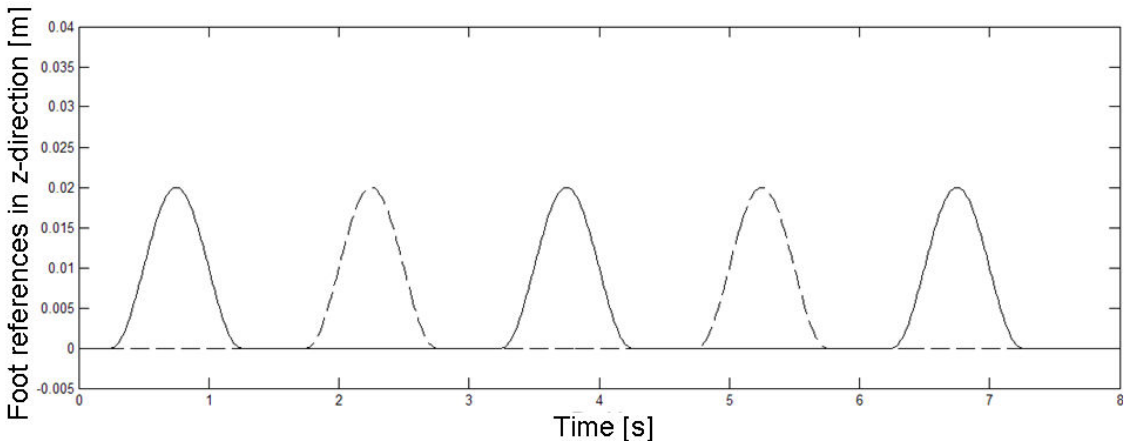

Figure 5.10: Right foot (solid) and left foot (dashed) references in the z -direction during a walk

5.4 Foot References in the x-Direction

The foot references in the x-direction are defined in the world frame too. These references are constant in their respective right and left support phases and in the double support phase. They move forward (they increase) in their respective swing phases. Again, for smoothness of the motion (*1-cosine)*-type of rising to the step destination is employed. The "one-shot" version of this x-direction swing reference is shown in Figure 5.11. The expression describing this curve is

$$x = \tfrac{1}{2} A_s \left(1 - \cos(t \frac{\pi}{T_s}) \right) \tag{31}$$

The maximum value A_s of the function shown in this figure is equal to s_s in the first and last foot swings of the walk and is $2s_s$ for all other swings. In order to create x-direction foot references for a complete stepping sequence and for both of the two feet, the curve in Figure 5.11 is shifted in temporally and spatially. Figure 5.12 shows the final x-references for a sequence of 5 foot swings. T_s is 1 s, T_d is 0.5 s, and s_s is 0.1 m in this plot. Note that the initial values of the references are not zero. As discussed in Section 5.1 and illustrated in Figure 5.5 the initial position references have an offset with respect to the hip and body coordinate frames. This offset between them is $x_{ref\ asymmetry}$ and this parameter is -0.11 m in Figure 5.12.

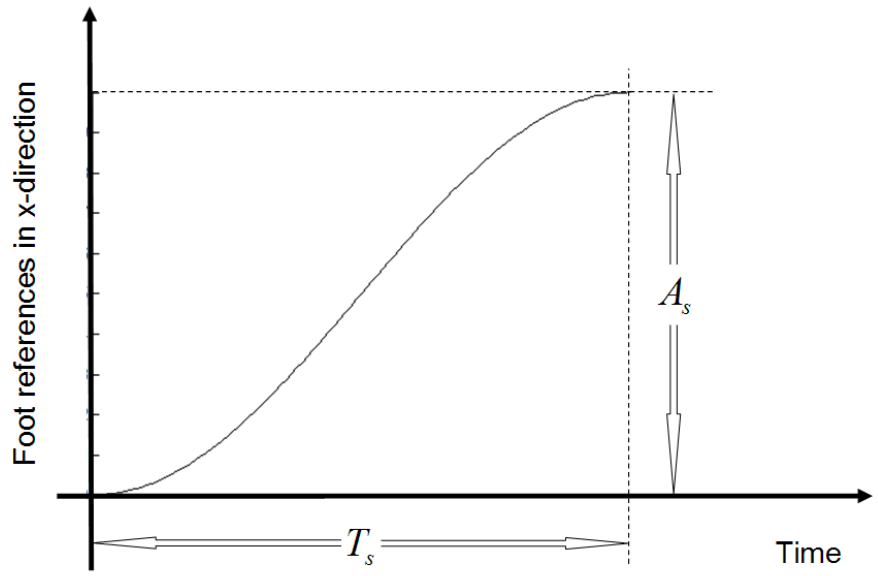

Figure 5.11: Foot reference in the x-direction in the form of "*1-cosine*" curve during a swing phase

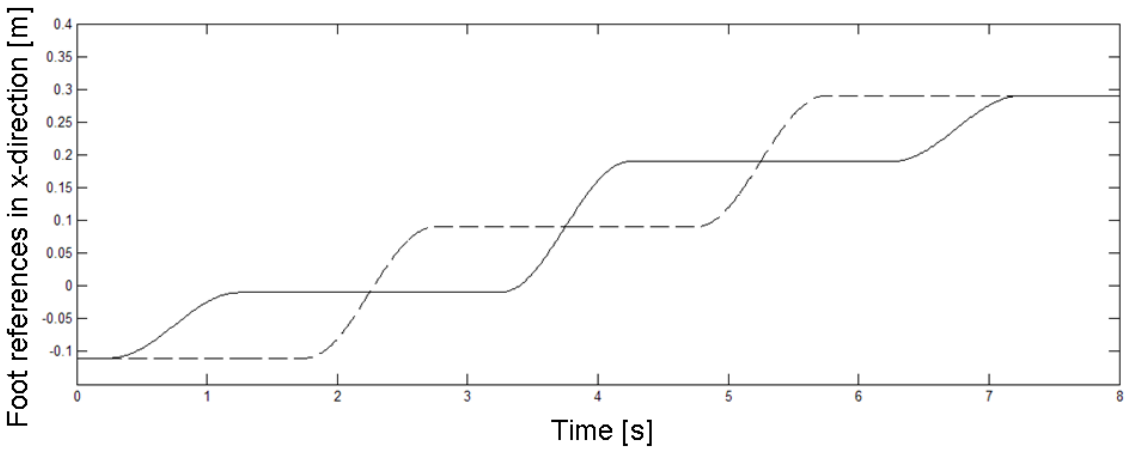

Figure 5.12: Right foot (solid) and left foot (dashed) references in the x-direction during a walk

5.5 Foot References in the y-Direction

The y-direction references in the world coordinate frame are constant. The right foot reference function is

$$y = -A \tag{32}$$

and the left foot y-reference is

$$y = A, \tag{33}$$

where A is the ZMP reference in the y-direction specified in the previous chapter.

5.6 Modifications on the CoM Reference

The CoM reference discussed in the previous chapter is created by the assumption that the origin of the robot coordinate frame and the CoM coincide. However, as discussed in this chapter, in general there can be a nonzero offset vector $\hat{s}_b^b$ between the body coordinate frame and CoM. Therefore the CoM references are shifted in such a way that the origin of the body is aligned with the world coordinate frame in the x and y directions and that the CoM is positioned with this offset. Typically, the y-component of $\hat{s}_b^b$ is not significant because of the symmetric build of humanoid robots. x-direction CoM offsets are more common. This is the case in Figure 5.13 too,

where a shift on c_x^{ref} is displayed. The CoM is assumed to be 0.05 m behind the body frame origin in this figure.

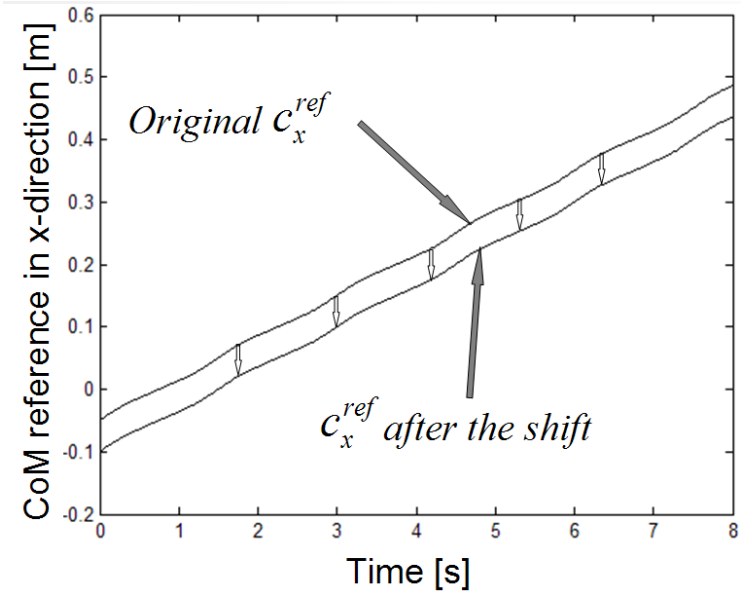

Figure 5.13: Original and the shifted (with $\hat{s}_b^b$) c_x^{ref} references together

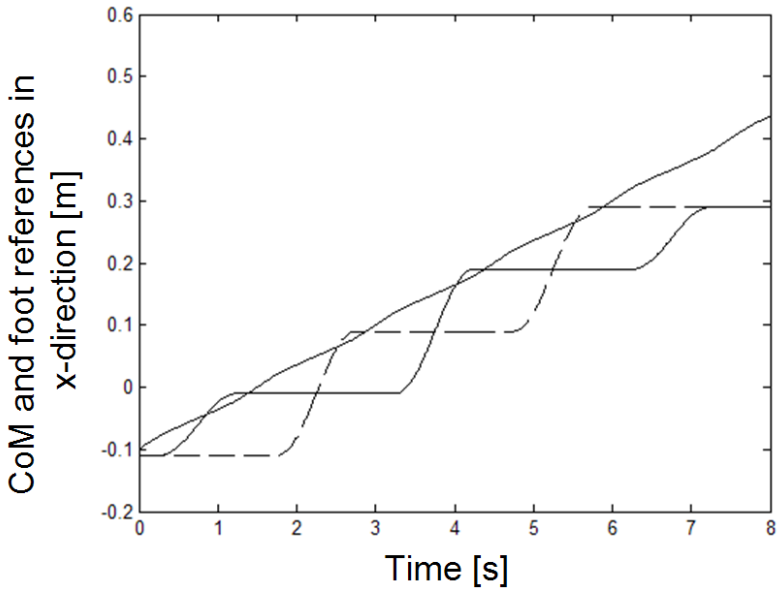

Figure 5.14: Shifted CoM reference and foot references in the x-direction

The newly obtained shifted CoM reference and the foot references in the x-direction are displayed in Figure 5.14 which indicates that another modification on the CoM trajectory has to be carried out: The CoM trajectory is an "infinitely running" one, whereas the foot trajectories are planned with a finite number of swing motions in mind. This problem can be cured, however, by saturating the CoM trajectory at the beginning and at the end of the walk. The saturation positions are computed by considering the

relative positions of the body and the feet with respect to the body frame. The feet are behind the body by $x_{ref\ asymmetry}$ and the CoM is behind the body by the magnitude of the x-direction component of $\hat{s}_b^b$. Therefore, the CoM trajectory is saturated at $-\hat{s}_{b\,x}^b$ at the beginning of the walk and at the end of the walk it is saturated in front of the final foot positions with an offset of $-x_{ref\ asymmetry}+\hat{s}_{b\,x}^b$. The saturated CoM trajectory is shown in Figure 5.15 together with x-direction foot references.

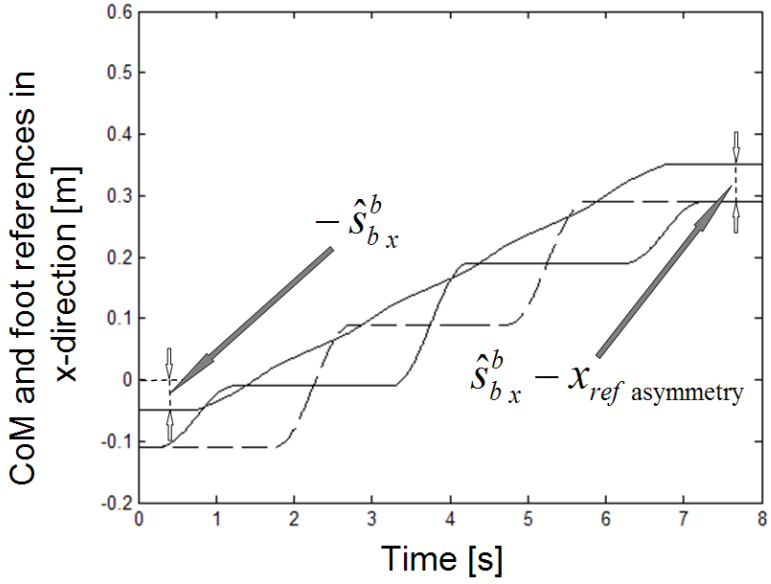

Figure 5.15: Saturated CoM reference with the foot references in the x-direction

The newly generated, saturated version of the x-direction CoM reference still has a drawback. It is no more a smooth reference. The saturation corners cause sharply changing position references. In order to soften them, again sinusoidal functions are employed. These functions, as smooth patches, replace the saturated CoM reference in the vicinities of the saturation corners. Figure 5.16 shows the saturation corners and the smooth curves which replaced them. The smoothing interpolation at the beginning uses the following replacement function

$$c_x^{ref}(t)=\hat{s}_{b\,x}^b+A_1\left(1-\cos\left(\left(t-\frac{1}{2}T_d\right)\frac{\pi}{2T_s}\right)\right) \quad \text{for} \quad \frac{1}{2}T_d \le t < \frac{1}{2}T_d+T_s \tag{34}$$

where A_1 is computed from the saturated CoM reference as

$$A_1=c_x^{ref}\left(\frac{1}{2}T_d+T_s\right)-\hat{s}_{b\,x}^b \tag{35}$$

The interpolation at the end is described by

$$c_x^{ref}(t) = \hat{s}_{b\,x}^{b} + \frac{1}{2}(N_{phase}-3)s_s - A_1\left(1-\cos\left(\left(t-\left[\frac{1}{2}(N_{phase}-3)T+\frac{1}{2}T_d+T_s\right]\right)\frac{\pi}{2T_s}\right)\right)$$

$$\text{for} \quad \frac{1}{2}(N_{phase}-3)T+\frac{1}{2}T_d \le t < \frac{1}{2}(N_{phase}-3)T+\frac{1}{2}T_d+T_s \tag{36}$$

Here, N_{phase} is the phase description number of Section 5.2. This parameter is equal to 11 in the example plots in this section. T is the step timing parameter of Chapter 4 and it is equal to the sum of the single and double support periods, namely of T_s and T_d, respectively.

Similar modifications are carried out on the y-direction CoM reference c_y^{ref} too. To start with, this function is truncated at the end of the step sequence. Figure 5.17 shows c_y^{ref} before (Figure 5.17.a) and after the truncation (Figure 5.17.b). The non-smooth beginning and en of c_y^{ref} are smoothed as in the case of c_x^{ref} too. The resulting reference function is shown in (Figure 5.17.c). The smoothing is achieved by a rise to the first peak value of c_y^{ref} and drop from the last peak value of it via *1-cosine* type curves of period $T_s + T_d$. The x-direction foot references are included in the figure in order to convey the step timing information to it in more detail.

Figure 5.18 summarizes the generated CoM and foot references.

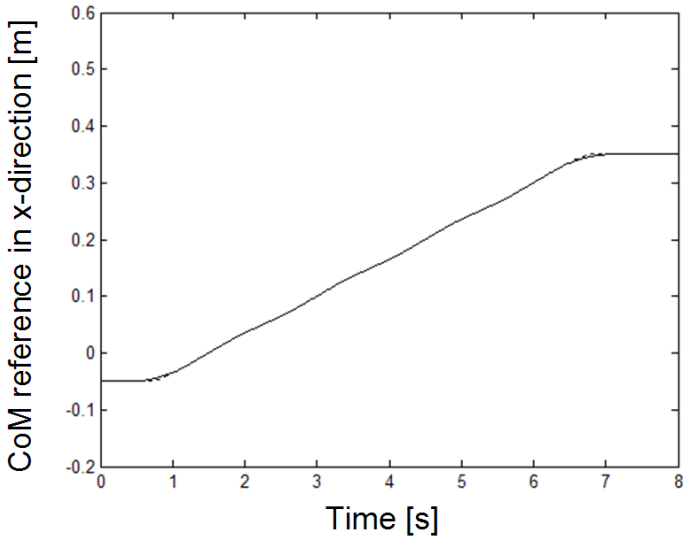

a)

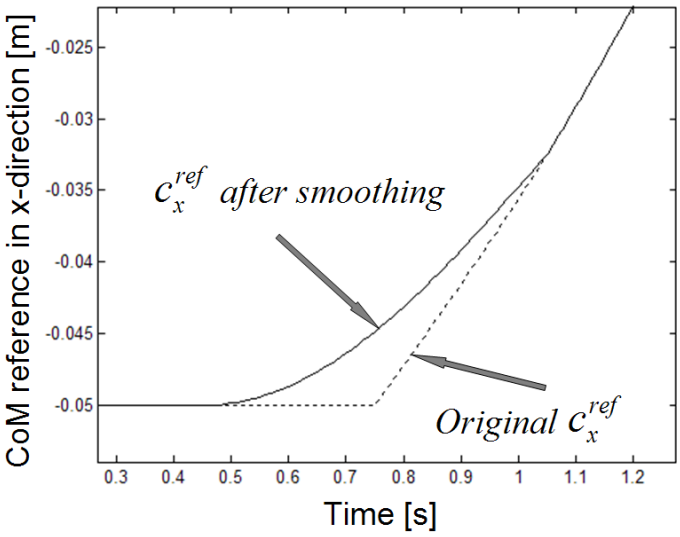

b)

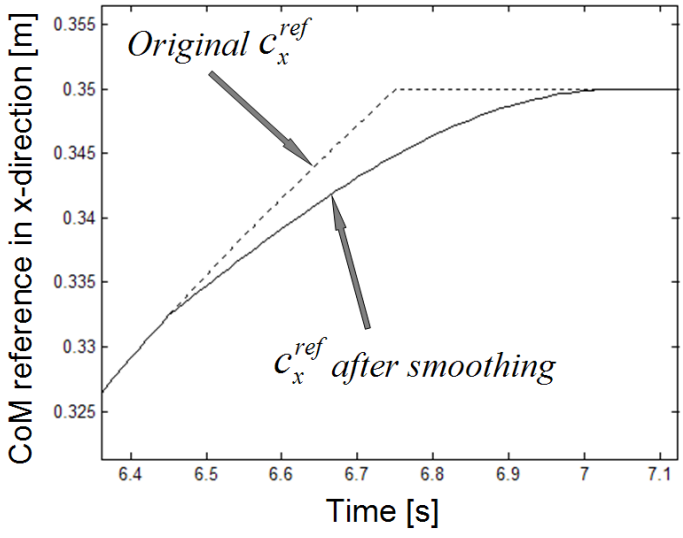

c)

Figure 5.16: Smoothed CoM reference in the x-direction a) Smoothed CoM reference together with the original CoM reference in the x-direction b) Smoothing at the lower part c) Smoothing at the upper part

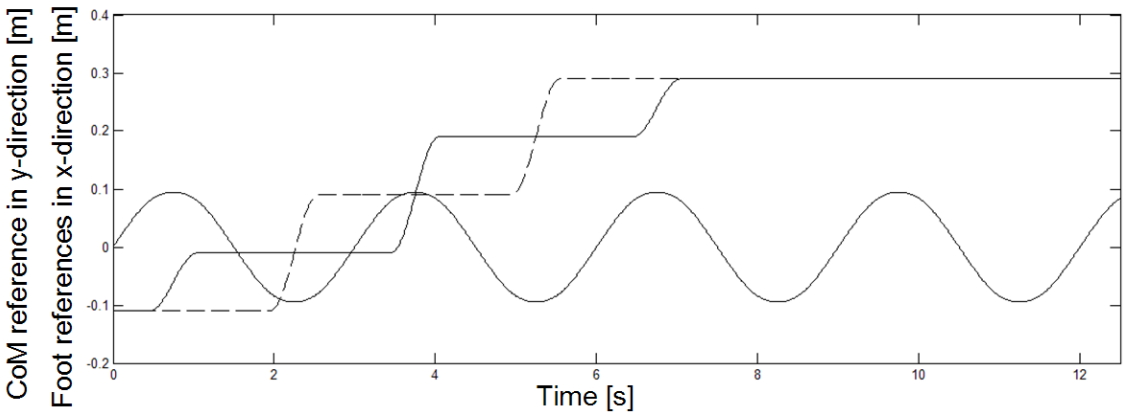

a)

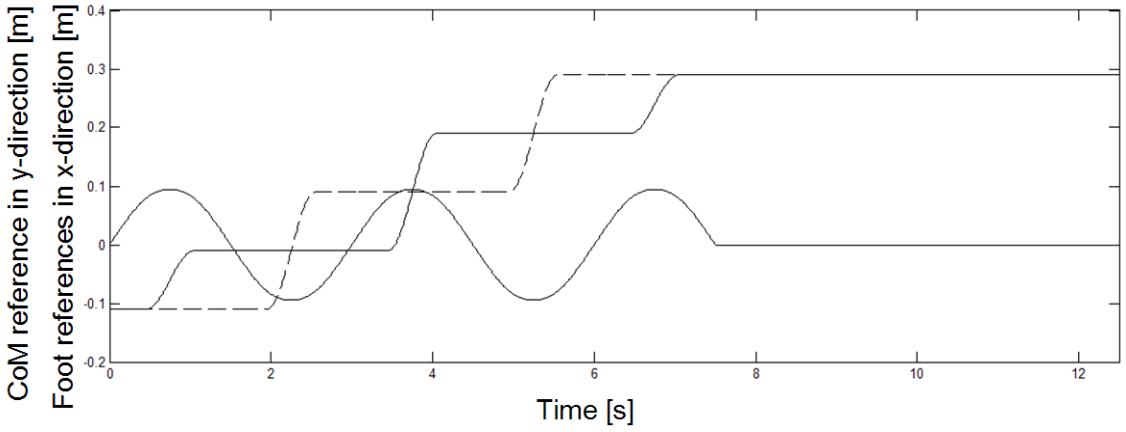

b)

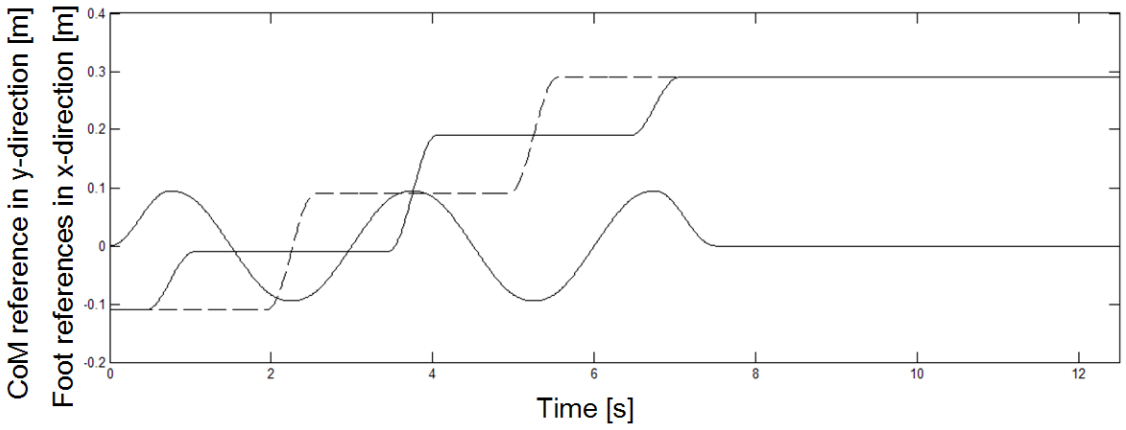

c)

Figure 5.17: Smoothed CoM reference in the y-direction a) Original CoM reference in the y-direction together with the foot references in the x-direction b) Saturated CoM reference in the y-direction c) Smoothed CoM reference in the y-direction

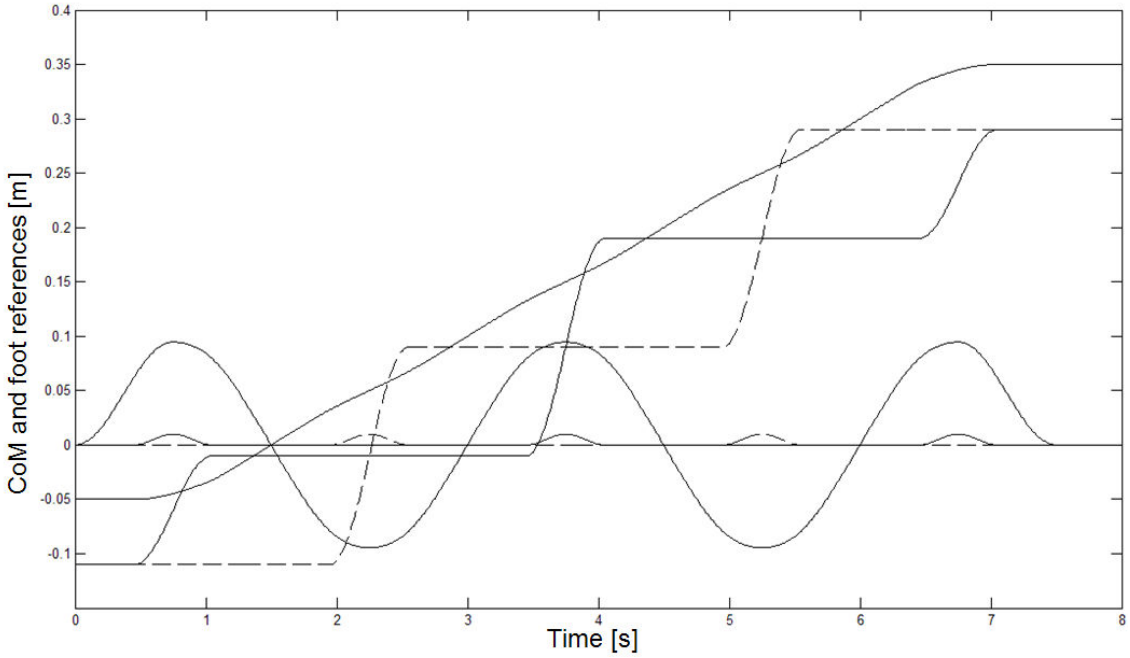

Figure 5.18: Overall generated CoM and foot references

5.7 Hip Frame Foot References and Inverse Kinematics

As stated earlier in this chapter, our ultimate objective in reference generation is obtaining joint position references which will be directly used in joint servo routines. The joint references are obtained by solving inverse kinematics from the foot configuration as expressed in the hip frames. One part of the foot configuration information is orientation. The reference orientation matrices are already found in Section 5.1 above. What remains is obtaining the foot coordinate frame center reference positions as expressed in the respective hip frames.

Provided in the Figure 5.18 are the CoM and foot position references in the world frame. As the body and world frame orientations, as per our assumptions, are identical, the body frame position can be computed as

$$d_w^b = c^{ref} - R_w^b \hat{s}_b^b = c^{ref} - \hat{s}_b^b \tag{37}$$

Since the hip coordinate frames are fixed to the body of the robot, their center positions are fixed as expressed in the body frame. Calling the right hip and left hip center positions in the body frame, d_b^{R0} and d_b^{L0}, respectively, we can find the world frame coordinates of the hip centers as

$$d_w^{Ro} = d_w^b + R_w^b d_b^{R0} = d_w^b + d_b^{R0} \tag{38}$$

Similarly,

$$d_w^{Lo} = d_w^b + R_w^b d_b^{L0} = d_w^b + d_b^{L0} \tag{39}$$

Now, we have the foot positions d_w^R, d_w^L, and the corresponding hip coordinates d_w^{Ro}, d_w^{Lo} expressed in the world frame. Since the world, body and hip frame orientations are the same, the foot position references expressed in the hip frames are computed as

$$d_{R0}^R = R_{R0}^w \left(d_w^R - d_w^{Ro} \right) = \left(d_w^R - d_w^{Ro} \right) \tag{40}$$

and

$$d_{L0}^L = R_{L0}^w \left(d_w^L - d_w^{Lo} \right) = \left(d_w^L - d_w^{Lo} \right) \tag{41}$$

The two equations above complete the position reference parts of the foot reference configurations as expressed in the corresponding hip frames.

Now, we are equipped with the desired foot configurations for the inverse kinematics process. The details of the inverse kinematics algorithm are the same as in [44]. Therefore they will not be presented in this thesis.

The next chapter is devoted to experimental walking results obtained with the humanoid robotic platform SURALP, with the reference generation mechanism described presented above.

Chapter 6

6. EXPERIMENTAL RESULTS

In this chapter, experiment results are presented. Walking experiments are carried out with the bipedal humanoid robot platform SURALP introduced in Chapter 3 and the results of one of these experiments are given. As reference trajectories, CoM references generated based on the forward moving ZMP references in Chapter 4, foot and leg joint references created in Chapter 5 are employed.

In order to have a stable bipedal walk, a stable reference generation mechanism and several control algorithms modifying these reference trajectories have to be implemented together, as mentioned in chapters 1 and 2. Since this thesis is concentrated on reference generation, rather than on implementing control algorithms, control algorithms introduced in [35-36, 45-46] are employed in order to achieve a stable bipedal walk.

Figure 6.1 shows the body roll and pitch angles during a 20 seconds walk. Reference generation parameters phase description number N_{phase}, single support period T_s, double support period T_d, distance between the foot centers A and range of the ZMP motion under the sole b are given in Table 6.1.

Table 6.1: Reference generation parameters

N_{phase}	23
T_s	1 s
T_d	0.9 s
A	7 cm
b	2 cm
s_s	12 cm

With these reference generation parameters, SURALP successfully walked with the generated reference trajectories based on forward moving natural ZMP trajectories

and the control algorithms in [35-36, 45-46] for an eleven swing step sequence with the step size of $s_s = 12\,\text{cm}$. Snapshots from this experiment are given in Figure 6.2.

With the generated ZMP reference trajectories in this thesis, stability of the walk is increased dramatically when compared to the previous walks of SURALP in [35-36, 45]. In this thesis, a walk with 12 cm step size is achieved while maximum step size was 6 cm in the previous works with SURALP. The newly presented reference generation method doubled the step size for the biped robot without any loss of stability. Other results showing the stability of the robot are the body inclination angles given in Figure 6.1. As it is seen from this figure, the body roll angle oscillates between $+2.5\,\text{deg}$ to $-3.5\,\text{deg}$ and the body pitch angle oscillates between $+2.1\,\text{deg}$ to $-1.7\,\text{deg}$. Oscillations in these ranges are quite acceptable for a bipedal robot whose upper body is much heavier than the legs which are traveling 24 cm distance in the swing phase. These results are achieved with the generated continuous and natural ZMP references and with the flexibility of adjusting single support and double support phase durations as separate parameters.

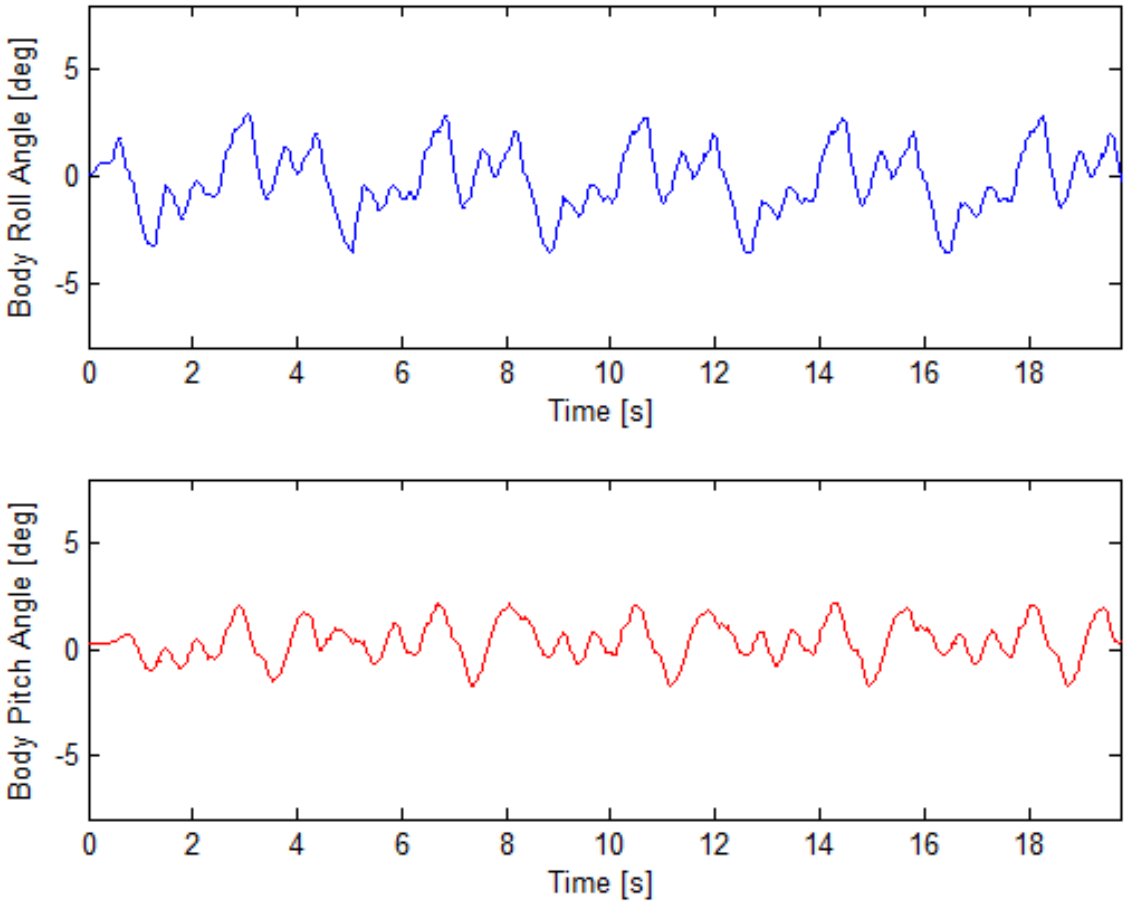

Figure 6.1: Body Roll and Pitch Angles

Figure 6.2: Snapshots of the experiment for an eleven swing step sequence with the step size $s_s = 12\,\text{cm}$

In the next chapter, conclusions of this thesis are presented.

Chapter 7

7. CONCLUSION AND FUTURE WORK

In this thesis, a forward moving (under the foot sole) continuous Zero Moment Point based reference trajectory generation is presented for a stable and human-like walk of the bipedal humanoid robots. The relation between the Zero Moment Point and the robot Center of Mass coordinates is obtained via the Linear Inverted Pendulum Model. In order to obtain the Center of Mass reference trajectory, ZMP reference trajectories are approximated with Fourier series approximation. Continuous nature of the ZMP reference trajectories provides non-oscillatory references, so that the smoothing with Lanczos sigma factors are not necessary unlike it is the case in [33].

Another contribution in this thesis is that the single support and double support phase durations are introduced as predefined separate parameters to be able to adjust them in the final parameter tuning of the generated references. In addition, a walk planning algorithm which generates a step sequence for a predefined number of steps with smooth starting and stopping motion is designed, in contrast to infinitely cycling references in [33].

Experimental results show that the generated stable human-like ZMP reference trajectories successfully enables a stable bipedal walk without a fall with a step size of 12 cm and limited oscillations of the robot upper body roll and pitch angles.

A natural extension of this thesis could be ZMP based reference generation for directional walk and turning motion.

Chapter 8

8. APPENDIX

A. Computation of the Fourier Coefficients for p_y^{ref}

$$p_y^{ref} = \sum_{k=1}^{\infty} \mathrm{A}(-1)^k \left[\begin{array}{l} \frac{2}{2\tau}(t-kT)\left[u(t-(kT-\tau))-u(t-(kT+\tau))\right] \\ +\left[u(t-(kT+\tau))-u(t-(kT+T-\tau))\right] \end{array} \right] \tag{42}$$

The Fourier coefficients b_k are computed as:

$$b_k\left(1+\frac{\pi^2k^2}{\omega_n^2T^2}\right) = \frac{2}{2T}\int_0^{2T} p_y^{ref}\sin\left(\frac{2\pi kt}{2T}\right)dt \tag{43}$$

Because of the symmetry of the functions p_y^{ref} and $\sin\left(\frac{2\pi kt}{2T}\right)$ about T we have

$$b_k\left(1+\frac{\pi^2k^2}{\omega_n^2T^2}\right) = \frac{2}{T}\int_0^{T} p_y^{ref}\sin\left(\frac{2\pi kt}{2T}\right)dt \tag{44}$$

Let

$$\begin{aligned} I_1 &\equiv \int_0^{T} p_y^{ref}\sin\left(\frac{2\pi kt}{2T}\right)dt \\ &= \int_0^{\tau} p_y^{ref}\sin\left(\frac{2\pi kt}{2T}\right)dt + \int_{\tau}^{T-\tau} p_y^{ref}\sin\left(\frac{2\pi kt}{2T}\right)dt + \int_{T-\tau}^{T} p_y^{ref}\sin\left(\frac{2\pi kt}{2T}\right)dt \end{aligned} \tag{45}$$

If $I_1 \neq 0$ (if k is odd) then

$$I_1 \equiv \underbrace{2\int_0^{\tau} p_y^{ref}\sin\left(\frac{2\pi kt}{2T}\right)dt}_{I_2} + \underbrace{\int_{\tau}^{T-\tau} p_y^{ref}\sin\left(\frac{2\pi kt}{2T}\right)dt}_{I_4} \tag{46}$$

$$I_2 = \int_0^{\tau} p_y^{ref}\sin\left(\frac{2\pi kt}{2T}\right)dt = \int_0^{\tau}\frac{A}{\tau}t\sin\left(\frac{2\pi kt}{2T}\right)dt = \frac{A}{\tau}\underbrace{\int_0^{\tau} t\sin\left(\frac{2\pi kt}{2T}\right)dt}_{I_3} \tag{47}$$

$$\begin{aligned} I_3 &= \int_0^{\tau} t\sin\left(\frac{2\pi kt}{2T}\right)dt = \underbrace{-\frac{2T}{2\pi k}t\cos\left(\frac{2\pi kt}{2T}\right)\Big|_0^{\tau}}_{-\frac{2T}{2\pi k}\tau\cos\left(\frac{2\pi k\tau}{2T}\right)} + \underbrace{\frac{2T}{2\pi k}\int_0^{\tau} 1\cos\left(\frac{2\pi kt}{2T}\right)dt}_{\frac{4T^2}{4\pi^2k^2}\sin\left(\frac{2\pi k\tau}{2T}\right)} \\ &= \frac{4T^2}{4\pi^2k^2}\sin\left(\frac{2\pi k\tau}{2T}\right) - \frac{2T}{2\pi k}\tau\cos\left(\frac{2\pi k\tau}{2T}\right) \end{aligned} \tag{48}$$

$$I_4 = \int_{\tau}^{T-\tau} p_y^{ref} \sin(\frac{2\pi kt}{2T})dt = \int_{\tau}^{T-\tau} A\sin(\frac{2\pi kt}{2T})dt = A\int_{\tau}^{T-\tau} \sin(\frac{2\pi kt}{2T})dt$$
$$= -A\frac{2T}{2\pi k}\cos(\frac{2\pi kt}{2T})\Big|_{\tau}^{T-\tau} = A\frac{2T}{2\pi k}\left[\cos(\frac{2\pi k\tau}{2T}) - \cos(\frac{2\pi k(T-\tau)}{2T})\right] \quad (49)$$

If k is odd, then

$$b_k(1+\frac{\pi^2k^2}{\omega_n^2T^2}) = \frac{2}{T}I_1 = \frac{2}{T}\{2I_2 + I_4\}$$
$$= \frac{2}{T}\left\{2\left[\frac{A}{\tau}I_3\right] + I_4\right\}$$
$$= \frac{2}{T}\left\{\begin{array}{l} 2\left[\frac{A}{\tau}\left\langle\frac{4T^2}{4\pi^2k^2}\sin(\frac{2\pi k\tau}{2T}) - \frac{2T}{2\pi k}\tau\cos(\frac{2\pi k\tau}{2T})\right\rangle\right] \\ \qquad + A\frac{2T}{2\pi k}\left[\cos(\frac{2\pi k\tau}{2T}) - \cos(\frac{2\pi k(T-\tau)}{2T})\right] \end{array}\right\}$$
$$= \frac{2}{T}\left\{\begin{array}{l} 2\left[\frac{A}{\tau}\left\langle\frac{T^2}{\pi^2k^2}\sin(\frac{\pi k\tau}{T}) - \frac{T}{\pi k}\tau\cos(\frac{\pi k\tau}{T})\right\rangle\right] \\ \qquad + A\frac{T}{\pi k}\left[\cos(\frac{\pi k\tau}{T}) - \cos(\frac{\pi k(T-\tau)}{T})\right] \end{array}\right\}$$
$$= 2\left\{\begin{array}{l} 2\left[\frac{A}{\tau}\left\langle\frac{T}{\pi^2k^2}\sin(\frac{\pi k\tau}{T}) - \frac{1}{\pi k}\tau\cos(\frac{\pi k\tau}{T})\right\rangle\right] \\ \qquad + A\frac{1}{\pi k}\left[\cos(\frac{\pi k\tau}{T}) - \cos(\frac{\pi k(T-\tau)}{T})\right] \end{array}\right\}$$
$$= 2\frac{A}{\pi k}\left\{2\left[\frac{1}{\tau}\left\langle\frac{T}{\pi k}\sin(\frac{\pi k\tau}{T}) - \tau\cos(\frac{\pi k\tau}{T})\right\rangle\right] + \left[\cos(\frac{\pi k\tau}{T}) - \cos(\frac{\pi k(T-\tau)}{T})\right]\right\} \quad (50)$$
$$= 2\frac{A}{\pi k}\left\{\left[\frac{2}{\tau}\left\langle\frac{T}{\pi k}\sin(\frac{\pi k\tau}{T}) - \tau\cos(\frac{\pi k\tau}{T})\right\rangle\right] + \left[\cos(\frac{\pi k\tau}{T}) - \cos(\frac{\pi k(T-\tau)}{T})\right]\right\}$$

$\Rightarrow$

$$b_k = \left\{\begin{array}{ll} \frac{\omega_n^2T^2}{\omega_n^2T^2+\pi^2k^2}2\frac{A}{\pi k}\left\{\begin{array}{l}\left[\frac{2}{\tau}\left\langle\frac{T}{\pi k}\sin(\frac{\pi k\tau}{T}) - \tau\cos(\frac{\pi k\tau}{T})\right\rangle\right] \\ \qquad + \left[\cos(\frac{\pi k\tau}{T}) - \cos(\frac{\pi k(T-\tau)}{T})\right]\end{array}\right\} & \text{if } k \text{ is odd} \\ 0 & \text{if } k \text{ even} \end{array}\right. \quad (51)$$

B. Computation of the Fourier Coefficients for p_x^{ref}

By definition $p_x^{ref} = \frac{B}{T}(t - \frac{T}{2}) + p_x'^{ref}$

where

$$p_x'^{ref} = \begin{cases} \Omega_1 + \sigma_1 t & \text{if} \quad 0 \le t \le \tau \\ \Omega_2 + \sigma_2 t & \text{if} \quad \tau < t \le T - \tau \\ \Omega_3 + \sigma_3 t & \text{if} \quad T - \tau < t \le T \end{cases} \tag{52}$$

with

$$\begin{aligned} &\Omega_1 = 0, \\ &\sigma_1 = \frac{\delta}{\tau}, \\ &\sigma_2 = \frac{-2\delta}{T - 2\tau}, \\ &\Omega_2 = \delta - \tau\sigma_2, \\ &\sigma_3 = \sigma_1; \\ &\Omega_3 = -\delta - (T - \tau)\sigma_3, \\ &\delta = \frac{\frac{T}{2} - \tau}{\frac{T}{2}}(\frac{B}{2} - b). \end{aligned} \tag{53}$$

From (20)

$$\beta_k(1 + \pi^2 k^2 / \omega_n^2 T^2) = \frac{2}{T}\int_0^T p_x'^{ref}(t)\sin(\frac{2\pi kt}{T})dt \equiv I_0 \tag{54}$$

Because of the symmetry of $p_x'^{ref}(t)\sin(\frac{2\pi kt}{T})$ about $\frac{T}{2}$ we can write I_0 as

$$\begin{aligned} I_0 &= \frac{2}{T}\int_0^T p_x'^{ref}(t)\sin(\frac{2\pi kt}{T})dt = \frac{4}{T}\int_0^{\frac{T}{2}} p_x'^{ref}(t)\sin(\frac{2\pi kt}{T})dt \\ &= \frac{4}{T}\left[\underbrace{\int_0^{\tau} f_1(t)\sin(\frac{2\pi kt}{T})dt}_{\equiv I_1} + \underbrace{\int_{\tau}^{\frac{T}{2}} f_2(t)\sin(\frac{2\pi kt}{T})dt}_{\equiv I_2}\right] \end{aligned} \tag{55}$$

where $f_1(t)$ and $f_2(t)$ are the two line segments in the function $p_x'^{ref}(t)$ before time $\frac{T}{2}$ in Figure 4.12.

The sub-integral I_1 can be computed as

$$\begin{aligned} I_1 &= \int_0^{\tau} f_1(x)\sin(\frac{2\pi kt}{T})dt = \int_0^{\tau}\left[\Omega_1 + \sigma_1 t\right]\sin(\frac{2\pi kt}{T})dt \\ &= \int_0^{\tau}\Omega_1\sin(\frac{2\pi kt}{T})dt + \int_0^{\tau}\sigma_1 t\sin(\frac{2\pi kt}{T})dt \\ &= \Omega_1\underbrace{\int_0^{\tau}\sin(\frac{2\pi kt}{T})dt}_{\equiv I_3} + \sigma_1\underbrace{\int_0^{\tau} t\sin(\frac{2\pi kt}{T})dt}_{\equiv I_4} \end{aligned} \tag{56}$$

In this expression

$$I_3 = \int_0^{\tau}\sin(\frac{2\pi kt}{T})dt = -\frac{T}{2\pi k}\cos(\frac{2\pi kt}{T})\Big|_0^{\tau} = \frac{T}{2\pi k}\left(1-\cos\left(\frac{2\pi k\tau}{T}\right)\right) \tag{57}$$

and

$$I_4 = \int_0^{\tau} t\sin(\frac{2\pi kt}{T})dt = \underbrace{-t\frac{T}{2\pi k}\cos(\frac{2\pi kt}{T})\Big|_0^{\tau}}_{=-\tau\frac{T}{2\pi k}\cos(\frac{2\pi k\tau}{T})} + \frac{T}{2\pi k}\underbrace{\int_0^{\tau}\cos(\frac{2\pi kt}{T})dt}_{\equiv I_5} \tag{58}$$

where

$$I_5 = \int_0^{\tau}\cos(\frac{2\pi kt}{T})dt = \frac{T}{2\pi k}\sin(\frac{2\pi kt}{T})\Big|_0^{\tau} = \frac{T}{2\pi k}\sin(\frac{2\pi k\tau}{T}) \tag{59}$$

This yields

$$\begin{aligned} I_4 &= -\tau\frac{T}{2\pi k}\cos(\frac{2\pi k\tau}{T}) + \frac{T}{2\pi k}\frac{T}{2\pi k}\sin(\frac{2\pi k\tau}{T}) \\ &= -\tau\frac{T}{2\pi k}\cos(\frac{2\pi k\tau}{T}) + \frac{T^2}{4\pi^2 k^2}\sin(\frac{2\pi k\tau}{T}) \end{aligned} \tag{60}$$

Hence I_1 is given by the following expression.

$$I_1 = \Omega_1\frac{T}{2\pi k}\left(1-\cos\left(\frac{2\pi k\tau}{T}\right)\right) + \sigma_1\left[-\tau\frac{T}{2\pi k}\cos(\frac{2\pi k\tau}{T}) + \frac{T^2}{4\pi^2 k^2}\sin(\frac{2\pi k\tau}{T})\right] \tag{61}$$

The second sub-integral I_2 is given by

$$\begin{aligned} I_2 &= \int_{\tau}^{\frac{T}{2}} f_2(x)\sin(\frac{2\pi kt}{T})dt = \int_{\tau}^{\frac{T}{2}}\left[\Omega_2 + \sigma_2 t\right]\sin(\frac{2\pi kt}{T})dt \\ &= \int_{\tau}^{\frac{T}{2}}\Omega_2\sin(\frac{2\pi kt}{T})dt + \int_{\tau}^{\frac{T}{2}}\sigma_2 t\sin(\frac{2\pi kt}{T})dt \\ &= \Omega_2\underbrace{\int_{\tau}^{\frac{T}{2}}\sin(\frac{2\pi kt}{T})dt}_{\equiv I_6} + \sigma_2\underbrace{\int_{\tau}^{\frac{T}{2}} t\sin(\frac{2\pi kt}{T})dt}_{\equiv I_7} \end{aligned} \tag{62}$$

The integral I_6 in (62) is obtained as

$$I_6 = \int_{\tau}^{\frac{T}{2}} \sin(\frac{2\pi kt}{T})dt = -\frac{T}{2\pi k}\cos(\frac{2\pi kt}{T})\Big|_{\tau}^{\frac{T}{2}} = \frac{T}{2\pi k}\left((-1)^{k+1} + \cos\left(\frac{2\pi k\tau}{T}\right)\right) \tag{63}$$

$$I_7 = \int_{\tau}^{\frac{T}{2}} t\sin(\frac{2\pi kt}{T})dt = \underbrace{-t\frac{T}{2\pi k}\cos(\frac{2\pi kt}{T})\Big|_{\tau}^{\frac{T}{2}}}_{\substack{=-\frac{T^2}{4\pi k}\cos(\pi k)+\tau\frac{T}{2\pi k}\cos(\frac{2\pi k\tau}{T}) \\ =\frac{T^2}{4\pi k}(-1)^{k+1}+\tau\frac{T}{2\pi k}\cos(\frac{2\pi k\tau}{T})}} + \frac{T}{2\pi k}\underbrace{\int_{\tau}^{\frac{T}{2}}\cos(\frac{2\pi kt}{T})dt}_{\equiv I_8} \tag{64}$$

where

$$I_8 = \int_{\tau}^{\frac{T}{2}} \cos(\frac{2\pi kt}{T})dt = \frac{T}{2\pi k}\sin(\frac{2\pi kt}{T})\Big|_{\tau}^{\frac{T}{2}} = 0 - \frac{T}{2\pi k}\sin(\frac{2\pi k\tau}{T}) \tag{65}$$

Therefore I_7 can be computed as

$$\begin{aligned} I_7 &= \frac{T}{2}\frac{T}{2\pi k}(-1)^{k+1} + \tau\frac{T}{2\pi k}\cos(\frac{2\pi k\tau}{T}) - \frac{T}{2\pi k}\frac{T}{2\pi k}\sin(\frac{2\pi k\tau}{T}) \\ &= \frac{T^2}{4\pi k}(-1)^{k+1} + \tau\frac{T}{2\pi k}\cos(\frac{2\pi k\tau}{T}) - \frac{T^2}{4\pi^2 k^2}\sin(\frac{2\pi k\tau}{T}) \end{aligned} \tag{66}$$

For the sub-integral I_2 we have

$$\begin{aligned} I_2 = \Omega_2 &\frac{T}{2\pi k}\left((-1)^{k+1} + \cos\left(\frac{2\pi k\tau}{T}\right)\right) \\ &+ \sigma_2\left[\frac{T^2}{4\pi k}(-1)^{k+1} + \tau\frac{T}{2\pi k}\cos(\frac{2\pi k\tau}{T}) - \frac{T^2}{4\pi^2 k^2}\sin(\frac{2\pi k\tau}{T})\right] \end{aligned} \tag{67}$$

Thus

$$\begin{aligned} I_0 = \frac{4}{T}\Bigg[&\Omega_1\frac{T}{2\pi k}\left(1-\cos\left(\frac{2\pi k\tau}{T}\right)\right) \\ &+ \sigma_1\left[-\tau\frac{T}{2\pi k}\cos(\frac{2\pi k\tau}{T}) + \frac{T^2}{4\pi^2 k^2}\sin(\frac{2\pi k\tau}{T})\right] \\ &+ \Omega_2\frac{T}{2\pi k}\left((-1)^{k+1} + \cos\left(\frac{2\pi k\tau}{T}\right)\right) \\ &+ \sigma_2\left[\frac{T^2}{4\pi k}(-1)^{k+1} + \tau\frac{T}{2\pi k}\cos(\frac{2\pi k\tau}{T}) - \frac{T^2}{4\pi^2 k^2}\sin(\frac{2\pi k\tau}{T})\right] \Bigg] \end{aligned} \tag{68}$$

with $\Omega_1 = 0$ we obtain

$$I_0 = \frac{4}{T}\left\{\begin{array}{l}\sigma_1\left[-\tau\frac{T}{2\pi k}\cos(\frac{2\pi k\tau}{T})+\frac{T^2}{4\pi^2k^2}\sin(\frac{2\pi k\tau}{T})\right] \\ \quad +\Omega_2\frac{T}{2\pi k}\left((-1)^{k+1}+\cos\left(\frac{2\pi k\tau}{T}\right)\right) \\ \quad +\sigma_2\left[\frac{T^2}{4\pi k}(-1)^{k+1}+\tau\frac{T}{2\pi k}\cos(\frac{2\pi k\tau}{T})-\frac{T^2}{4\pi^2k^2}\sin(\frac{2\pi k\tau}{T})\right]\end{array}\right\} \quad (69)$$

Further with $\Omega_2 = \frac{\delta T}{2(\frac{T}{2}-\tau)}$ and $\sigma_2 = -\frac{\delta}{\frac{T}{2}-\tau}$ we reach the following expression for Ω_2:

$$\Omega_2 = -\frac{\sigma_2 T}{2} \quad (70)$$

$$\Rightarrow I_0 = \frac{4}{T}\left[\begin{array}{l}\sigma_1\left[-\tau\frac{T}{2\pi k}\cos(\frac{2\pi k\tau}{T})+\frac{T^2}{4\pi^2k^2}\sin(\frac{2\pi k\tau}{T})\right] \\ -\frac{\sigma_2 T}{2}\frac{T}{2\pi k}\left((-1)^{k+1}+\cos\left(\frac{2\pi k\tau}{T}\right)\right) \\ +\sigma_2\left[\frac{T^2}{4\pi k}(-1)^{k+1}+\tau\frac{T}{2\pi k}\cos(\frac{2\pi k\tau}{T})-\frac{T^2}{4\pi^2k^2}\sin(\frac{2\pi k\tau}{T})\right]\end{array}\right]$$

$$= \frac{4}{T}\left[\begin{array}{l}\sigma_1\left[-\tau\frac{T}{2\pi k}\cos(\frac{2\pi k\tau}{T})+\frac{T^2}{4\pi^2k^2}\sin(\frac{2\pi k\tau}{T})\right] \\ -\frac{\sigma_2 T^2}{4\pi k}\left((-1)^{k+1}+\cos\left(\frac{2\pi k\tau}{T}\right)\right) \\ +\sigma_2\left[\frac{T^2}{4\pi k}(-1)^{k+1}+\tau\frac{T}{2\pi k}\cos(\frac{2\pi k\tau}{T})-\frac{T^2}{4\pi^2k^2}\sin(\frac{2\pi k\tau}{T})\right]\end{array}\right]$$

$$= \frac{4}{T}\left[\begin{array}{l}\sigma_1\left[-\tau\frac{T}{2\pi k}\cos(\frac{2\pi k\tau}{T})+\frac{T^2}{4\pi^2k^2}\sin(\frac{2\pi k\tau}{T})\right] \\ -\frac{\sigma_2 T^2}{4\pi k}\left(\cos\left(\frac{2\pi k\tau}{T}\right)\right)+\sigma_2\left[\tau\frac{T}{2\pi k}\cos(\frac{2\pi k\tau}{T})-\frac{T^2}{4\pi^2k^2}\sin(\frac{2\pi k\tau}{T})\right]\end{array}\right]$$

$$= \frac{4}{T}\left[\begin{array}{l}\sigma_1\left[-\tau\frac{T}{2\pi k}\cos(\frac{2\pi k\tau}{T})+\frac{T^2}{4\pi^2k^2}\sin(\frac{2\pi k\tau}{T})\right] \\ +\sigma_2\left[\tau\frac{T}{2\pi k}\cos(\frac{2\pi k\tau}{T})-\frac{T^2}{4\pi k}\left(\cos\left(\frac{2\pi k\tau}{T}\right)\right)-\frac{T^2}{4\pi^2k^2}\sin(\frac{2\pi k\tau}{T})\right]\end{array}\right] \quad (71)$$

$$
\begin{aligned}
I_0 &= \frac{4}{T}\frac{T}{2\pi k}\left[\begin{array}{l}\sigma_1\left[-\tau\cos(\frac{2\pi k\tau}{T})+\frac{T}{2\pi k}\sin(\frac{2\pi k\tau}{T})\right] \\ \qquad +\sigma_2\left[\tau\cos(\frac{2\pi k\tau}{T})-\frac{T}{2}\left(\cos\left(\frac{2\pi k\tau}{T}\right)\right)-\frac{T}{2\pi k}\sin(\frac{2\pi k\tau}{T})\right]\end{array}\right] \\
&= \frac{2}{\pi k}\left[\begin{array}{l}\sigma_1\left[-\tau\cos(\frac{2\pi k\tau}{T})+\frac{T}{2\pi k}\sin(\frac{2\pi k\tau}{T})\right] \\ \qquad +\sigma_2\left[\tau\cos(\frac{2\pi k\tau}{T})-\frac{T}{2}\left(\cos\left(\frac{2\pi k\tau}{T}\right)\right)-\frac{T}{2\pi k}\sin(\frac{2\pi k\tau}{T})\right]\end{array}\right]
\end{aligned}
\tag{72}
$$

Finally, from (54) the coefficients β_k are obtained as

$$
\begin{aligned}
\beta_k &= \frac{\omega_n^2 T^2}{\pi^2 k^2+\omega_n^2 T^2} I_0 \\
&= \frac{\omega_n^2 T^2}{\pi^2 k^2+\omega_n^2 T^2}\frac{2}{\pi k}\left[\begin{array}{l}\sigma_1\left[-\tau\cos(\frac{2\pi k\tau}{T})+\frac{T}{2\pi k}\sin(\frac{2\pi k\tau}{T})\right] \\ \qquad +\sigma_2\left[\tau\cos(\frac{2\pi k\tau}{T})-\frac{T}{2}\left(\cos\left(\frac{2\pi k\tau}{T}\right)\right)-\frac{T}{2\pi k}\sin(\frac{2\pi k\tau}{T})\right]\end{array}\right]
\end{aligned}
\tag{73}
$$

REFERENCES

[1] http://www.becomehealthynow.com/images/organs/planes_bh.jpg

[2] Wang, J. W., Xiong, W. L., Liu, H. and Ma, H., "Locomotion Planning Research for a Humanoid Robot Based on the ZMP", *Proceedings of the 2003 IEEE International Conference on Robotics, Intelligent Systems and Signal Processing,* pp. 942-947, Changsha, China, October 2003.

[3] Feng, S. and Sun, Z., "A Simple Trajectory Generation Method for Biped Walking", *Proceedings of the 2008 10th International Conference on Control, Automation, Robotics and Vision,* pp. 2078-2082, Hanoi, Vietnam, December 2008.

[4] Villeda, L. L., Frisoli, A. and Vega, V. P., "A Mechatronic Analysis and Synthesis of Human Walking Gait", *Proceedings of the 2009 IEEE International Conference on Mechatronics,* pp. 1-6, Malaga, Spain, April 2009.

[5] http://sprojects.mmi.mcgill.ca/gait/normal/walk.gif

[6] Seven, U., "Linear Inverted Pendulum Model and Swing Leg Dynamics in Biped Robot Walking Trajectory Generation", Thesis (MS), Department of Mechatronics Engineering of the Graduate School of Engineering and Natural Sciences of Sabanci University, July 2007.

[7] http://en.wikipedia.org/wiki/Zero_Moment_Point

[8] Lim, S. H. and Kim, J. G., "Adaptive Gait Algorithm for IWR Biped Robot", *Proceedings of the 1995 International Conference on Power Electronics and Drive Systems,* pp. 438-443, February 1995.

[9] Zhang, Y., Wang, Q. and Fu, P., "A New Method of Desired Gait Synthesis in Biped robot", *Proceedings of the 3rd World Congress on Intelligent Control and Automation,* pp. 1300-1304, Hefei, China, June-July 2000.

[10] Kajita, S., Kanehiro, F., Kaneko, K., Fujiwara, K., Yokoi, K. and Hirukawa, H., "A Realtime Pattern Generator for Biped Walking", *Proceedings of the 2002 IEEE International Conference on Robotics & Automation,* pp. 31-37, Washington, USA, May 2002.

[11] Nishiwaki, K., Kagami, S., Kuniyoshi, Y., Inaba, M. and Inoue, H., "Online Generation of Humanoid Walking Motion based on a Fast Generation Method of Motion Pattern that Follows Desired ZMP", *Proceedings of the 2002 IEEE/RSJ*

International Conference on Intelligent Robots and Systems, pp. 2684-2689, Lausanne, Switzerland, October 2002.

[12] Lim, H. O., Kaneshima, Y. and Takanishi, A., "Online Walking Pattern Generation for Biped Humanoid Robot with Trunk", *Proceedings of the 2002 IEEE International Conference on Robotics & Automation,* pp. 3111-3116, Washington, USA, May 2002.

[13] Peng, Z., Huang, Q., Zhang, L., Jafri, A. R., Zhang, W. and Li, K., "Humanoid On-line Pattern Generation Based on Parameters of Off-line Typical Walk Patterns", *Proceedings of the 2005 IEEE International Conference on Robotics & Automation,* pp. 3758-3763, Barcelona, Spain, April 2005.

[14] Sugihara, T., Nakamura, Y. and Inoue, H., "Realtime Humanoid Motion Generation through ZMP Manipulation based on Inverted Pendulum Control", *Proceedings of the 2002 IEEE International Conference on Robotics & Automation,* pp. 1404-1409, Washington, USA, May 2002.

[15] Harada, K., Kajita, S., Kaneko, K. and Hirukawa, H., "An Analytical Method on Real-time Gait Planning for a Humanoid Robot", *Proceedings of the 2004 IEEE/RAS International Conference on Humanoid Robots,* pp. 640-655, November 2004.

[16] Nishiwaki, K., Kagami, S., Kuffner, J. J., Inaba, M. and Inoue, H., "Online Humanoid Walking Control System and a Moving Goal Tracking Experiment", *Proceedings of the 2003 IEEE International Conference on Robotics & Automation,* pp. 911-916, Taipei, Taiwan, September 2003.

[17] Kajita, S., Kanehiro, F., Kaneko, K., Fujiwara, K., Harada, K., Yokoi, K. and Hirukawa, H., "Biped Walking Pattern Generation by using Preview Control of Zero-Moment Point", *Proceedings of the 2003 IEEE International Conference on Robotics& Automation*, pp. 1620-1626, Taipei, Taiwan, September 2003.

[18] Tanaka, T., Takubo, T., Inuoe, K. and Arai, T., "Emergent Stop for Humanoid Robots", *Proceedings of the 2006 IEEE/RSJ International Conference on Intelligent Robots and Systems,* pp. 3970-3975, Beijing, China, October 2006.

[19] Verrelst, B., Stasse, O., Yokoi, K. and Vanderborght, B., "Dynamically Stepping Over Obstacles by the Humanoid Robot HRP-2", *Proceedings of the 2006 IEEE/RAS International Conference on Humanoid Robots,* pp. 117-123, December 2006.

[20] Nishiwaki, K. and Kagami, S., "High Frequency Walking Pattern Generation based on Preview Control of ZMP", *Proceedings of the 2006 IEEE International Conference on Robotics& Automation*, pp. 2667-2672, Florida, USA, May 2006.

[21] Huang, W., Chew, C. M., Zheng, Y. and Hong, G. S., "Pattern Generation for Bipedal Walking Slopes and Stairs", *Proceedings of the 2008 IEEE/RAS International Conference on Humanoid Robots,* pp. 205-210, Daejeon, Korea, December 2008.

[22] Kong, J. S., Lee, B. H. and Kim, J. G., "A Study on the Gait Generation of a Humanoid Using Genetic Algorithm", *SICE 2004 Annual Conference,* pp. 187-191, Sapporo, Japan, August 2004.

[23] Dau, V. H., Chew, C. M. and Poo, A. N., "Optimal Trajectory Generation for Bipedal Robots", *Proceedings of the 2007 IEEE/RAS International Conference on Humanoid Robots,* pp. 603-608, November 2007.

[24] Ha, S., Han, Y. and Hahn, H., "Natural Gait Generation of Biped Robot based on Captured Human Motion Image", *Proceedings of the 2008 IEEE International Conference on Multisensor Fusion and Integration for Intelligent Systems,* pp. 522-525, Seoul, Korea, August 2008.

[25] Hoonsuwan, P., Sillapaphiromsuk, S., Sukvichai, K. and Fish, Jr. A., "Designing a Stable Humanoid Robot Trajectory using a Real Human Motion", *Proceedings of the 2009 6th International Conference on Electrical Engineering/Electronics, Computer, Telecommunications and Information Technology,* pp. 336-339, May 2009.

[26] Ayhan, O. and Erbatur, K., "Biped Robot Walk Control via Gravity Compensation Techniques", *Proceedings of the 2004 30th Annual Conference of IEEE Industrial Electronics Society,* pp. 621-626, Busan, Korea, November 2004.

[27] Naksuk, N., Mei, Y. and Lee, C. S. G., "Humanoid Trajectory Generation: An Iterative Approach Based on Movement and Angular Momentum Criteria", *Proceedings of the 2004 IEEE/RAS International Conference on Humanoid Robots,* pp. 576-591, November 2004.

[28] Kim, J. Y., Park, I. W. and Oh, J. H., "Experimental Realization of Dynamic Walking of the Biped Humanoid Robot KHR-2 Using Zero Moment Point Feedback and Inertial Measurement", *Proceedings of the 2006 International Conference on Advanced Robotics*, pp. 707-736, 2006.

[29] Erbatur, K. and Seven, U., “An Inverted Pendulum based Approach to Biped Trajectory Generation with Swing Leg Dynamics”, *Proceedings of the 2007 IEEE/RAS International Conference on Humanoid Robots,* pp. 216-221, November 2007.

[30] Morisawa, M., Harada, K., Kajita, S., Nakaoka, S., Fujiwara, K., Kanehiro, F., Kaneko, K. and Hirukawa, H., “Experimentation of Humanoid Walking Allowing Immediate Modification of Foot Place Based on Analytical Solution”, *Proceedings of the 2007 IEEE International Conference on Robotics& Automation*, pp. 3989-3994, Roma, Italy, April 2007.

[31] Tang, Z. and Er, M. J., “Humanoid 3D Gait Generation Based on Inverted Pendulum Model”, *Proceedings of the 2007 IEEE 22nd International Symposium on Intelligent Control*, pp. 339-344, Singapore, October 2007.

[32] Lee, B. J., Stonier, D., Kim, Y. D. and Yoo, J. K., “Modifiable Walking Pattern of a Humanoid Robot by Using Allowable ZMP Variation”, *IEEE Transactions on Robotics,* pp. 917-925, August 2008.

[33] Erbatur, K. and Kurt, O., “Natural ZMP Trajectories for Biped Robot Reference Generation”, *IEEE Transactions on Industrial Electronics,* vol. 56, no. 3, pp. 835-845, March 2009.

[34] Erbatur, K. and Kawamura, A., “A New Penalty based Contact Modeling and Dynamics Simulation Method as Applied to Biped Walking Robots," *Proceedings of the 2003 FIRA World Congress*, Vienna, Austria, October 2003.

[35] Erbatur, K., Seven U., Taşkıran E., Koca Ö., Kızıltaş G., Ünel M., Sabanovic A. and Onat A., “SURALP-L, The Leg Module of a New Humanoid Platform,” *Proceedings of the 2008 IEEE/RAS International Conference on Humanoid Robots*, pp. 168-173, Daejeon, Korea, December 2008.

[36] Erbatur, K., Seven U., Taşkiran E. and Koca Ö., “Walking Trajectory Generation and Force Feedback Control for The Humanoid Robot Leg Module SURALP-L” *Proceedings of the IASTED International Conference on Intelligent Systems and Control*, Orlando, USA, November 2008.

[37] Erbatur, K., Okazaki, A., Obiya, K., Takahashi, T. and Kawamura, A., “A Study on the Zero Moment Point Measurement for Biped Walking Robots,”, *Proceedings of the AMC 2002, 7th International Workshop on Advanced Motion Control*, pp. 431-436, Maribor, Slovenia, July 2002.

[38] Fujimoto, Y. and Kawamura, A., “Simulation of an Autonomous Biped Walking Robot Including Environmental Force Interaction”, *IEEE Robotics and Automation Magazine,* pp. 33-42, June 1998.

[39] Dasgupta, A. and Nakamura, Y., “Making Feasible Walking Motion of Humanoid Robots from Human Motion Capture Data” *Proceedings of the 1999 IEEE International Conference on Robotics and Automation*, pp. 1044-1049, Detroit, Michigan, May 1999.

[40] Kajita, S., Kanehiro, F., Kaneko, K., Yokoi, K. and Hirukawa, H., “The 3D Linear Inverted Pendulum Mode: A Simple Modeling for a Biped Walking Pattern Generation,” *Proceedings of the 2001 IEEE/RSJ International Conference on Intelligent Robots and Systems,* pp. 239-246, Hawaii, USA, November 2001.

[41] Vukobratovic, M., Borovac, B., Surla, D. and Stokic, D., *Biped Locomotion: Dynamics, Stability and Application*. Springer-Verlag, 1990.

[42] Choi, Y., You, B. J. and Oh, S. R., “On the Stability of Indirect ZMP Controller for Biped Robot Systems”, *Proceedings of the 2004 IEEE/RSJ International Conference on Intelligent Robots and Systems,* pp. 1966–1971*,* Sendal, Japan, October 2004.

[43] Bebek, O., and Erbatur, K., "A Fuzzy System for Gait Adaptation of Biped Walking Robots," *Proceedings of the 2003 IEEE Conference on Control Applications,* pp. 669-673, June 2003.

[44] Erbatur, K. and Seven, U., “An Inverted Pendulum Based Approach to Biped Trajectory Generation with Swing Leg Dynamics”, *Proceedings of the 2007 IEEE/RAS International Conference on Humanoid Robots,* pp. 216-221, November 2007.

[45] Erbatur, K., Seven, U., Taskiran, E., Koca, O., Unel, M., Kiziltas, G., Sabanovic, A., and Onat, A., “SURALP: A New Full-Body Humanoid Robot Platform”, *accepted for publication in the Proceedings of the 2009 IEEE/RSJ International Conference on Intelligent Robots and Systems,* Missouri, USA, October 2009.

[46] Taşkıran, E., “Walking Trajectory Generation and Control of a Humanoid Robot: SURALP”, Thesis (MS), Department of Mechatronics Engineering of the Graduate School of Engineering and Natural Sciences of Sabanci University, August 2009.